UNIVERSITY OF SOUTHAMPTON

FACULTY OF PHYSICAL SCIENCES AND ENGINEERING

Physics

Hadronic kaon decays from lattice QCD

by

Tadeusz Janowski

Thesis for the degree of Doctor of Philosophy

October 2015

UNIVERSITY OF SOUTHAMPTON

ABSTRACT

FACULTY OF PHYSICAL SCIENCES AND ENGINEERING
Physics

Doctor of Philosophy

HADRONIC KAON DECAYS FROM LATTICE QCD

by Tadeusz Janowski

We present the most recent results for the $\Delta I = 3/2$ $K \to \pi\pi$ scattering amplitude calculated directly at physical kinematics using two lattice ensembles with Iwasaki gauge action and Möbius Domain Wall Fermion action with the Möbius parameter $\alpha = 2$. The ensembles have dimension $48^3 \times 96 \times 24$ and $64^3 \times 128 \times 12$ respectively with inverse lattice spacings of 1.728(4) GeV and 2.357(7) GeV respectively. We find that the continuum value of the $K \to \pi\pi$ $\Delta I = 3/2$ decay amplitude is $\mathrm{Re}A_2 = 1.50(4)(14) \times 10^{-8}$ GeV and $\mathrm{Im}A_2 = -6.99(20)(84) \times 10^{-13}$ GeV, which are consistent with the both the experiment and the previous lattice calculation. This is the first calculation of this quantity which involves the continuum extrapolation, which keeps the discretisation errors under control and by doing so addresses the largest source of systematic error in the previous calculation. The new dominant source of systematic error is due to Wilson coefficient calculation.

We also confirm our previous observation about the cancellation of contraction within the $\mathrm{Re}A_2$ amplitude. We believe that this cancellation gives the significant contribution to the $\Delta I = 1/2$ rule.

Finally, we present the results of $K\pi$ scattering lengths calculated using the same ensembles. The results are $a_0^{3/2} m_\pi = -0.06(1)$ in the I=3/2 channel and $a_0^{1/2} m_\pi = 0.16(2)$ in the I=1/2 channel. These results agree with both the dispersive calculations and previous lattice findings. Unlike previous lattice computations, ours is the first calculation of these quantities directly at a physical point, making it independent of the chiral perturbation theory.

Contents

List of Figures

List of Tables

Declaration of Authorship

I, Tadeusz Janowski , declare that the thesis entitled *Hadronic kaon decays from lattice QCD* and the work presented in the thesis are both my own, and have been generated by me as the result of my own original research. I confirm that:

- this work was done wholly or mainly while in candidature for a research degree at this University;
- where any part of this thesis has previously been submitted for a degree or any other qualification at this University or any other institution, this has been clearly stated;
- where I have consulted the published work of others, this is always clearly attributed;
- where I have quoted from the work of others, the source is always given. With the exception of such quotations, this thesis is entirely my own work;
- I have acknowledged all main sources of help;
- where the thesis is based on work done by myself jointly with others, I have made clear exactly what was done by others and what I have contributed myself;
- parts of this work have been published as: [2], [3] and [4].

Signed:.....

Date:.....

Acknowledgements

I would like to thank first and foremost my supervisor, Prof. Chris Sachrajda, for his guidance and support during all stages of this project.

I would also like to thank Dr. Andreas Jüttner for his extensive help with the numerical issues, especially for the careful checks of the $K\pi$ scattering length calculations, which took a lot of time and effort to get right!

This thesis wouldn't be possible without the input of all the colleagues from the RBC-UKQCD collaboration. I worked especially closely with Dr. Andrew Lytle, Daiqian Zhang and Dr. Chris Kelly.

I learned a lot about the Standard Model and beyond from our unofficial 'Weinberg reading group', which I found both fun and interesting, so I would like to thank all the members: Dr. Daniele Barducci, Dr. Maien Binjonaid, Miguel Crispim-Romao, Juri Fiaschi, Dr. Jason Hammett, Dr. Venus Keus, Anthony Preston and Dr. Dr. Marc Thomas.

Last, but certainly not least, I would like to thank the SHEP group, especially my fellow 4007 office mates, who made my everyday life at Southampton more enjoyable and a bit crazy (in a positive sense).

Chapter 1

Introduction

Combined charge conjugation and parity symmetry (CP) violation is one of the requirements for large matter-antimatter asymmetry in the Universe that we observe today. First of all, there is a possibility of CP-violation in the strong sector, where the inclusion of the so-called θ term would induce explicit breaking of CP symmetry, however studies of electric dipole moment of the neutron show that this term is negligibly small. This is known as the strong CP problem and will not be discussed here. This leaves weak interactions as the only source of CP-violation in the Standard Model. At low energies the relevant parameters are the Pontecorvo-Maki-Nakagawa-Sakata (PMNS) matrix in the lepton sector and the Cabibbo-Kobayashi-Maskawa matrix in the quark sector. The CKM matrix is discussed in more detail in Chapter 2. By studying weak interactions we can hope to find out where the large matter-antimatter symmetry comes from as well as improving constraints on the Standard Model with hope of finding new physics.

In this thesis I will focus on CP violation in neutral kaon decays, specifically in $K \to \pi\pi$ processes. As discussed in Chapter 3 these can be classified as *indirect* CP-violation which is a result of physical neutral kaon states not being CP-eigenstates, *direct* CP violation referring to the possibility of CP-even state decaying into a CP-odd state or vice versa, and *interference* CP violation, which can arise from a difference between indirect and direct CP phases. Historically, indirect CP violation in $K \to \pi\pi$ decay was first observed in [5] and direct CP-violation was discovered later in [6; 7; 8; 9].

As will be discussed in Chapter 3, there are several interesting measurable quantities. Two of them are the parameters ϵ and ϵ', the former being associated to the indirect and interference CP violation and the latter to direct CP violation. The ratio of the two has been determined experimentally to be $\mathrm{Re}(\epsilon'/\epsilon) = 1.65(26) \times 10^{-3}$. The third quantity is the ratio of the real parts of the decay amplitude to two pions in the isospin 0 state (A_0) to the decay amplitude to two pions in the isospin 2 state (A_2). Experimentally the ratio $\mathrm{Re}A_0/\mathrm{Re}A_2 \approx 22.5$. This is a surprisingly large number, as naively one may expect

only a factor of 2 enhancement [10; 11]. This observation, known as the $\Delta I = 1/2$ rule has been an unresolved issue for almost fifty years.

From the theory side until recently we did not have any predictions. This is because the calculation of strong matrix elements is non-perturbative, which means that it can be done most reliably with lattice QCD. Thanks to both hardware and theoretical developments this calculation can now be done directly at physical kinematics. The two most important calculations prior to the one which is the subject of this thesis are the calculation of both $\mathrm{Re}A_0$ and $\mathrm{Re}A_2$ at threshold ($m_K \approx 2m_\pi$) at two different pion masses [2] and the calculation of $\mathrm{Re}A_2$ directly at the physical point [12]. The threshold calculation is interesting because it gave us the first insight into the reason behind the $\Delta I = 1/2$ enhancement, which appears to be significantly affected by a cancellation of contraction in the $\mathrm{Re}A_2$ amplitude. The physical point calculation of the $\mathrm{Re}A_2$ was the first calculation of this type and it gave results which could be compared directly to the experiment. The major weakness of this calculation however was that it was done using a single lattice spacing, which meant that the discretisation errors were not well controlled and a conservative estimate of 15 % was used.

The work described in this thesis follows [3] and attempts to address this issue by repeating the measurement of the A_2 amplitude using two physical-point ensembles which have the same volume but different lattice spacings. This allows us to take the continuum extrapolation and thus get a handle on the size of systematic errors.

The calculation of A_0 at physical kinematics is significantly more challenging. The main difficulty comes from ensuring that the pions have equal and opposite momenta, which requires the introduction of G-parity boundary conditions. The first calculation of A_0 at physical kinematics has recently been completed [13].

A separate calculation described in this thesis which we used the same ensembles for is the calculation of $K\pi$ scattering lengths. While conceptually the calculation is identical to $\pi\pi$ scattering, we found significant contribution from finite time effects in this calculation.

This thesis is structured as follows. Chapter 2 gives an introduction to the Standard Model explaining in particular where the CKM matrix comes from and how it gives rise to CP-violation, gives a brief summary of C, P and T symmetries. This is followed by the description of Fermi effective theory, which is a useful description for studying the low-energy flavour-changing processes such as $K \to \pi\pi$. The last section in chapter 2 gives a brief introduction to the chiral perturbation theory and explains how it can be used to study $K \to \pi\pi$ decays. Chapter 3 explains the phenomenology of $K \to \pi\pi$ decays, defining various types of CP violation (direct, indirect and interference), introduces the measurable quantities which can be used to parametrise CP violation and quotes some experimental results. The last section of this chapter describes the phenomenology of two-particle scattering, which is important in understanding the finite volume effects.

Chapter 4 introduces lattice QCD describing both concepts and computational tools used for this analysis. Section 4.1 describes our choice of gauge field and fermion field formulation, section 4.2 describes how the rotational symmetry is broken to the cubic symmetry and the effect of this breaking on particle states. Section 4.3 and 4.4 introduce the Euclidean correlation functions, describing the calculation from the path integral and their spectral decomposition respectively. Section 4.5 introduces propagator smearing which can be used to improve the overlap of interpolating operators with physical states. Section 4.6 and 4.7 describe the correlation functions used in $K \to \pi\pi$ projects, which are $\pi\pi \to \pi\pi$ and $K \to \pi\pi$ correlation functions respectively. Section 4.8 describes the technique of all mode averaging, which can be used to significantly reduce statistical error at a cost increasing the computational time. Section 4.9 describes how the fitting procedure used to fit the correlation functions works. Section 4.10 describes the Maiani-Testa no-go theorem, which states that matrix elements of multi-particle states can not be extracted from infinite volume Euclidean correlation functions. This restriction is lifted in the finite volume. Section 4.11 discusses the continuum scaling and explains why $K \to \pi\pi$ matrix elements are $O(a)$ improved. Section 4.12 describes the finite volume effects and explains how phase shifts can be calculated and how finite volume matrix elements are related to the infinite volume ones by the Lellouch-Lüscher factor. Section 4.13 discusses the nonperturbative renormalisation, in particular how matrix elements calculated on the lattice can be related to $\overline{MS}$ matrix elements. Finally, section 4.14 outlines the main differences between $\Delta I = 3/2$ and $\Delta I = 1/2$ calculations. Chapter 5 discusses the ensembles which are used for this project and gives results. Finally, Chapter 6 summarises and concludes this thesis. There is one appendix, which contains transformation matrices corresponding to transformations of a 3-vector under cubic symmetry transformations sorted by their conjugacy classes. This is relevant for section 4.2.

Chapter 2

The Standard Model

The Standard Model of particle physics is a very successful theory, which explains all fundamental interactions (except gravity) and is consistent with all experimental observations (with the exception of neutrino masses). While there are slight tensions between theory and experiment such as the measurement of the anomalous magnetic moment of the muon [14] or the discrepancy in $B \to K^* \mu^+ \mu^-$ [15] which may point towards new physics at high energies, the Standard Model remains an excellent tool for describing low energy physics, such as kaon decays. When working at low energies it is convenient to 'integrate out' the high-energy degrees of freedom and work with an effective theory. In section 2.1 I will introduce the Standard Model Lagrangian, then in section 2.2 I will describe how going below the electroweak symmetry breaking scale leads to flavour mixing and CP violation by means of the Cabibbo-Kobayashi-Maskawa matrix. I will then proceed to remove the heavy vector boson degrees of freedom which results in Fermi effective theory and describe how to renormalise the theory at a desired scale. This will be the subject of section 2.4. Section 2.3 describes the symmetries of QCD which will be useful throughout the thesis. Finally, section 2.5 introduces chiral perturbation theory, which is a useful tool for studying low energy QCD.

2.1 Matter content of the Standard Model

The Standard Model has an $SU(3) \times SU(2) \times U(1)$ gauge structure, with the particle content shown in Table 2.1. The most general Lorentz invariant, gauge invariant and

Field	$SU(3)$	$SU(2)$	$U(1)$	spin
G (gluon)	8	1	0	1
W (W, Z and photon)	1	3	0	1
B (Z and photon)	1	1	0	1
H (Higgs)	1	2	-1/2	0
L_i (left-handed lepton)	1	2	-1/2	1/2
Q_i (left-handed quark)	3	2	1/6	1/2
e_i (right-handed electron)	1	1	-1	1/2
u_i (right handed up-type quark)	3	1	2/3	1/2
d_i (right handed down-type quark)	3	1	-1/3	1/2

Table 2.1: Matter content of the Standard Model: fields and their representations under gauge and spin groups.

renormalisable Lagrangian than can be built of out these fields is:

$$\mathcal{L} = \mathcal{L}_{gauge} + \mathcal{L}_{fermion} + \mathcal{L}_{Higgs} + \mathcal{L}_{Yukawa}, \tag{2.1}$$

$$\mathcal{L}_{gauge} = \sum_{\alpha \in B,W,G} -\frac{1}{4} F_{\alpha}^{\mu\nu a} F_{\alpha\mu\mu}^{a}, \tag{2.2}$$

$$\mathcal{L}_{fermion} = \sum_{\alpha \in L_i,Q_i,e_i,u_i,d_i} \bar{\psi}_{\alpha} \left(i \not{D}_{\alpha} \right) \psi_{\alpha}, \tag{2.3}$$

$$\mathcal{L}_{Higgs} = \frac{1}{2} D_{\mu} H^{\dagger} D^{\mu} H - \mu^2 H^{\dagger} H - \lambda \left(H^{\dagger} H \right)^2, \tag{2.4}$$

$$\mathcal{L}_{Yukawa} = -Y_{ij}^{l} \bar{L}_i H e_j - Y_{ij}^{d} \bar{Q}_i H d_j - Y_{ij}^{u} \bar{Q}_i (i\sigma^2) H^* u_j + h.c., \tag{2.5}$$

where i and j are the family indices, ‘ h.c.’ stands for ‘ hermitian conjugate terms’ which are required to make the Lagrangian real. Explicitly, $u_i = (u \quad c \quad t)^T$ and $d_i = (d \quad s \quad b)^T$.

2.2 Electroweak symmetry breaking

Although the Standard Model is a very successful theory, for the purpose of studying kaon physics it is more convenient to use the low energy approximation to the Standard Model. In this section I will show the steps we use to achieve a convenient approximation.

2.2.1 Higgs vacuum expectation value

The most important feature of the Higgs sector is the spontaneous symmetry breaking mechanism. The Higgs potential can be read off from $\mathcal{L}_{Higgs}$ to be:

$$V(H) = \lambda \left(H^{\dagger} H \right)^2 + \mu^2 H^{\dagger} H. \tag{2.6}$$

When $\lambda > 0$ and $\mu^2 < 0$, this potential is minimised for $|H| = \sqrt{\frac{-\mu^2}{2\lambda}} \equiv \frac{v}{\sqrt{2}}$. Without loss of generality, we may choose the vacuum state to be $H_{vac} = \begin{pmatrix} 0 \\ v/\sqrt{2} \end{pmatrix}$. The Higgs field can then be rewritten in terms of four scalar fields:

$$H = e^{\frac{i\pi^a(x)\sigma^a}{v}} \begin{pmatrix} 0 \\ \frac{v}{\sqrt{2}} + \frac{h(x)}{\sqrt{2}} \end{pmatrix}, \tag{2.7}$$

where σ^a are the Pauli matrices. The coefficients here were chosen such that the fields π^a and h are canonically normalised, i.e. the kinetic terms are $\frac{1}{2}(\pi^a)^2$ and $\frac{1}{2}h^2$. The π^a fields correspond to the Goldstone bosons (which should not be confused with QCD pions) while the h field corresponds to the Higgs boson. The change in the π^a fields acts on this doublet like an SU(2) gauge transformation. We can therefore choose the gauge such that $\pi^a(x) = 0$, known as the unitary gauge. As will become apparent in the following section, the choice of unitary gauge gives masses to W and Z bosons. The original four degrees of freedom of the Higgs doublet then become a Higgs boson and longitudinal polarisations of W^+, W^- and Z bosons (recall that massless bosons have only two transverse polarisations).

2.2.2 Masses of vector bosons

Above the electroweak scale all gauge bosons are massless and therefore have two spin degrees of freedom. In the unitary gauge, the degrees of freedom of Goldstone bosons combine with degrees of freedom of gauge bosons. As a result, the gauge bosons gain mass (massive spin 1 particles have 3 degrees of freedom). Their masses can be found from the $(D^\mu H)^\dagger D_\mu H$ term, where the covariant derivative is in this case:

$$D_\mu = \partial_\mu + i\frac{g}{2}W_\mu^a\sigma^a + \frac{ig'}{2}B_\mu \tag{2.8}$$

$$= \begin{pmatrix} \partial_\mu + \frac{ig}{2}W_\mu^3 + \frac{ig'}{2}B_\mu & \frac{ig}{2}(W_1 - iW_2) \\ \frac{ig}{2}(W_1 + iW_2) & \partial_\mu - \frac{ig}{2}W_\mu^3 + \frac{ig'}{2}B_\mu \end{pmatrix}. \tag{2.9}$$

In the unitary gauge the $(D^\mu H)^\dagger D_\mu H$ term contains the following contributions to the gauge boson mass:

$$\frac{g^2v^2}{4}W^+W^- + \frac{g^2v^2}{8}\left(\frac{g'}{g}B_\mu - W_\mu^3\right)^2, \tag{2.10}$$

where $W^\pm \equiv \frac{1}{\sqrt{2}}(W_1 \pm iW_2)$. The first term can be compared with the mass term for charged vector field $m_W^2W^+W^-$ to give $m_W = \frac{gv}{2}$. The second term mixes W^3 and B fields, so the mass can not be read off directly. Instead we can remove the mixing by making the rotation:

$$\begin{pmatrix} W_\mu^3 \\ B_\mu \end{pmatrix} = \begin{pmatrix} \cos\theta_W & \sin\theta_W \\ -\sin\theta_W & \cos\theta_W \end{pmatrix} \begin{pmatrix} Z_\mu \\ A_\mu \end{pmatrix}. \tag{2.11}$$

This rotation results in kinetic terms for A and Z, which are canonically normalised. Choosing

$$\tan\theta_W = \frac{g'}{g} \tag{2.12}$$

gives for the second term:

$$\frac{g^2v^2}{8}\left(\frac{Z_\mu}{\cos\theta_W}\right)^2 \equiv \frac{m_Z^2}{2}Z_\mu Z^\mu. \tag{2.13}$$

θ_W is known as Weinberg angle. As a result, we have a massless field A corresponding to a photon, and a massive Z boson with mass

$$m_Z = \frac{gv}{2\cos\theta_W} = \frac{m_W}{\cos\theta_W}. \tag{2.14}$$

2.2.3 Charged and neutral currents

The interactions of electroweak gauge bosons with fermions can be read off from $\mathcal{L}_{fermion}$. This term can be written as:

$$\begin{aligned} i\bar{\psi}\not{D}\psi &= i\bar{\psi}\gamma^\mu\left(\partial_\mu - igT_R^aW_\mu^a - ig\tan\theta_W Y B_\mu\right)\psi & (2.15)\\ &= i\bar{\psi}\gamma^\mu\left(\partial_\mu - igT_R^+W_\mu^- - igT_R^-W_\mu^+ - ig\sin\theta_W(T_R^3+Y)A_\mu\right.\\ &\left. - ig(T_R^3\cos\theta_W - Y\frac{\sin^2\theta_W}{\cos\theta_W})Z_\mu\right)\psi, & (2.16)\end{aligned}$$

where $T_R^\pm = \frac{1}{\sqrt{2}}(T_R^1 \pm iT_R^2)$ and T_R^i are the generators of $SU(2)$ in representation R. The right-handed fields in the Standard Model are in the trivial representation of SU(2), so for these fields $T^+ = T^- = T^3 = 0$. These fields can't couple to the W bosons and their coupling to photon is given by $ig\sin\theta_W Y\bar{\psi}\not{A}\psi$ and to the Z boson is given by $ig\tan\theta_W Y\bar{\psi}\not{Z}\psi$. Comparing the former with the electron-photon coupling in QED ($e\bar{\psi}\not{A}\psi$) we have:

$$e = g\sin\theta_W. \tag{2.17}$$

Left-handed fields transform under the fundamental representation of SU(2) with $T_F^i = \sigma^i/2$. The couplings are as follows:

- W_μ^+

$$\frac{ie}{\sqrt{2}\sin\theta_W}\begin{pmatrix}0 & 0\\ 1 & 0\end{pmatrix} \tag{2.18}$$

- W_μ^-

$$\frac{ie}{\sqrt{2}\sin\theta_W}\begin{pmatrix}0 & 1\\ 0 & 0\end{pmatrix} \tag{2.19}$$

- A_μ

$$ie \begin{pmatrix} Y+\frac{1}{2} & 0 \\ 0 & Y-\frac{1}{2} \end{pmatrix} \tag{2.20}$$

- Z_μ

$$ie \begin{pmatrix} \frac{1}{2}\cot\theta_W + Y\tan\theta_W & 0 \\ 0 & -\frac{1}{2}\cot\theta_W + Y\tan\theta_W \end{pmatrix} \tag{2.21}$$

2.2.4 Quark masses and mixings

Now consider the Yukawa sector, $\mathcal{L}_{Yukawa}$. Below the electroweak scale, the term giving mass to the down-type quarks (ignoring the fermion-Higgs interaction coming from the same term) is:

$$Y^d_{ij}\bar{Q}_i H d_j + h.c. \rightarrow M^d_{ij}\bar{d}_{Li}d_{Rj} + h.c., \tag{2.22}$$

with

$$M^d_{ij} = \frac{v}{\sqrt{2}}Y^d_{ij}. \tag{2.23}$$

Similarly, for the up type quarks we get:

$$Y^u_{ij}\bar{Q}_i(i\sigma^2)H^* d_j + h.c. \rightarrow M^u_{ij}\bar{u}_{Li}u_{Rj} + h.c., \tag{2.24}$$

with

$$M^u_{ij} = \frac{v}{\sqrt{2}}Y^u_{ij}. \tag{2.25}$$

To find the (tree-level bare) fermion masses, we change the basis as follows:

$$u_{L/Ri} \rightarrow U^u_{L/Rij}u_{L/Rj} \tag{2.26}$$

$$d_{L/Ri} \rightarrow U^d_{L/Rij}d_{L/Rj} \tag{2.27}$$

$$M^{u/d}_{ij} \rightarrow U^{u/d}_L \begin{pmatrix} m_{u/d} & 0 & 0 \\ 0 & m_{c/s} & 0 \\ 0 & 0 & m_{t/b} \end{pmatrix} U^{u/d\dagger}_R. \tag{2.28}$$

This is known as the mass basis. Changing to the mass basis has no effect on the kinetic and neutral current interactions, but the charged interactions become:

$$\frac{ie}{\sqrt{2}\cos\theta_W}\bar{u}_{Li}\not{W}^+ d_{Li} + h.c. \rightarrow \frac{ie}{\sqrt{2}\cos\theta_W}\bar{u}_{Li}\not{W}^+ V_{ij}d_{Lj} + h.c. \tag{2.29}$$

with

$$V_{ij} \equiv U^{u\dagger}_L U^d_L. \tag{2.30}$$

V_{ij} is the Cabibbo-Kobayashi-Maskawa (CKM) matrix and it is the source of CP violation in the weak sector as discussed below.

With these results, the Standard Model Lagrangian below the electroweak scale can be written as

$$\mathcal{L} = \mathcal{L}_{QCD} + \mathcal{L}_W \tag{2.31}$$

$$\mathcal{L}_{QCD} = \frac{1}{4} G^a_{\mu\nu} G^{\mu\nu a} + \sum_{\psi \in u,d,s,c,b,t} \bar{\psi}(i \not{D}_{QCD} - m_\psi)\psi \tag{2.32}$$

$$\mathcal{L}_W = -\frac{1}{4} W^{\mu\nu a} W^a_{\mu\nu} - \frac{1}{4} F^{\mu\nu} F_{\mu\nu} + \frac{m_Z^2}{2} Z^\mu Z_\mu + m_W^2 W_\mu W^\mu \tag{2.33}$$

$$+ \frac{ie}{\sqrt{2}\cos\theta_W} \bar{u}_{Li} \not{W}^+ V_{ij} d_{Lj} + h.c. \tag{2.34}$$

While the following section describes in more detail the CP transformations of asymptotic states, in order to examine the effect of the CKM matrix on CP violation I will introduce the CP transformations of fermion fields now. Under CP, the fields transform as:

$$\psi \to \gamma^2 \bar{\psi}^T, \tag{2.35}$$

$$\bar{\psi} \to \psi^T \gamma^2, \tag{2.36}$$

$$W^\mu \to -W_\mu. \tag{2.37}$$

where

$$\gamma^i = \begin{pmatrix} 0 & \sigma^i \\ -\sigma^i & 0 \end{pmatrix} \tag{2.38}$$

and σ^i are the Pauli matrices. Using these relation in Eq. (2.29) shows that the Lagrangian will be CP invariant only if $V^* = V$, i.e. if the CKM matrix is real.

The CKM matrix, being a 3×3 unitary matrix, has $3^2 = 9$ real parameters. Five of these parameters can be absorbed into quark field phases (there are 6 phases corresponding to the 6 fields, but an overall phase doesn't change the form of the CKM matrix). This leaves $9-5 = 4$ independent parameters. If the CKM matrix were real (so that there is no CP violation) and orthogonal (unitary and real), it would have $(3-1)3/2 = 3$ parameters (recall than an orthogonal matrix of size N has N(N-1)/2 independent parameters). This means that one of the CKM matrix parameters must be CP-violating.

Using the PDG parametrisation of the CKM matrix we have

$$V_{CKM} = \begin{pmatrix} c_{12}c_{13} & s_{12}c_{13} & s_{13}e^{i\delta} \\ -s_{12}c_{23} - c_{12}s_{23}s_{13}e^{i\delta} & c_{12}c_{23} - s_{12}s_{23}s_{13}e^{i\delta} & s_{23}c_{13} \\ s_{12}s_{23} - c_{12}c_{23}s_{13}e^{i\delta} & -c_{12}s_{23} - s_{12}c_{23}s_{13}e^{i\delta} & c_{23}c_{13} \end{pmatrix} \tag{2.39}$$

where the following shorthand notation is used

$$c_{ij} \equiv \cos\theta_{ij} \qquad s_{ij} \equiv \sin\theta_{ij} \tag{2.40}$$

and θ_{12},θ_{13}, θ_{23} and δ are four independent parameters of the CKM matrix. In particular, the values of the CKM matrix elements I'll be using in this thesis are ([16]):

$$V_{ud} = 0.2252 \tag{2.41}$$

$$V_{us} = 0.97425 \tag{2.42}$$

$$\tau \equiv -\frac{V_{ts}^* V_{td}}{V_{us}^* V_{ud}} = 0.0014148 - 0.0005558i. \tag{2.43}$$

2.3 Symmetries of QCD

Other than Lorentz and gauge invariance, the QCD Lagrangian exhibits a number of useful symmetries, which will be the topic of this section.

2.3.1 C,P and T

C and P are the charge conjugation and parity transformations respectively. C is defined as the transformation that changes the particle to a corresponding particle with opposite charge (i.e. its antiparticle), while leaving its four-momentum and spin unchanged. Therefore, if we write our single-particle states as $\mid \mathbf{p}, s_z, Q, n\rangle$ with quantum numbers corresponding to the momentum, component of the spin in z-direction, charge (which can refer to any conserved charge, not necessarily electromagnetic) and particle species (e.g. electron, positron etc.) respectively, the action of the operator C on this state will be:

$$C \mid \mathbf{p}, s_z, Q, n\rangle = e^{i\xi_C} \mid \mathbf{p}, s_z, -Q, \bar{n}\rangle. \tag{2.44}$$

The charge conjugation changes the particle n into its antiparticle $\bar{n}$. The phase ξ_C is the charge conjugation phase and, if the particle is not its own antiparticle, it can be absorbed by redefinition of the anti-particle state (states differing by an overall phase correspond to the same physics). The ξ_C phase has therefore no physical meaning in this case. On the other hand, if the particle is its own antiparticle, it is an eigenstate of C and such a redefinition can not take place. The charge conjugation phase then becomes a real physical quantity.

P is the parity symmetry which corresponds to the spatial reflection $\mathbf{x} \to -\mathbf{x}$. The effect of this symmetry on single-particle states is:

$$P \mid \mathbf{p}, s_z, Q, n\rangle = e^{i\xi_P} \mid -\mathbf{p}, s_z, Q, n\rangle \tag{2.45}$$

for massive particles. Unlike C, the phases of P operator are always physical (strictly speaking, the parity operator can always be modified by multiplying it by a global U(1) phase, which in QCD are the electric charge, baryon number or lepton number; choosing parities of proton, neutron and electron to be +1 fixes the parities of all the remaining

particles). This is because any state can be written as a Lorentz boost acing on a momentum 0 state, and it is clear from the above equation that momentum 0 states are eigenstates of P operator.

Combined C and P transformations gives a CP transformation:

$$CP \mid \mathbf{p}, s_z, Q, n\rangle = e^{i\xi} \mid -\mathbf{p}, s_z, -Q, n'\rangle. \tag{2.46}$$

For brevity, from now on I am going to use the notation where CP transformed states are denoted with a bar, e.g.:

$$CP \mid a\rangle = e^{i\xi_a} \mid \bar{a}\rangle. \tag{2.47}$$

If CP is the symmetry of the system, the S-matrix must satisfy:

$$(CP)S(CP)^{-1} = S, \tag{2.48}$$

which implies that

$$\langle f \mid S \mid i\rangle = e^{i(\xi_i - \xi_f)}\langle \bar{f} \mid S \mid \bar{i}\rangle. \tag{2.49}$$

It follows from there that decay rates for particles are the same as decay rates for antiparticles:

$$\Gamma(i \to f) = \int |\langle f \mid S \mid i\rangle|^2 \, dLIPS = \int \left|\langle \bar{f} \mid S \mid \bar{i}\rangle\right|^2 dLIPS = \Gamma(\bar{i} \to \bar{f}), \tag{2.50}$$

where $dLIPS$ denotes the Lorentz-invariant phase space volume element.

The third useful discrete symmetry is the time reversal symmetry, defined as the operator that switches the time direction $t \to -t$. What makes the time reversal operator unique is that, unlike other operators, it's antiunitary and antilinear, meaning that:

$$\langle f \mid i\rangle \xrightarrow{T} \langle i \mid f\rangle, \tag{2.51}$$

$$T\left(\alpha \mid \phi_1\rangle + \beta \mid \phi_2\rangle\right) = \alpha^* T \mid \phi_1\rangle + \beta^* T \mid \phi_2\rangle. \tag{2.52}$$

This is necessary to ensure that the energy spectrum of the theory is bounded from below. Time reversal has the following effect on massive particle states:

$$T \mid \mathbf{p}, s_z, Q, n\rangle = e^{i\xi_T}(-1)^{s-s_z} \mid \mathbf{p}, -s_z, Q, n\rangle, \tag{2.53}$$

where s is the total spin of the particle. Unlike C and P, the phase ξ_T is *never* physical. This is a direct consequence of antilinearity of T:

$$Te^{i\eta} \mid \mathbf{p}, s\rangle = e^{-i(2\eta - \xi_T)}(-1)^{j-s}e^{i\eta} \mid \mathbf{p}, -s\rangle. \tag{2.54}$$

This shows that simply rephasing the state (which has no effect on physics) changes the value of the T phase.

An important property of any field theory is that, if we assume Lorentz invariance, the combined CPT transformation is a symmetry of the theory. One of the consequences of CPT is that CP violation (as observed in weak decays) also implies T violation. This is one of the reasons why CP violation is necessary to generate matter-antimatter asymmetry in the Universe - without it by, time reversal symmetry, all processes would have the same rates as the reverse processes.

2.3.2 Chiral symmetry

Chiral symmetry is an approximate flavour symmetry. One can see that if we exclude the mass terms of up, down and strange quarks, the QCD Lagrangian 2.32 will not mix left and right-handed fields of these quarks with each other. This is because $\bar{\psi}\not{D}\psi = \bar{\psi}_L\not{D}\psi_L + \bar{\psi}_R\not{D}\psi_R$, while the inclusion of the mass term would spoil this relation because $\bar{\psi}\psi = \bar{\psi}_L\psi_R + \bar{\psi}_R\psi_L$. This approximation is reasonable, because by ignoring these three quark masses we're introducing an error of order $m_s/\Lambda_{QCD} < 1$. Furthermore, if we ignore electric charges of these three quarks (which is reasonable for low energies where the electromagnetic interactions are much weaker than the strong interactions), the covariant derivatives acting on all three light flavours will become equal and the Lagrangian will remain invariant under the following transformation:

$$\begin{pmatrix} u \\ d \\ s \end{pmatrix}_{L/R} \rightarrow U_{L/R} \begin{pmatrix} u \\ d \\ s \end{pmatrix}_{L/R} , \tag{2.55}$$

with $U_{L/R} \in U(3)$. Even though the Lagrangian is invariant under $U(3)_L \times U(3)_R$, the S-matrix is not. This is a consequence of the axial anomaly - the QCD action in the chiral limit is invariant under $\psi \rightarrow e^{i\gamma^5\theta}$ but the integration measure in the path integral is not. As a consequence, $U(1)_A$ does not satisfy Ward identities and is not a valid symmetry transformation. The full chiral symmetry group is $SU(3)_L \times SU(3)_R \times U(1)_B$.

2.3.3 Isospin

A very useful subgroup of the chiral symmetry group is $SU(2)_V$ relating up and down quarks to each other. This symmetry is valid in the limit where $m_u = m_d$ and electromagnetic effects can be neglected as before.

Isospin is a quantum number associated with up and down quarks and antiquarks which form isospin doublets ($I = 1/2$) with the value of the 3rd component of the isospin I_3 given by:

Quark	I_3
u and $\bar{d}$	+1/2
d and $\bar{u}$	-1/2

I will use the convention where both quark and antiquark fields transform under the fundamental representation of $SU(2)_V$:

$$q_\alpha = \begin{pmatrix} u \\ d \end{pmatrix} \tag{2.56}$$

$$\bar{q}_\alpha = \begin{pmatrix} -\bar{d} \\ \bar{u} \end{pmatrix}. \tag{2.57}$$

A light quark and antiquark can form a bound state which can be either an isospin singlet or a triplet. An example of mesons forming such an isospin triplet are the pions, which have the following flavour composition:

Pion	I_3	Flavour content
π^+	+1	$-\bar{d}u$
π^0	0	$\frac{1}{\sqrt{2}}\left(\bar{u}u - \bar{d}d\right)$
π^-	-1	$\bar{u}d$

Kaons consist of one strange quark/antiquark (with strangeness -1/+1 and isospin 0) and one light antiquark/quark, and therefore form isospin doublets

Kaon	S	I_3	Flavour content
K^+	+1	+1/2	$\bar{s}u$
K^0	+1	-1/2	$\bar{s}d$
$\bar{K}^0$	-1	+1/2	$\bar{d}s$
K^-	-1	-1/2	$\bar{u}s$

.

A pair of pions, which are isospin 1 particles, can form an I=2, I=1 or I=0 state, which are

$$
\begin{aligned}
|\, I=2, I_3=2\rangle &= |\, \pi^+\pi^+\rangle && (2.58)\\
|\, I=2, I_3=1\rangle &= \frac{1}{\sqrt{2}}\left(|\, \pi^+\pi^0\rangle + |\, \pi^0\pi^+\rangle\right) && (2.59)\\
|\, I=2, I_3=0\rangle &= \frac{1}{\sqrt{6}}\left(|\, \pi^+\pi^-\rangle + |\, \pi^-\pi^+\rangle + 2\,|\, \pi^0\pi^0\rangle\right) && (2.60)\\
|\, I=2, I_3=-1\rangle &= \frac{1}{\sqrt{2}}\left(|\, \pi^-\pi^0\rangle + |\, \pi^0\pi^-\rangle\right) && (2.61)\\
|\, I=2, I_3=-2\rangle &= |\, \pi^-\pi^-\rangle && (2.62)\\
|\, I=1, I_3=1\rangle &= \frac{1}{\sqrt{2}}\left(|\, \pi^+\pi^0\rangle - |\, \pi^0\pi^+\rangle\right) && (2.63)\\
|\, I=1, I_3=0\rangle &= \frac{1}{\sqrt{2}}\left(|\, \pi^+\pi^-\rangle - |\, \pi^-\pi^+\rangle\right) && (2.64)\\
|\, I=1, I_3=-1\rangle &= \frac{1}{\sqrt{2}}\left(|\, \pi^0\pi^-\rangle - |\, \pi^-\pi^0\rangle\right) && (2.65)\\
|\, I=0, I_3=0\rangle &= \frac{1}{\sqrt{3}}\left(|\, \pi^+\pi^-\rangle + |\, \pi^-\pi^+\rangle - |\, \pi^0\pi^0\rangle\right). && (2.66)
\end{aligned}
$$

All kaons are pions are spin 0 particles, which means that in $K \to \pi\pi$ decays, the resultant pions will have total angular momentum $l = 0$ (i.e. they form an s-wave). Such a state must be even under parity transformation. This means that $I = 1$ two pion states, which are odd under parity, can not contribute to the overall decay amplitude. Consequently, in the isospin limit, there are only two possible $K \to \pi\pi$ channels:

- $\Delta I = 3/2$ where the two-pion final state is in $I = 2$ state.
- $\Delta I = 1/2$ where the two-pion final state is in $I = 0$ state.

2.3.4 G-parity

G-parity is a combination of charge conjugation and isospin rotation by π:

$$G = e^{i\pi\sigma_2}C. \tag{2.67}$$

It has the following effect on the light quarks:

$$u \xrightarrow{G} -C\bar{d}^T, \tag{2.68}$$

$$d \xrightarrow{G} C\bar{u}^T. \tag{2.69}$$

where C is the charge conjugation matrix $\gamma^0\gamma^2$. Taking $m_u = m_d$, the QCD Lagrangian preserves both the isospin and charge conjugation symmetries, so G-parity must be the symmetry of QCD as well.

All pions are G-parity odd. This will be useful for two reasons. First, it forbids $2\pi \to 3\pi$ scattering, which means that a two-pion system at centre-of-mass energy given by the kaon mass will scatter elastically, which is a necessary condition for calculating the two-pion phase shift as will be discussed in section 4.12.1. Second, this property will be very useful for construction of boundary conditions that result in a moving pion in the ground state in $\Delta I = 1/2$ $K \to \pi\pi$ decay. For details see section 4.14.3.

2.4 Fermi effective theory

When studying kaon decays, we are working at energy scales which are much lower than the W boson mass. This means that the W boson will never appear on-shell, so Green functions with an external W boson can be ignored and any internal W lines can be replaced with effective operators. This replacement can be understood in two (equivalent) ways:

Operator product expansion Operator product expansion is a technique which allows us to separate long-distance and short distance contributions in a product of two operators. In the regime where the two operators come close together, they can be replaced with series of local operators with (Wilson) coefficients, which can be worked out from perturbation theory. In the case of W-boson, we have a product of two left-handed currents

$$\frac{\eta_{\mu\nu} - \frac{p_\mu p_\nu}{m_W^2}}{p^2 - m_W^2 + i\epsilon} \int d^4x e^{ipx} J_L^\mu(x) J_L^\nu(0) = \sum_i C_i(p) O_i \tag{2.70}$$

$$= C(p^2) + C_{\bar{q}q}(p^2) m\bar{q}q + \cdots$$
$$+ C_1(p^2)(\bar{s}_i d_j)_L (\bar{u}_j u_i)_L + \cdots \tag{2.71}$$

We have thus separated the long-distance contribution (O_i) from the short-distance contribution $C_i(p)$. Not all of these operators will be relevant for $K \to \pi\pi$ scattering and in the remainder of this thesis I will focus only on the relevant ones, such as the four-quark operator in the last line.

Effective field theory The second approach is more straightforward - write down the effective field theory Lagrangian for energies below the W mass, which will include higher-dimension operators, and choose the low energy coefficients by matching to the full theory at m_W scale. This approach is equivalent to the operator product expansion, in particular the momentum (scale) dependence of Wilson coefficients is recovered by renormalisation as shown in section 2.4.3.2.

Figure 2.1: Lowest order short distance contributions to current-current operators with and without colour mixing

An important restriction on the operators mediating the $K \to \pi\pi$ transition is that they must be parity *odd* $PO(x^\mu)P^{-1} = -O(x_\mu)$. To see this consider a matrix element $\langle \pi(\mathbf{p}_1)\pi(\mathbf{p}_2) \mid O(x^\mu) \mid K(\mathbf{p}_K)\rangle$. Under parity it transforms as

$$\langle \pi(\mathbf{p}_1)\pi(\mathbf{p}_2) \mid O(x^\mu) \mid K(\mathbf{p}_K)\rangle = \langle \pi(\mathbf{p}_1)\pi(\mathbf{p}_2) \mid P^{-1}PO(x^\mu)P^{-1}P \mid K(\mathbf{p}_K)\rangle \quad (2.72)$$

$$= \eta_\pi^2 \eta_K \eta_O \langle \pi(-\mathbf{p_1})\pi(-\mathbf{p_2}) \mid O(x_\mu) \mid K(-\mathbf{p_K})\rangle \quad (2.73)$$

where $\eta_\pi = \eta_K = -1$ are the intrinsic parities of pion and kaon respectively and η_O is to be determined. The matrix element $\langle \pi(\mathbf{p}_1)\pi(\mathbf{p}_2) \mid O(x^\mu) \mid K(\mathbf{p}_K)\rangle$ is a Lorentz scalar and the above equation says that under simultaneous exchange of all upper and lower Lorentz indices ($p_i^\mu \leftrightarrow p_{i\mu}$) it picks up a phase ($-\eta_O$). However, there is no way of constructing a Lorentz scalar with a phase -1 using only p_1^μ, p_2^μ and p_K^μ (the simplest object with this property is $\epsilon_{\mu\nu\rho\sigma}p_1^\mu p_2^\nu p_3^\rho p_4^\sigma$, which requires four independent four-momenta). The conclusion is that $\eta_O = -1$ and only parity-odd operators contribute to $K \to \pi\pi$ decays.

2.4.1 Dimension-6 operators

Consider a four quark Green function:

$$\langle \bar{s}(p_1)u(p_2)\bar{u}(p_3)d(p_4)\rangle. \quad (2.74)$$

Various contributions to this diagram are shown in Figs. 2.1, 2.2 and 2.3. The contributions from various diagrams can be replaced in an effective field theory by a four-quark operators explicitly given by:

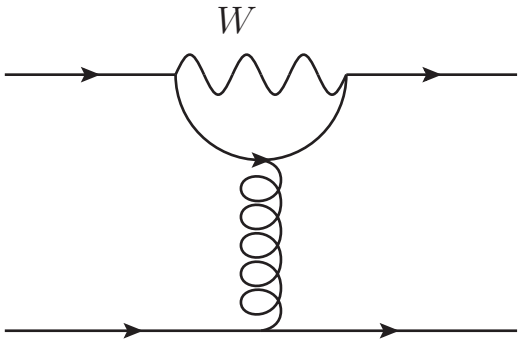

Figure 2.2: Lowest order short distance contributions to QCD penguin operators

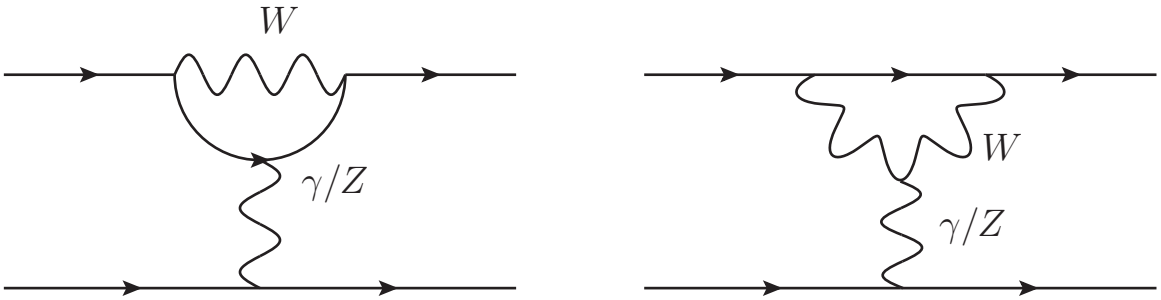

Figure 2.3: Lowest order short distance contributions to electroweak penguin operators

$$Q_1 = (\bar{s}_i d_i)_L (\bar{u}_j u_j)_L \tag{2.75}$$

$$Q_2 = (\bar{s}_i d_j)_L (\bar{u}_j u_i)_L \tag{2.76}$$

$$Q_3 = (\bar{s}_i d_i)_L \sum_{q\in\{u,d,s\}} (\bar{q}_j q_j)_L \tag{2.77}$$

$$Q_4 = (\bar{s}_i d_j)_L \sum_{q\in\{u,d,s\}} (\bar{q}_j q_i)_L \tag{2.78}$$

$$Q_5 = (\bar{s}_i d_i)_L \sum_{q\in\{u,d,s\}} (\bar{q}_j q_j)_R \tag{2.79}$$

$$Q_6 = (\bar{s}_i d_j)_L \sum_{q\in\{u,d,s\}} (\bar{q}_j q_i)_R \tag{2.80}$$

$$Q_7 = \frac{3}{2} (\bar{s}_i d_i)_L \sum_{q\in\{u,d,s\}} e_q (\bar{q}_j q_j)_R \tag{2.81}$$

$$Q_8 = \frac{3}{2} (\bar{s}_i d_j)_L \sum_{q\in\{u,d,s\}} e_q (\bar{q}_j q_i)_R \tag{2.82}$$

$$Q_9 = \frac{3}{2} (\bar{s}_i d_i)_L \sum_{q\in\{u,d,s\}} e_q (\bar{q}_j q_j)_L \tag{2.83}$$

$$Q_{10} = \frac{3}{2} (\bar{s}_i d_j)_L \sum_{q\in\{u,d,s\}} e_q (\bar{q}_j q_i)_L \tag{2.84}$$

In these expressions, lower case Roman letters denote colours, while the spins are contracted within each pair of brackets, which either have the left-chiral structure $(\bar{q}q)_L = \bar{q}\gamma^\mu(1-\gamma^5)q$ or right-chiral structure $(\bar{q}q)_R = \bar{q}\gamma^\mu(1+\gamma^5)q$ and the Lorentz indices μ are contracted between the brackets. For example, the explicit expression for Q_1 is $\left(\bar{s}_i\gamma^\mu(1-\gamma^5)d_i\right)\left(\bar{u}_j\gamma_\mu(1-\gamma^5)u_j\right)$. In this basis, operators Q_1 and Q_2 correspond to the current-current diagrams in Fig. 2.1, operators Q_3 to Q_6 correspond to the QCD penguin operators in Fig. 2.2 (the structure $\sum_q(\bar{q}q)_V$ with V=L+R mimics the coupling of a gluon to fermions) and operators Q_7 to Q_{10} correspond to electroweak penguin operators in Fig. 2.3 ($\sum_q e_q\bar{q}q$ comes from coupling of the photon to external quarks).

Because of the left-left Fierz identity

$$\left[\bar{q}_{1i}\gamma^\mu(1-\gamma^5)q_{2j}\right]\left[\bar{q}_{3k}\gamma^\mu(1-\gamma^5)q_{4l}\right] = \left[\bar{q}_{1i}\gamma^\mu(1-\gamma^5)q_{4l}\right]\left[\bar{q}_{3k}\gamma^\mu(1-\gamma^5)q_{2j}\right] \tag{2.85}$$

only 7 of these operators will be linearly independent. Indeed, we have:

$$Q_4 = -Q_1 + Q_2 + Q_3, \tag{2.86}$$

$$Q_9 = \frac{3}{2}Q_1 - \frac{1}{2}Q_3, \tag{2.87}$$

$$Q_{10} = \frac{1}{2}Q_1 + Q_2 - \frac{1}{2}Q_3. \tag{2.88}$$

2.4.2 Dimension 6 operators in chiral basis

It is convenient to express the remaining seven dimension-six operators in a basis that transform as irreducible representations of $SU(3)_L \times SU(3)_R$ chiral symmetry group. A generic four quark operator has the form:

$$O_{AB} = T^{\alpha\beta}_{\gamma\delta}(\bar{q}^\alpha q_\gamma)_A(\bar{q}^\beta q_\delta)_B \tag{2.89}$$

where Greek indices label flavours, A and B label spin structure (either left or right handed current). The colour structure of the operator is irrelevant for the following argument and so the colour indices will be suppressed. The lower indices transform according to 3 (i.e. fundamental) representation of SU(3) while upper indices transform according to $\bar{3}$ (antifundamental) representation.

We need to consider two cases here: LL and LR spin structures (RR is forbidden, since flavour changing is mediated by the W-boson which only couples to left-handed fields; on the other hand LR operators are allowed because of penguin diagrams in Figs. 2.2 and 2.3).

Recall that for SU(N) groups, one can construct a general irreducible representation from the fundamental representation by either symmetrising or antisymmetrising the group indices. For example, if ϕ_α and χ_α both transform under the fundamental representation

of SU(N), then $\phi_\alpha\chi_\beta + \phi_\beta\chi_\alpha$ and $\phi_\alpha\chi_\beta - \phi_\beta\chi_\alpha$ are the irreducible representations of SU(N) with dimensions N(N+1)/2 and N(N-1)/2 respectively. Similarly, one can create the irreducible representations from fundamental and antifundamental representations by taking either a trace or a traceless combination. For example if ϕ_i transforms under the fundamental representation and χ^j transforms under antifundamental representation, we can have a singlet representation $\chi^i\phi_i$ and an N^2-1 dimensional representation $\chi^\alpha\phi_\beta - \frac{1}{N}\chi^\gamma\phi_\gamma\delta^\alpha_\beta$.

- Case 1: LR operator
  By using
  $$3 \otimes \bar{3} = 8 \oplus 1 \tag{2.90}$$
  This means that the two possibilities for $\Delta S = 1$ LR operators are (8,1) and (8,8). Again, left handed singlets are forbidden, since they cannot contribute to flavour changing processes. We can write them explicitly by taking a trace and traceless component of the right handed current:
  $$Q^{(8,1)}_{LR\alpha} = (\bar{s}q_\alpha)_L \sum_\delta (\bar{q}^\delta q_\delta)_R \tag{2.91}$$
  $$Q^{(8,8)\,\beta}_{LR\ \ \alpha\gamma} = (\bar{s}q_\alpha)_L \left((\bar{q}^\beta q_\gamma)_R - \frac{1}{3}\delta^\beta_\gamma \sum_\delta (\bar{q}^\delta q_\delta)_R \right) \tag{2.92}$$
  From here one can immediately identify that Q_5 and Q_6 operators are in the (8,1) representation while Q_7 and Q_8 operators are in the (8,8) representation. It should be noted that the (8,1) operators can only contribute to $\Delta I = 1/2$ channel (since the only non-singlet contribution to the isospin comes from a single light quark, meaning these operators transform as isospin doublets). (8,8) operators contribute to both kaon decay channels.

- Case 2: LL operator
  The LL case is significantly more complicated. The irreducible representations can be obtained by (anti)symmetrising the upper/lower indices and taking traces/-traceless components between upper and lower indices of tensor T in equation 2.89. Noting that T is symmetric under simultaneous exchange of $\alpha \leftrightarrow \beta$ and $\gamma \leftrightarrow \delta$ it is clear that we either need to simultaneously symmetrise or antisymmetrise upper and lower indices. Furthermore, the singlet representations can again be ignored by flavour changing argument. Note that completely antisymmetric representation can be rewritten in terms of a two-index tensor using:
  $$T^{[\alpha\beta]}_{[\gamma\delta]} = \epsilon_{\gamma\delta\zeta}\epsilon^{\alpha\beta\eta}T'^{\zeta}_{\eta} \tag{2.93}$$
  and, as argued above, a tensor with one lower and one upper index can be in either a singlet or an octet representation. This leaves the following representations:

– Symmetric traceless - (27,1)

$$O^{(27,1)\,(\alpha\beta)}_{\quad\ (\gamma\delta)} = O^{(\alpha\beta)}_{(\gamma\delta)} - \frac{1}{5}\left(\delta^{\alpha}_{\gamma}O^{(\beta\eta)}_{(\delta\eta)} + 3\text{perm}\right) + \frac{1}{20}\left(\delta^{\alpha}_{\gamma}\delta^{\beta}_{\delta}O^{\eta\zeta}_{\eta\zeta} + 1\text{perm}\right) \quad (2.94)$$

In this equation ' perm' refers to other permutations of indices $\alpha \leftrightarrow \beta$ and $\gamma \leftrightarrow \delta$. The factors of 1/5 and 1/20 are chosen so that traces over all pairs of upper and lower indices vanish (in 3 flavour theory).

The operator we are interested in contains $(\bar{s}d)_L(\bar{u}u)_L$ and thus the above expression simplifies to:

$$O^{(27,1)} = 2(\bar{s}d)_L(\bar{u}u)_L + 2(\bar{s}u)_L(\bar{u}d)_L - (\bar{s}d)_L(\bar{d}d)_L - (\bar{s}d)_L(\bar{s}s)_L \quad (2.95)$$

– Symmetric one trace - $(8,1)_S$
The only operator of this form containing $\bar{s}d$ is:

$$O^{(8,1)}_S = (\bar{s}d)(\bar{u}u) + (\bar{s}u)(\bar{u}d) + 2(\bar{s}d)(\bar{d}d) + 2(\bar{s}d)(\bar{s}s) \quad (2.96)$$

– Antisymmetric one trace $(8,1)_A$ This operator takes the form:

$$O^{(8,1)}_A = (\bar{s}d)(\bar{u}u) - (\bar{s}u)(\bar{u}d) \quad (2.97)$$

A generic left-left (8,1) operator can be any linear combination of $Q^{(8,1)}_S$ and $Q^{(8,1)}_A$.

The complete set of seven linearly-independent operators in the chiral basis is then:

$$Q'_1 = 3Q_1 + 2Q_2 - Q_3 \quad (2.98)$$

$$Q'_2 = \frac{1}{5}(2Q_1 - 2Q_2 + Q_3) \quad (2.99)$$

$$Q'_3 = \frac{1}{5}(-3Q_1 + 3Q_2 + Q_3) \quad (2.100)$$

$$Q'_{5/6/7/8} = Q_{5/6/7/8} \quad (2.101)$$

It is worth noting that all (8,1) operators are isospin doublets. This can be seen easily by noting that $\bar{s}d$ is an isospin doublet and the remaining part of each (8,1) operator is an isospin singlet (which should be obvious given that it is a singlet of chiral symmetry group of which isospin is a subgroup). This means that (8,1) operators can only change the isospin by 1/2.

In the $\Delta I = 3/2$ decay only (27,1) and two (8,8) operators contribute and because (27,1) is left-left and (8,8) are left-right operators, they will be automatically in the chiral basis,

without the need to invoke Eqs. (2.99)-(2.101). Explicitly, the operators are given by:

$$Q^{\Delta I=3/2}_{(27,1)} = (\bar{s}_i d_i)_L \left(\bar{u}_j u_j - \bar{d}_j d_j\right)_L + (\bar{s}_i u_i)_L (\bar{u}_j d_j)_L, \tag{2.102}$$

$$Q^{\Delta I=3/2}_{(8,8)} = (\bar{s}_i d_i)_L \left(\bar{u}_j u_j - \bar{d}_j d_j\right)_R + (\bar{s}_i u_i)_L (\bar{u}_j d_j)_R, \tag{2.103}$$

$$Q^{\Delta I=3/2}_{(8,8)\mathrm{mx}} = (\bar{s}_i d_j)_L \left(\bar{u}_j u_i - \bar{d}_j d_i\right)_R + (\bar{s}_i u_j)_L (\bar{u}_j d_i)_R.. \tag{2.104}$$

This is the operator basis which we used for $\Delta I = 3/2$ operators. It is related to the chiral basis (which was used for all $\Delta I = 1/2$ calculations) by the relations

$$Q^{\Delta I=3/2}_{(27,1)} = \frac{3}{5} Q'_1 \tag{2.105}$$

$$Q^{\Delta I=3/2}_{(8,8)} = 2Q'_7 \tag{2.106}$$

$$Q^{\Delta I=3/2}_{(8,8)\mathrm{mx}} = 2Q'_8. \tag{2.107}$$

2.4.3 Renormalisation

Loop integrals that arise in quantum field theory are often divergent. On the other hand, Green functions (which are related to scattering matrix elements) must be finite. This can be achieved by choosing parameters in the Lagrangian to be infinite in such a way that the divergences cancel with the divergences coming from loop diagrams. The procedure that achieves this is renormalisation. It consists of two steps:

- Regularisation - a procedure which introduces a regulator, which makes the loop integrals convergent. Examples of regulators which are used here are the lattice spacing and ϵ in dimensional regularisation.
- Subtraction - regulated Green functions will contain a piece which depends on the cutoff (and is divergent as the cutoff is removed) and a finite piece. It is clear that the divergent piece must be removed, but this procedure is not unique - any part of finite piece can be removed as well. Two common subtraction prescriptions are the minimal subtraction scheme which just removes the divergent piece, and the on-shell subtraction scheme, where the subtraction is defined by demanding that the Green function satisfies a given condition.

2.4.3.1 Renormalisation of QCD

As an example of the above procedure, consider the QCD Lagrangian, Eq. 2.32. We can rewrite it in terms or renormalised quantities:

$$m_0 = Z_m m_R \tag{2.108}$$
$$\psi_0 = \sqrt{Z_q}\psi_R \tag{2.109}$$
$$A_0^{\mu a} = \sqrt{Z_A} A_R^{\mu a} \tag{2.110}$$
$$g_0 = Z_g g_R \mu^{\epsilon} \tag{2.111}$$

where the factor μ^{ϵ} arises in dimensional regularisation and is needed to correct the mass dimension of the interaction term.

Then the QCD Lagrangian can be written as:

$$\mathcal{L} = \mathcal{L}_R + \mathcal{L}_{ct} \tag{2.112}$$

The counterterm Lagrangian, $\mathcal{L}_{ct}$, contains additional interactions, which depend on renormalisation constants Z.

I will now illustrate this approach by considering the renormalisation of the strong coupling constant g. Consider the three-point amputated Green's function

$$\langle \bar{\psi}_R \psi_R A_R^{\mu a} \rangle_{amp} = \int \mathcal{D}\phi_i \bar{\psi}_R \psi_R A_R^{\mu a} e^{i\int d^4x \mathcal{L}_R + \mathcal{L}_{ct}} \Big|_{amp} \tag{2.113}$$

where 'amp' denotes removing the external propagators. For example, the tree-level formula for this Green function, which arises from $\bar{\psi}_R \gamma_\mu A_R^{\mu a} \frac{\lambda^a}{2} \psi$ in the renormalised Lagrangian would be

$$\langle \bar{\psi}_R \psi_R A_R^{\mu a} \rangle_{amp}^{tree} = \gamma^\mu \frac{\lambda^a}{2}. \tag{2.114}$$

The counterterm depends on the renormalisation constants, which are chosen such that the counterterm cancels the divergence arising from loops in the renormalised Lagrangian. This fixes the value of the product $Z_q Z_g \sqrt{Z_A}$. To extract Z_g, we can calculate Z_q and Z_A from quark and gluon two-point functions respectively.

Taking the derivative of Eq. (2.111) with respect to $\ln \mu$ gives

$$\beta(\mu) = -\frac{1}{Z_g} \frac{\partial Z_g}{\partial \ln \mu} g_R - \epsilon g_R \tag{2.115}$$

where the $\beta(\mu)$ function is defined by

$$\beta(\mu) \equiv \frac{\partial g_R}{\partial \ln \mu}. \tag{2.116}$$

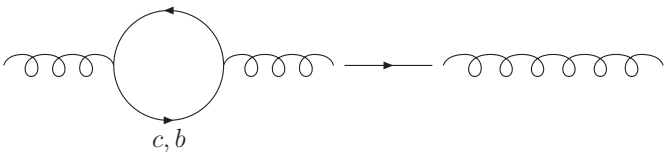

Figure 2.4: Example of processes corresponding to the threshold corrections at b/c scale.

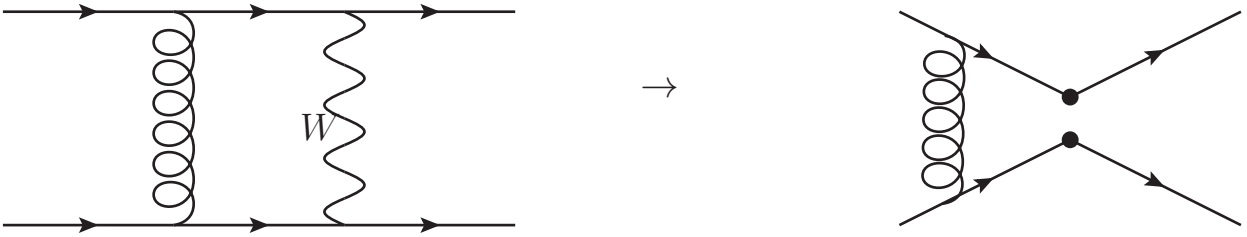

Figure 2.5: Comparison of a current-current operator with the corresponding effective four fermion operator

The β function can be calculated in perturbation theory and the renormalised coupling can be obtained by integrating the above equation. The advantage of this approach is that it results in summation of logarithmic contributions to the coupling constant.

I will now describe the procedure of obtaining the renormalised coupling at a given scale μ. The value of the coupling constant at the scale of the Z-boson mass in the $\overline{MS}$ scheme has been determined using experimental and lattice input to be $\alpha(m_Z) = 0.1185(6)$ [16]. We then use the 5-flavour running to go down to the b-quark scale, then c-quark scale and finally to the desired scale μ applying threshold corrections at each quark mass scale. The threshold corrections are calculated by comparing $Z_g(\mu)$ in (n+1)-flavour theory with $Z_g(\mu)$ in n-flavour theory. These will differ, as the former will contain more quark loops, the divergent parts of which will have to be absorbed by Z_g. An example of such a loop is shown in Fig. 2.4.

Following this procedure we find the value of α_s at 3 GeV in a three-flavour theory to be

$$\alpha_s(3\,\text{GeV}) = 0.24544. \tag{2.117}$$

2.4.3.2 Renormalisation of four-fermion operators

If we add the electroweak sector to the above considerations in the form of Fermi effective theory, we will find that the conditions (2.108)-(2.111) are no longer sufficient to renormalise the theory. To see this, consider the contribution to the four-point Green function shown in figure 2.5. Explicitly, they can be written as

$$\langle\bar{\psi}(x_1)\psi(x_2)\bar{\psi}(x_3)\psi(x_4)\rangle_{amp} = \int \mathcal{D}\phi_i \bar{\psi}(x_1)\psi(x_2)\bar{\psi}(x_3)\psi(x_4) e^{i(S_{QCD}+S_W)}\Big|_{amp} \tag{2.118}$$

$$= \int \mathcal{D}\phi_i \bar{\psi}(x_1)\psi(x_2)\bar{\psi}(x_3)\psi(x_4)\left(1 + i\int d^4x H_W(x)\right) e^{iS_{QCD}}\Big|_{amp} \tag{2.119}$$

$$= i\int d^4x \langle\bar{\psi}(x_1)\psi(x_2)\bar{\psi}(x_3)\psi(x_4)H_W(x)\rangle_{amp}^{QCD} \tag{2.120}$$

$$\equiv G_4[H_W]. \tag{2.121}$$

where $\bar{\psi}\psi\bar{\psi}\psi$ are four fields corresponding to external legs of an unamputated Green's function, which in our case will consist of one strange antiquark field and three light (up or down) quark fields. I introduced a shorthand notation $G_4[H_W]$ for future convenience. The diagram in the full theory (left) is convergent (counting powers of loop momentum gives d^4p from the loop itself,$1/p$ for each internal fermion line and $1/p^2$ for each internal boson line so it behaves like $\int \frac{d^4p}{p^6}$), while the corresponding diagram in the effective theory is logarithmically divergent (goes like $\int \frac{d^4p}{p^4}$). The additional divergence can only be absorbed by the coefficients in multiplying the operators, so we have:

$$G_4[H_W] = \sum_i C_i(\mu) G_4[O_i(\mu)]. \tag{2.122}$$

The coefficients C_i are called Wilson coefficients and depend on both the renormalisation scheme and scale. The index i runs over all relevant operators in the theory. If we are considering transitions that change isospin by 3/2 there are 3 such operators: one (27,1) and two (8,8). Transitions that change the isospin by 1/2 have the index i running over 7 operators: one (27,1), four (8,1) and two (8,8).

The operator (or equivalently Wilson coefficient) renormalisation works just like renormalisation in full theory, i.e. define the renormalised Wilson coefficient in terms of the bare one in the effective Hamiltonian as

$$C_i^0 = C_j(\mu) Z_{ji}(\mu), \tag{2.123}$$

so the effective Hamiltonian can be written as

$$H_{eff} = C_i^0 O_i^0 = C_i(\mu) O_i + (Z_{ji}(\mu) Z_q^2 - \delta_{ij}) O_j, \tag{2.124}$$

where Z_q factors come from renormalisation of quark fields in the four-quark operator. The second term is the counterterm, which is later tuned to remove the divergences from Green functions. Then the renormalisation matrix can be absorbed into the amputated Green function

$$G_4[H_W] = \sum_i C_i^0 G_4[O_i^0] = \sum_{i,j} C_j(\mu) \underbrace{Z_{ji}(\mu) Z_q^2 G_4[O_i^0]}_{G_4[O_j(\mu)]}. \tag{2.125}$$

This is equivalent to the operator renormalisation

$$O_i = Z_{ij}(\mu) O_j^0. \tag{2.126}$$

The additional factor of Z_q^2 comes from the fact that we're considering the amputated Green functions.

Note that in general operators will mix under renormalisation. This can be seen most easily by considering the diagrams in Figs. 2.7, 2.8. The gluon exchange diagram in Fig. 2.7 will mix colour unmixed and colour mixed operators $\bar{q}_i \Gamma q_i \bar{q}_j \Gamma q_j \leftrightarrow \bar{q}_i \Gamma q_j \bar{q}_i \Gamma q_j$. This is because the additional gluon line will introduce a factor $T^a_{ij} T^a_{kl} = -\frac{1}{2N}\delta_{ij}\delta_{kl} + \frac{1}{2}\delta_{ik}\delta_{jl}$. The first term of this expression preserves the colour structure, but the second one does not. This introduces mixings between operators Q_{2n-1} and O_{2n} in the original ten operator basis (2.75-2.84).

A different mixing is introduced by QCD penguin diagrams (also called 'eye' diagrams in the literature) as shown in Fig. 2.8. These diagrams will have the flavour structure $\bar{s}\gamma^\mu(1-\gamma^5)d \sum_{q\in u,d,s} \bar{q}\gamma_\mu q$, which will mix any operator with Q_3 to Q_6 in the ten-operator basis (or equivalently with (8,8) operators in the chiral basis).

If we assume chiral symmetry then the basis of seven linearly independent dimension-six operators in Eq. (2.99)-(2.101) is complete - no new operators will arise as a result of renormalisation procedure. To see this, first consider the symmetry which combines CP with simultaneous exchange of d and s flavours (CPS symmetry). This is a symmetry of the QCD Lagrangian and hence it will forbid mixings between operators with different CPS parity. All six-fermion operators considered so far have CPS= +1. This puts a strong constraint on the operator mixing. Other operators that we may have to consider are:

1. dim-6 pseudoscalar-scalar operators of the form

$$(\bar{s}d)(\bar{d}d - \bar{s}s)_{PS\pm SP} = (\bar{s}d)_P(\bar{d}d - \bar{s}s)_S \pm (\bar{s}d)_S(\bar{d}d - \bar{s}s)_P \tag{2.127}$$

   where

$$(\bar{q}_1 q_2)_S = \bar{q}_1 q_2, \tag{2.128}$$
$$(\bar{q}_1 q_2)_P = \bar{q}_1 \gamma^5 q_2. \tag{2.129}$$

2. dim-5 operators (dim-6 including the mass factor) of the form

$$O_\gamma \equiv (m_s - m_d)\bar{s}\sigma^{\mu\nu} F_{\mu\nu}(1-\gamma^5)d \tag{2.130}$$
$$O_g \equiv (m_s - m_d)\bar{s}\sigma^{\mu\nu} G^a_{\mu\nu} T^a (1-\gamma^5)d \tag{2.131}$$

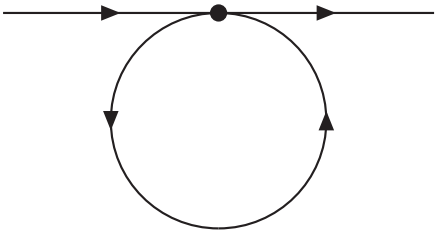

Figure 2.6: Loop diagrams which give rise to the $\bar{s}\gamma^5 d$ counterterm.

3. dim-3 (dim-4 including mass factor) operator

$$O_P \equiv (m_s - m_d)\bar{s}\gamma^5 d \tag{2.132}$$

I will now argue that given chiral symmetry none of these operators can contribute to the weak Hamiltonian.

1. (a) PS+SP These operators arise as a parity odd component of $(\bar{s}_L d_R)(\bar{s}_L s_R - \bar{d}_L d_R)$ (or a similar operator with $L \leftrightarrow R$). In the chiral limit, such an operator can not be constructed in the Standard Model and therefore will not contribute to the operator product expansion. In practice we do not have an exact chiral symmetry, but chiral symmetry breaking effects will have an additional mass dependence. Because construction of these operators requires two mass insertions, the chiral symmetry breaking term will appear as a dimension-8 operator and can be neglected for our purposes.

   (b) PS-SP These operators can be related to VA-AV operators by Fierz identity [17].

   $$(\bar{q}_{1i}q_{2i})(\bar{q}_{3j}q_{4j})_{PS-SP} = \frac{1}{2}(\bar{q}_{1i}q_{2j})(\bar{q}_{3j}q_{4i})_{AV-VA}. \tag{2.133}$$

   Because VA-AV operators are already included in the analysis, adding PS-SP operators will not add any new information to the theory.

2. In principle the dim-5 electromagnetic and chromomagnetic penguin operators should be included, however their Wilson coefficients are known to be small (proportional to m_π^2/m_K^2 in chiral perturbation theory) [18] and as a first approximation can be neglected.

3. The dim-3 operator can arise from the diagram shown in figure 2.6. The function of the additional $\bar{s}\gamma^5 d$ operator is to act as a counterterm for the quadratic divergence in these diagrams. It is useful to notice that the operator $\bar{s}\gamma^5 d$ satisfies the partially-conserved axial current (PCAC) relation

   $$\partial_\mu \left(\bar{s}\gamma_\mu\gamma^5 d\right) = (m_s + m_d)\bar{s}\gamma^5 d \tag{2.134}$$

   and is therefore proportional to a total derivative.

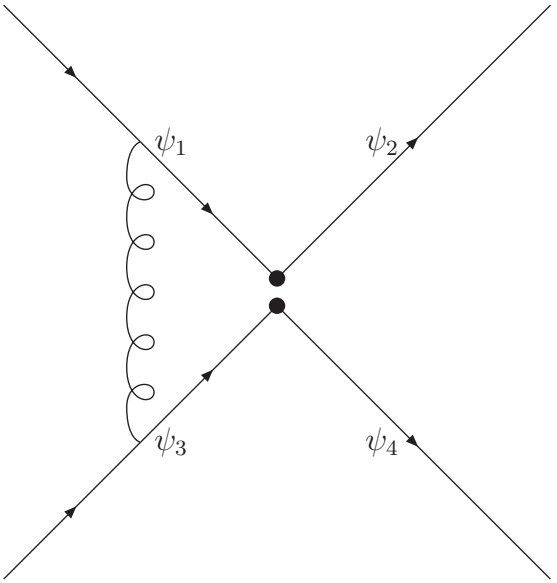

Figure 2.7: An example of a gluon exchange diagram

As a consequence, any on-shell matrix element of this operator must vanish because

$$\langle f \mid \partial_\mu O^\mu(x) \mid i\rangle = \partial_\mu \langle f \mid e^{iP^\nu x_\nu} O e^{-iP^\nu x_\nu} \mid i\rangle \tag{2.135}$$

$$= i(p_f - p_i)_\mu \langle f \mid O \mid i\rangle e^{i(p_f - p_i)^\nu x_\nu} \tag{2.136}$$

where P^μ is the four-momentum operator. Because on-shell matrix elements conserve energy and momentum, this additional contribution will vanish identically. This statement does not hold on the lattice, as will be discussed in section 4.14.2.

2.4.3.3 Dimension-6 operators without chiral symmetry

It is interesting to note that even without full chiral symmetry, if the flavour $SU(3)_V$ symmetry is present the parity-odd four-fermion operators exhibit the same mixing pattern as in the case where the chiral symmetry is present. This was pointed out in [19] and their discussion is summarised in the remainder of this section.

The proof is split in two parts corresponding to two types of diagrams that enter the renormalisation procedure: gluon exchange diagrams (see Fig. 2.7) and penguin diagrams (Fig. 2.8).

For the choice of operators, most of the discussion from the previous section applies, however without chiral symmetry we need to include the PS+SP operators:

$$O_X = (\bar{s}_i d_i)(\bar{d}_j d_j - \bar{s}_j s_j)_{PS+SP} \tag{2.137}$$

$$O_Y = (\bar{s}_i d_j)(\bar{d}_j d_i - \bar{s}_j s_i)_{PS+SP}. \tag{2.138}$$

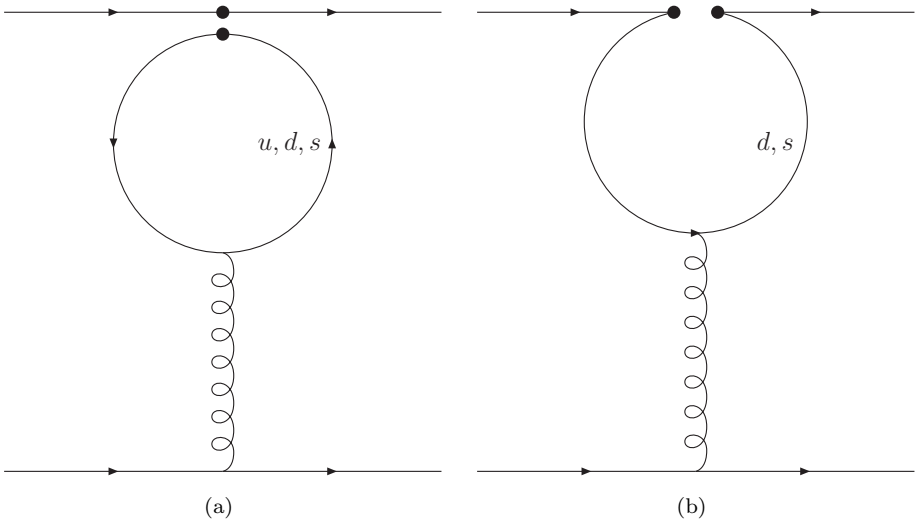

Figure 2.8: Penguin diagrams

Gluon-exchange diagrams In $SU(3)_V$ limit, the u, d and s quarks all have the same masses, which means that the gluon exchange diagrams will all contribute the same way regardless of the flavours of the external quark lines. This allows us to use a clever trick by [20], which is to work in a four-flavour theory with flavours labelled $\psi_1, \psi_2, \psi_3, \psi_4$, which has the following symmetries:

S'	$\psi_1 \leftrightarrow \psi_2,\ \psi_3 \leftrightarrow \psi_4$
S"	$\psi_1 \leftrightarrow \psi_4,\ \psi_2 \leftrightarrow \psi_3$

The four-fermion operators of the form $(\bar{\psi}_1\psi_2)(\bar{\psi}_3\psi_4)$ have the following transformation properties under CPS' and CPS":

	CPS'	CPS"
VA+AV	+1	+1
VA-AV	+1	-1
PS+SP	-1	-1

This means that these 3 types of operators cannot mix under renormalisation. Because gluon exchange diagrams are flavour-blind, the same conclusion will hold for any choice of flavours.

Consider an (8,8) operator, which is a LR operator, with parity-odd component VA-AV. The above considerations forbid mixings to LL (parity-odd component VA+AV) operators (27,1) and $(8,1)_{LL}$, but leave the possibility of mixing with $(8,1)_{LR}$. However, these two types of operators have different flavour structure - see Eq. (2.101) and (2.75-2.84).

Because gluon exchange diagrams preserve flavours, they won't mix the above two operators. As a consequence, there is no mixing between (8,8) operators and any other operators.

This leaves the mixing (27,1) and (8,1) operators. These operators transform as 27 and 8 representations of $SU(3)_V$ respectively, and since $SU(3)_V$ is an approximate symmetry broken by terms of order $m_s - m_d$, we conclude that there is no mixing between these operators at dimension 6.

To conclude, gluon exchange diagrams won't induce mixings between any of the four types of operators: (27,1), $(8,1)_{LL}$, $(8,1)_{LR}$, (8,8).

Penguin diagrams We can't use the CPS' and CPS" trick here, because we need to work in a 3-flavour theory (u,d and s quarks going in a loop). Penguin operators can, in principle, mix any operator with an (8,1) operator. There are two types of penguin diagrams shown in figure 2.8.

- Fig. 2.8 (left) diagram In the (8,8) operator case, the self contraction gives (in terms of propagators) 2U-D-S, which in the isospin limit reduces to D-S. Similarly, the $Q_{X,Y}$ operators are proportional to D-S.
- Fig. 2.8 (right) diagram Here we use the fact that the (8,8) operator has a LR structure, so its parity-odd component has the VA-AV chiral structure. In the following I will label the penguin contractions $P^{d/s}_{VA/AV}$, where the superscript denotes the quark going inside the loop and the chiral structure is defined such that the first label is the coupling to the external strange quark and the second is to the external down quark.

  For example the contribution from $(\bar{s}d)_V(\bar{d}d)_A$ is P^d_{VA} and the contribution from $(\bar{s}d)_V(\bar{s}s)_A$ is P^s_{AV}. The contractions to the VA operator give $P^d_{VA} + P^s_{AV}$, while the contractions to the AV operator give $P^d_{AV} + P^s_{VA}$. The contribution to the full operator is then $P^d_{VA} - P^s_{VA} + P^s_{AV} - P^d_{AV}$. Similarly, the PS+SP operator is proportional to $P^d_{SP} - P^s_{SP} - P^s_{PS} + P^d_{PS}$.

In both cases the penguin contractions are proportional to the difference between s and d penguins, which means that the mixing with (8,1) operators must be proportional to $m_s - m_d$, resulting in a scale suppression. The above argument forbids mixing between (8,1) and (8,8) and $Q_{X/Y}$ operators. The mixing of (27,1) and (8,8) operators is again suppressed by $SU(3)_V$ symmetry, just like in the case of gluon exchange diagrams.

The above arguments show that the mixing pattern of dimension-6 operators is the same with $SU(3)_V$ symmetry as with the full chiral symmetry. Before we mark chiral symmetry as redundant, it is worth noting that it prevents mixings at dimension 7, arising

both from $(m_s - m_d)$ times the dimension-6 operator terms mentioned above as well as additional dimension-7 operators such as $(\bar{s}(1-\gamma^5)d)(\bar{q}\not{D}(1-\gamma^5)q)$ (these operators can have $(15,\bar{3})$, $(\bar{6},\bar{3})$ or $(3,\bar{3})$ chiral structure). The magnitude of these higher-order effects (and in lattice calculations their effect on scaling) is currently unknown.

2.4.3.4 Calculation of Wilson coefficients

All the discussion so far has been valid for three-flavour theory. The calculation of Wilson coefficient will depend on running from m_W scale down to the charm quark scale, which will depend on 5- and 4-flavour theories as well. There are three main differences with respect to three-flavour theory:

- All the flavour sums in Eq. (2.75)-(2.84) run over all available flavours: u,d,s,c,b in 5-flavour and u,d,s,c in 4-flavour theory.
- There are two additional operators:

$$Q_1^c = (\bar{s}_i d_i)_L (\bar{c}_j c_j)_L, \tag{2.139}$$

$$Q_2^c = (\bar{s}_i d_j)_L (\bar{c}_j c_i)_L. \tag{2.140}$$

- There are no penguin contributions proportional to $V_{us}^* V_{ud}$ due to GIM mechanism.

GIM cancellation in this case works as follows. From the unitarity of CKM-matrix we have $V_{is}^* V_{id} = \delta_{sd} = 0$. Then, labelling the penguin diagrams with quark q inside the loop by P_q we can conclude that the penguin diagram contribution to any Green's function will be proportional to

$$\sum_i V_{is}^* V_{id} P_i = V_{us}^* V_{ud}(P_u - P_c) + V_{ts}^* V_{td}(P_t - P_c). \tag{2.141}$$

The $V_{us}^* V_{ud}$ coefficient is proportional to the difference of charm and up penguin diagrams. If up and charm quarks were both massless, the difference would be zero. At the scale $\mu = m_W$ the up and charm quark masses are small and we can think of up and charm penguins as a massless quark penguins with two mass term insertions (we require two insertions because the mass term changes chirality and the W boson only couples to left-handed fields). The difference $P_u - P_c$ at m_W scale is therefore proportional to $(m_c - m_u)^2/m_W^2$, which we can neglect in our approach, because we're only expanding up to order $1/m_W$. Furthermore, working in a massless renormalisation scheme (see below) the renormalisation group running will preserve this difference for all scales all the way down to $\mu = m_c$, at which point threshold corrections will re-introduce the penguin diagrams.

We can calculate the (renormalised) Wilson coefficients as well as the renormalisation matrices $Z_{ij}(\mu)$ at $\mu = m_W$ scale by calculating amputated Green functions both in full QCD theory and in the effective five-flavour theory and comparing the results:

$$\langle O \rangle_{full} = \langle O \rangle^{(5)}_{eff}, \tag{2.142}$$

where the angle brackets denote the amputated Green functions:

$$\langle O \rangle_{full/eff} = \int \mathcal{D}\phi_i O e^{iS_{full/eff}} \Big|_{amp}, \tag{2.143}$$

where the integral runs over all the fields in the theory. This must be true for any operator O.

Just like in the case of the running coupling, Wilson coefficients will contain terms of the form $\ln(\mu/m_W)$, which become large when the difference in scales $m_W - \mu$ becomes large and have to be resummed as before. Acting with $\mu\frac{d}{d\mu}$ on both sides of Eq. (2.123) gives

$$0 = \frac{dC_j}{d\mu} Z_{ji} + C_j \frac{dZ_{ji}}{d\mu}. \tag{2.144}$$

Defining the anomalous dimension matrix γ as

$$\gamma_{ij} \equiv \frac{dZ_{ik}}{d\log\mu} Z^{-1}_{kj} \tag{2.145}$$

gives

$$\frac{dC_i}{d\log\mu} = -C_j \gamma_{ji}. \tag{2.146}$$

This expression can be integrated using Dyson's formula:

$$U(\mu_f, \mu_i) = T_\mu e^{i\int_{\mu_i}^{\mu_f} d\ln\mu \gamma(\mu)} \tag{2.147}$$

$$= T_g e^{i\int_{g(\mu_i)}^{g(\mu_f)} dg \frac{\gamma(\mu)}{\beta(\mu)}} \tag{2.148}$$

In a mass-independent renormalisation scheme the coefficients Z_{ij} do not depend on mass and therefore the anomalous dimension matrices (and hence the running) will not depend on quark masses either. This means that we have the same running for operators proportional to $V^*_{us}V_{ud}$ as for the operators proportional to $V^*_{ts}V_{td}$. Another advantage of mass-independent schemes is that because the anomalous dimension matrices do not depend on masses, they must be identical to the anomalous dimension matrices in a massless theory. In a massless theory the chiral symmetry is exact, which means that the anomalous dimension matrices (and hence operator mixing) will preserve exact chiral symmetry, even though it is only an approximate symmetry of the Lagrangian. This argument does not apply to threshold corrections however, which can re-introduce the mass dependence.

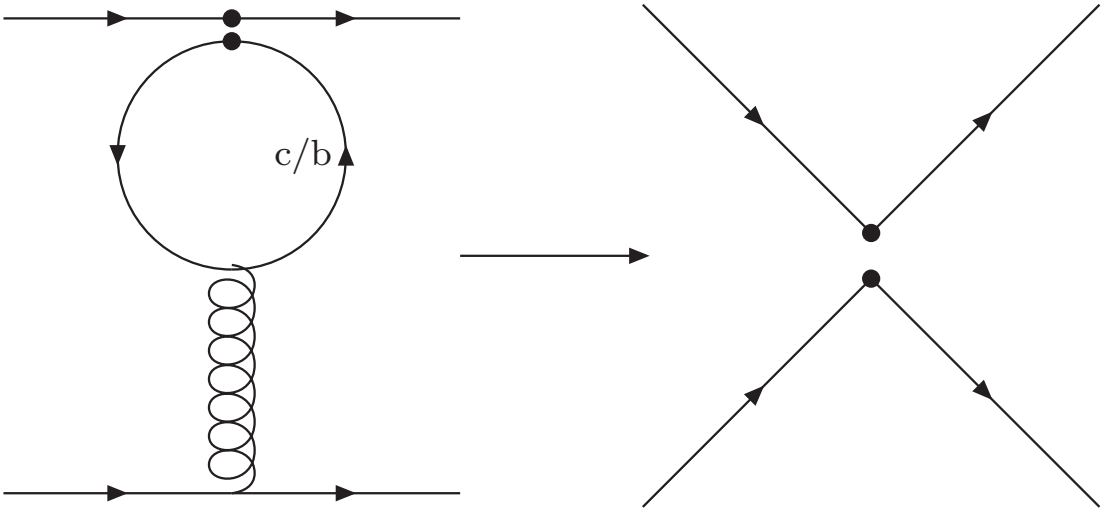

Figure 2.9: Example diagrams that are relevant for threshold matching at charm/bottom scale.

Because $\overline{MS}$ scheme does not satisfy the decoupling theorem, we need to apply threshold corrections by hand. This is done by comparing Green functions in n-flavour theory with the ones in (n+1)-flavour theory

$$\langle O \rangle_{eff}^{(n)} = \langle O \rangle_{eff}^{(n+1)}, \tag{2.149}$$

which can be done because the Wilson coefficients in (n+1)-flavour theory are known from the running. An example of diagrams which need to be integrated for threshold matching are shown in figure 2.9.

Above the charm scale it is convenient exploit the GIM mechanism by parametrising the weak Hamiltonian in the following way:

$$H_W = \frac{G_F}{\sqrt{2}} V_{us}^* V_{ud} \left((1-\tau) \sum_{i=1,2} z_i(\mu)(O_i - O_i^c) + \tau \sum_{i=1}^{10} v_i(\mu) O_i \right) \tag{2.150}$$

with $\tau \equiv -V_{ts}^* V_{td} / V_{us}^* V_{ud}$ and operators defined in Eqs. (2.75) - (2.84) and (2.139) - (2.140) . The coefficient proportional to $V_{cs}^* V_{cd}$ does not appear because of the CKM matrix unitarity relation:

$$V_{us}^* V_{ud} + V_{cs}^* V_{cd} + V_{ts}^* V_{td} = 0. \tag{2.151}$$

The first sum runs only over the current-current operators due to GIM suppression. Matching to three-flavour theory reintroduces the penguin diagrams via processes with charm quark loop in figure 2.9. In a three-flavour theory the weak Hamiltonian is instead parametrised as:

$$H_W = \frac{G_F}{\sqrt{2}} V_{us}^* V_{ud} \left(\sum_{i=1}^{10} (z_i(\mu) + \tau y_i(\mu)) O_i \right) \tag{2.152}$$

z_i	3 GeV LO	3 GeV NLO	y_i	3 GeV LO	3 GeV NLO
1	-0.391608	-0.241415	1	0	0
2	1.19262	1.11228	2	0	0
3	-0.00590226	-0.00392423	3	0.0245797	0.0211096
4	0.0227256	0.0169695	4	-0.0592354	-0.0558734
5	-0.00818322	-0.00349963	5	0.0180197	0.0117843
6	0.0199481	0.0120747	6	-0.0698914	-0.0610235
7	-0.0000852011	0.0000940198	7	0.000405289	-0.000161911
8	0.000020126	-0.000104478	8	0.000489482	0.000652032
9	-0.0000708857	0.0000275290	9	-0.0103101	-0.0103828
10	-0.0000233252	0.0000798557	10	0.00327317	0.00243775

Table 2.2: Wilson coefficients at 3 GeV in $\overline{MS}$ scheme calculated at leading (LO) and next-to-leading(NLO) order in α_s and α.

with

$$y_i(m_c) = v_i(m_c) - z_i(m_c). \tag{2.153}$$

As a final step, we can calculate the running in a three-flavour theory up to a desired scale.

The anomalous dimension matrices (including QED corrections) as well as the threshold matching matrices are given in [21].

Wilson coefficients calculated by running down to 3 GeV using LO and NLO running are shown in table 2.2.

2.5 Chiral perturbation theory

A popular way of studying low energy QCD is by means of chiral perturbation theory (ChPT). In this approach the spontaneous breaking of flavour $SU(N_f)$ axial symmetry by the chiral condensate, which gives rise to $N_f^2 - 1$ Goldstone bosons, which are treated as fundamental degrees of freedom. Chiral perturbation theory can be done either for $N_f = 2$ flavours, in which case the theory describes pions, or $N_f = 3$ flavours, in which case the Goldstone bosons are 3 pions, 4 kaons and an eta meson.

The importance of chiral perturbation theory for this project is twofold:

1. It is used for a (short) chiral extrapolation to correct for the differences in observables arising from small differences in physical and simulated meson masses. See section 5.6.1.

2. It is used to evaluate the magnitude of finite volume effects - see section 4.12.

Specifically, the theory is formulated in terms of $SU(N_f)$ fields $\Sigma(x)$, which transform under $SU(N_f)_L \times SU(N_f)_R$ as

$$\Sigma(x) \to U_L \Sigma(x) U_R^\dagger. \tag{2.154}$$

Furthermore, $\Sigma(x)$ can be written in terms of elementary (Goldstone boson) fields as

$$\Sigma(x) = e^{\frac{2i\sum_{a=1}^{N_f^2-1}\phi^a(x)T^a}{f_0}} \tag{2.155}$$

where T^a are the generators of $SU(N_f)$ and f_0 is a constant, which turns out to be the tree-level approximation of the pion decay constant. For example, taking $N_f = 3$ we have

$$\sum_{a=1}^{8}\phi^a\lambda^a = \begin{pmatrix} \pi^0 + \frac{1}{\sqrt{3}}\eta & \sqrt{2}\pi^+ & \sqrt{2}K^+ \\ \sqrt{2}\pi^- & -\pi^0 + \frac{1}{\sqrt{3}}\eta & \sqrt{2}K^0 \\ \sqrt{2}K^- & \sqrt{2}\bar{K}^0 & -\frac{2}{\sqrt{3}}\eta \end{pmatrix} \tag{2.156}$$

where λ^a are the Gell-Mann matrices, which are the generators of the fundamental representation of SU(3).

Chiral symmetry forbids quark masses, but the chiral symmetry breaking effects due to the mass terms can be included by using the following trick. First, note that in the QCD Lagrangian the mass term has the form $\bar{\psi}M\psi$, where $\psi = (u\ d\ s)^T$ and M=diag(m_u, m_d, m_s). This term is not invariant under chiral transformations, but if we upgrade M to a field χ ('spurion'), which transforms as $\chi \to U_L \chi U_R^\dagger$ then the term would be invariant. In a similar way, we can use χ in the effective field theory to construct all possible terms which are invariant under chiral symmetry and replace them with M matrices later.

The leading order ($O(p^2)$) ChPT Lagrangian can then be written as:

$$\mathcal{L}^{(0)} = \frac{f^2}{8}\mathrm{Tr}\left(\partial_\mu\Sigma^\dagger\partial^\mu\Sigma\right) + \frac{B_0 f^2}{4}\mathrm{Tr}\left(\chi^\dagger\Sigma + \Sigma^\dagger\chi\right). \tag{2.157}$$

To study $K \to \pi\pi$ transitions, we need to add operators corresponding to $\Delta S = 1$ transitions. As we have seen in section 2.4.2, such operators can be in a (27,1), (8,1) or (8,8) representation of $SU(3)_L \times SU(3)_R$. In ChPT the $O(p^2)$ contributions to the Lagrangian coming from these operators are ([22], [23]):

$$\mathcal{L}_{(27,1)} = \alpha_{27} t^{ij}_{kl}(\Sigma\partial_\mu\Sigma^\dagger)^k_i(\Sigma\partial_\mu\Sigma^\dagger)^k_i + h.c. \tag{2.158}$$

$$\mathcal{L}_{(8,1)} = \alpha_1\mathrm{Tr}\left(\lambda_6\partial_\mu\Sigma\partial^\mu\Sigma^\dagger\right) + \alpha_2 2B_0\mathrm{Tr}\left(\lambda_6(\chi\Sigma^\dagger + \Sigma\chi^\dagger)\right) \tag{2.159}$$

$$\mathcal{L}_{(8,8)} = \alpha_{88}\mathrm{Tr}\left(\lambda_6\Sigma Q\Sigma^\dagger\right) \tag{2.160}$$

where t^{ij}_{kl} is a completely symmetric and traceless tensor with $t^{13}_{12} = 1$,$t^{23}_{22} = 1/2$ and $t^{33}_{32} = -3/2$, $Q = \mathrm{diag}(2/3, -1/3, -1/3)$ and λ_6 (not to be confused with the Gell-Mann matrix λ^6) is given by $(\lambda_6)_{ij} = \delta_{i3}\delta_{j2}$. The matrix λ_6 was introduced because we are interested in $\Delta S = 1$ transitions. It can be easily verified that (8,1) and (8,8) operators transform in the desired way by recalling the discussion in section 2.4.2 and noting that Q and λ_6 are traceless. Similarly the (27,1) operators transforms as desired, because the t^{ij}_{kl} tensor is symmetric and traceless.

This Lagrangian can be used to derive the $K \to \pi\pi$ matrix elements. For the $\Delta I = 3/2$ transitions only the (27,1) and (8,8) operators contribute. Their matrix elements have been calculated to next-to-leading order of ChPT in [24; 25]. The result is:

$$\mathcal{M}^{27}_{\mathrm{LO}} = \langle\pi^+\pi^-|\mathcal{O}^{(27,1),3/2}|K^0\rangle_{\mathrm{LO}} = -\frac{4i\alpha_{27}}{f_K f_\pi^2}(m_K^2 - m_\pi^2)\,, \tag{2.161}$$

$$\begin{aligned}\mathcal{M}^{27}_{\mathrm{log}} =& \langle\pi^+\pi^-|\mathcal{O}^{(27,1),3/2}|K^0\rangle_{\mathrm{log}} \\ =& -\frac{4i\alpha_{27}}{f_K f_\pi^2}\frac{1}{f^2}\left[-\frac{1}{12}m_K^4\left(1-\frac{m_K^2}{m_\pi^2}\right)\beta(m_\pi^2, m_K^2, m_\eta^2) + m_K^2\left(\frac{5}{4}\frac{m_K^4}{m_\pi^2}\right.\right. \\ & \left. -\frac{13}{4}m_K^2 + 2m_\pi^2\right)\beta(m_\pi^2, m_K^2, m_\pi^2) + (m_K^4 - 3m_\pi^2 m_K^2 + 2m_\pi^4) \\ & \times\beta(m_K^2, m_\pi^2, m_\pi^2) + \left(-\frac{1}{4}\frac{m_K^4}{m_\pi^2} - \frac{1}{12}m_K^2 + \frac{1}{3}m_\pi^2\right)\ell(m_\eta^2) + \left(\frac{-m_K^4}{m_\pi^2}\right. \\ & \left.\left. -4m_K^2 + 4m_\pi^2\right)\ell(m_K^2) + \left(\frac{5}{4}\frac{m_K^4}{m_\pi^2} - \frac{45}{4}m_K^2 + 11m_\pi^2\right)\ell(m_\pi^2)\right]\,,\end{aligned} \tag{2.162}$$

$$\mathcal{M}^{88}_{\mathrm{LO}} = \langle\pi^+\pi^-|\mathcal{O}^{(8,8),3/2}|K^0\rangle_{\mathrm{LO}} = -\frac{4i\alpha_{88}}{f_K f_\pi^2}\,, \tag{2.163}$$

$$\begin{aligned}\mathcal{M}^{88}_{\mathrm{log}} =& \langle\pi^+\pi^-|\mathcal{O}^{(8,8),3/2}|K^0\rangle_{\mathrm{log}} \\ =& -\frac{4i\alpha_{88}}{f_K f_\pi^2}\frac{1}{f^2}\left[\left(\frac{5}{4}\frac{m_K^4}{m_\pi^2} - 2m_K^2\right)\beta(m_\pi^2, m_K^2, m_\pi^2) + (m_K^2 - 2m_\pi^2)\right. \\ & \times\beta(m_K^2, m_\pi^2, m_\pi^2) + \frac{1}{4}\frac{m_K^4}{m_\pi^2}\beta(m_\pi^2, m_K^2, m_\eta^2) - \left(4 + \frac{1}{2}\frac{m_K^2}{m_\pi^2}\right)\ell(m_K^2) \\ & \left. + \left(\frac{5}{4}\frac{m_K^2}{m_\pi^2} - 8\right)\ell(m_\pi^2) - \frac{3}{4}\frac{m_K^2}{m_\pi^2}\ell(m_\eta^2)\right]\,.\end{aligned} \tag{2.164}$$

At this order m_η is given by the Gell-Mann-Okubo relation: $3m_\eta^2 = 4m_K^2 - m_\pi^2$. The functions $\ell(m^2)$ and $\beta(q^2, m_1^2, m_2^2)$ correspond to diagrams with one and two pseudo Goldstone boson propagators respectively as illustrated in Fig. 2.10.

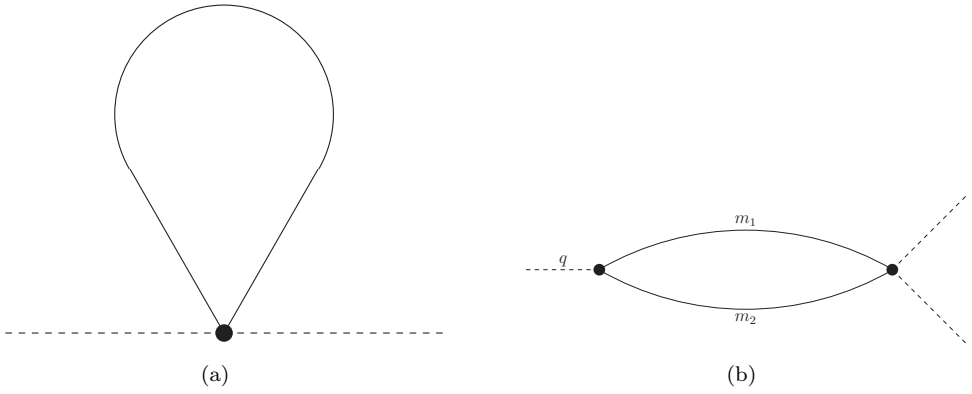

Figure 2.10: Loop diagrams which contribute to $K \to \pi\pi$ matrix elements in ChPT: (a) $\ell(m^2)$, where m is the mass of the boson in the loop and (b) $\beta(q^2, m_1^2, m_2^2)$.

Chapter 3

Phenomenology of hadronic kaon decays

3.1 Review of CP-violation

One of the biggest puzzles in modern physics is the abundance of matter over antimatter in the Universe. This means that there must be a fundamental law which generates matter-antimatter asymmetry. The conditions necessary for this asymmetry to arise are the Sakharov conditions:

1. Baryon number violation
2. Out of thermal equilibrium
3. **CP violation**

Condition 1 is self-explanatory - we start in a symmetric phase with baryon number equal to 0 and end in a phase with a large baryon number corresponding (approximately) to the sum of the numbers of all protons and neutrons in the Universe. This can only be achieved if the baryon number is violated. In the Standard Model the baryon number violation is present because the baryon number is anomalous, which can lead to baryon number violation via sphaleron processes.

Condition 2 is necessary, because in thermal equilibrium the rate of any process $A \to B$ is the same as the rate of the reverse process $B \to A$. This means that in equilibrium the total numbers of particles and antiparticles will, on average, remain constant.

Condition 3, CP-violation, as discussed in section 2.3.1, generates the matter-antimatter asymmetry and it will be the topic of the remainder of this chapter.

3.2 Neutral kaon mixing

Experimentally, CP violation was first discovered in the neutral kaons. Neutral kaon has an interesting property that it is the lightest neutral meson, which is not its own antiparticle, which makes it an ideal candidate for studying CP-violation at low energies.

Neutral kaon flavour eigenstates are $\mid K^0\rangle$ and $\mid \bar{K}^0\rangle$ with flavour content of $\bar{s}d$ and $\bar{d}s$ respectively. Because these states have the same conserved quantum numbers they can be thought of as components of some state $\mid \psi\rangle$ such that

$$\mid \phi(t)\rangle = \psi_1(t) \mid K^0\rangle + \psi_2(t) \mid \bar{K}^0\rangle + \sum_n c_n(t) \mid n\rangle \tag{3.1}$$

where the sum runs over all states with the same quantum numbers as K^0 and $\bar{K}^0$, such as e.g. $\mid \pi^+\pi^-\rangle$, $\mid \pi^+ e\nu\rangle$ etc. The state $\mid \phi(t)\rangle$ satisfies the Schrödinger equation

$$H \mid \phi(t)\rangle = i\frac{d}{dt} \mid \phi(t)\rangle. \tag{3.2}$$

To proceed we need to restrict ourselves to states $\mid K^0\rangle$ and $\mid \bar{K}^0\rangle$. This pair of states satisfies a similar equation

$$R \begin{pmatrix} \psi_1(t) \\ \psi_2(t) \end{pmatrix} = i\frac{d}{dt} \begin{pmatrix} \psi_1(t) \\ \psi_2(t) \end{pmatrix}. \tag{3.3}$$

The main difference between this equation and the Schrödinger equation is that the matrix R is not required to be Hermitian. Indeed, we find for the probability density

$$\frac{d}{dt}(|\psi_1(t)|^2 + |\psi_2(t)|^2) = -(\psi_1^*(t)\psi_2^*(t))\Gamma \begin{pmatrix} \psi_1 \\ \psi_2 \end{pmatrix} \tag{3.4}$$

where $\Gamma = i(R - R^\dagger)$. Because kaons decay, the rate of change of the probability density is negative, and Γ is a Hermitian, positive-definite matrix. R can then be written as

$$R = M - \frac{i}{2}\Gamma. \tag{3.5}$$

We can write explicit expression for the matrices M and Γ using second order time-independent perturbation theory

$$M_{ij} = m_0\delta_{ij} + \langle i \mid H_W \mid j\rangle + \sum_n P\frac{\langle i \mid H_W \mid n\rangle\langle n \mid H_W \mid j\rangle}{m_0 - E_n} \tag{3.6}$$

$$\Gamma_{ij} = 2\pi\sum_n \delta m_0 - E_n\langle i \mid H_W \mid n\rangle\langle n \mid H_W \mid j\rangle. \tag{3.7}$$

where H_W is the weak Hamiltonian and the states now exclude weak interactions.

Now consider CP and CPT transformations of neutral kaon states:

$$\begin{aligned} CP \mid K^0\rangle &= e^{i\xi} \mid \bar{K}^0\rangle, \\ CP \mid \bar{K}^0\rangle &= e^{-i\xi} \mid K^0\rangle, \\ CPT \mid K^0\rangle &= e^{i\eta} \mid \bar{K}^0\rangle, \\ CPT \mid \bar{K}^0\rangle &= e^{i\eta} \mid K^0\rangle. \end{aligned}$$

The states $\mid K^0\rangle$ and $\mid \bar{K}^0\rangle$ have opposite CP phases because we require that $(CP)^2 = 1$ and equal CPT phases because $(CPT)^2 = 1$ and CPT is antilinear. As before, the phases $e^{i\xi}$ are unphysical and can be absorbed by redefinition of $\mid \bar{K}^0\rangle$. Without loss of generality we can choose the phase to be $\xi = 0$.

For the remainder of the chapter I will assume that CPT is conserved so that $(CPT)H_W(CPT)^{-1} = H_W$. Then we have from Eqs. (3.6)-(3.7) it follows that $M_{11} = M_{22}$ and $\Gamma_{11} = \Gamma_{22}$.

From Eq. (3.3) we can infer the masses and mixings between $\mid K^0\rangle$ and $\mid \bar{K}_0\rangle$ states by calculating the eigenvalues and eigenvectors of the matrix R. Assuming CPT invariance, the eigenvectors are of the form $(p \quad \pm q)^T$ with $q/p = R_{21}/\sqrt{R_{12}R_{21}}$. We also choose the overall normalisation so that $|p|^2 + |q|^2 = 1$. Then the physical states $\mid K_L\rangle$ and $\mid K_S\rangle$ are given by

$$\mid K_L\rangle = p \mid K_0\rangle + q \mid \bar{K}_0\rangle, \tag{3.8}$$

$$\mid K_S\rangle = p \mid K_0\rangle - q \mid \bar{K}_0\rangle. \tag{3.9}$$

If on top of that we assume CP invariance, $(CP)^{-1}H_W(CP) = H_W$, we will have an additional condition on the off-diagonal matrix elements:

$$M_{12}^* = M_{12}e^{2i\xi}, \tag{3.10}$$

$$\Gamma_{12}^* = \Gamma_{12}e^{2i\xi}. \tag{3.11}$$

This allows us to construct a CP-violating quantity

$$\delta \equiv \frac{|R_{12}| - |R_{21}|}{|R_{12}| + |R_{21}|}, \tag{3.12}$$

which quantifies the amount of CP-violation in the mixing. Finally, δ can be rewritten in terms of $|p|$ and $|q|$:

$$\delta = |p|^2 - |q|^2 = \langle K_L \mid K_S\rangle. \tag{3.13}$$

Using $|p|^2 + |q|^2 = 1$ we can rewrite

$$|p|^2 = \frac{1+\delta}{2} \tag{3.14}$$

$$|q|^2 = \frac{1-\delta}{2}. \tag{3.15}$$

Another useful consequence of CP-symmetry is

$$\frac{p}{q} = \sqrt{\frac{M_{12}^* - i\Gamma_{12}^*}{M_{12} - i\Gamma_{12}}} \tag{3.16}$$

$$= \pm e^{i\xi} \tag{3.17}$$

or in terms of magnitudes

$$\left|\frac{q}{p}\right| = 1, \tag{3.18}$$

which will be used in defining the interference CP violation below.

3.3 Direct CP violation

Another possible source of CP violation can arise in kaon interactions. Suppose that CP is conserved. Then, for any process, the transition matrix (related to the S-matrix by $S = 1 + iT$) will satisfy:

$$(CP)^{-1}T(CP) = T. \tag{3.19}$$

Consider a system with two possible final states, $\langle f \mid$, $\langle g \mid$ which are CP-eigenstates so that:

$$CP \mid f\rangle = \eta_f \mid f\rangle, CP \mid g\rangle = \eta_g \mid g\rangle. \tag{3.20}$$

The phase factors η_f and η_g can not be removed by rephasing $\mid f\rangle$ or $\mid g\rangle$ and are therefore physical quantities. Furthermore, the condition $(CP)^2 = 1$ constrains them to be ± 1. The matrix elements will transform as:

$$\langle f \mid T \mid i\rangle = e^{i\xi_i}\eta_f\langle f \mid T \mid \bar{i}\rangle, \tag{3.21}$$

$$\langle g \mid T \mid i\rangle = e^{i\xi_i}\eta_g\langle g \mid T \mid \bar{i}\rangle. \tag{3.22}$$

This is a system of two equations with one unphysical phase ξ, which can be solved to give the following constraints on the matrix elements:

$$|\langle f \mid T \mid i\rangle| = |\langle f \mid T \mid \bar{i}\rangle| \tag{3.23}$$

$$|\langle g \mid T \mid i\rangle| = |\langle g \mid T \mid \bar{i}\rangle| \tag{3.24}$$

$$\epsilon' \equiv \langle f \mid T \mid i\rangle\langle g \mid T \mid \bar{i}\rangle - \eta_f\eta_g\langle f \mid T \mid \bar{i}\rangle\langle g \mid T \mid i\rangle = 0. \tag{3.25}$$

The first two equations can not be used to measure CP violation, because they are also a consequence of CPT. The third equation on the other hand defines ϵ', which is the measure of *direct* CP violation. Note that in order to define it, at least two possible finite state interactions are needed.

3.4 Interference CP-violation

We can define a parameter λ_f, which mixes direct and indirect CP-violation

$$\lambda_f \equiv \frac{\bar{A}_f q}{A_f p}. \tag{3.26}$$

where

$$\langle f \mid T \mid K^0 \rangle \equiv \sqrt{2} A_f e^{i\delta_f} \tag{3.27}$$

$$\langle f \mid T \mid \bar{K}^0 \rangle \equiv \sqrt{2} \bar{A}_f e^{i\delta_f} \tag{3.28}$$

where δ_f are the phase shifts associated with the final state $\mid f\rangle$ defined as usual $\langle f \mid f; in\rangle = e^{2i\delta_f}$ where $\mid f; in\rangle$ is the 'in' state corresponding to the 'out' state $\mid f\rangle$. This is explained in more detail in section 3.7. For example, if the final state is the I=2 or I=0 two-pion state, then the phase will be the two-pion phase shift in I=2 (δ_2) or I=0 (δ_0) channel respectively.

The reason for excluding the phase shifts from the definitions of A_f and $\bar{A}_f$ is that, if time reversal invariance holds, one can show that A_f and $\bar{A}_f$ become purely real. This is known as Watson's theorem, which I will now prove. Starting from the definition in Eq. (3.28) we have:

$$\sqrt{2} A_f e^{i\delta_f} = \langle f \mid T \mid K^0 \rangle \tag{3.29}$$

$$= \langle f; in \mid T \mid K^0 \rangle^* e^{i(\xi_f^T - \xi_K)} \tag{3.30}$$

$$= \langle f \mid T \mid K^0 \rangle^* e^{i(\xi_f^T - \xi_K^T + 2\delta_f} \tag{3.31}$$

$$= \sqrt{2} A_f^* e^{i(\xi_f^T - \xi_K^T + \delta_f)} \tag{3.32}$$

where in the second line I used time reversal invariance of the transfer matrix combined with the fact that time reversal changes the outgoing partial waves $\mid f\rangle$ into incoming partial waves $\mid f; in\rangle$ and in the third line I used $\mid f; in\rangle = e^{2i\delta_f} \mid f\rangle$. Recalling that the time-reversal phases are unphysical, we can choose the phase convention such that $\xi_f^T = \xi_K^T = 0$. This gives $A_f = A_f^*$, which is the statement of Watson's theorem. In practice time reversal (and equivalently CP) is not conserved, but because the the amount of CP-violation is small we still have $|A_f| \approx \mathrm{Re} A_f$.

If CP were conserved, we would have from Eq. (3.17) and (3.21):

$$\lambda_f^2 = 1. \tag{3.33}$$

On the other hand, treating direct and indirect CP violation separately only imposes constraints Eq. (3.18) and (3.23) which give

$$|\lambda_f| = 1. \tag{3.34}$$

This means that even if $|\lambda_f| = 1$, if $\mathrm{Im}\lambda_f \neq 0$ there is still a CP-violation, which is a consequence of a mismatch between direct and indirect CP phases. Hence $\mathrm{Im}\lambda_f$ (or equivalently $\mathrm{Arg}\lambda_f$) is the measure of interference CP-violation.

3.5 Measurable CP-violating parameters in the kaon system

We can define the following measurable (up to a phase) amplitudes:

$$\epsilon \equiv \frac{\langle \pi\pi; 0 \mid T \mid K_L \rangle}{\langle \pi\pi; 0 \mid T \mid K_S \rangle} \tag{3.35}$$

$$\epsilon_2 \equiv \frac{\langle \pi\pi; 2 \mid T \mid K_L \rangle}{\langle \pi\pi; 0 \mid T \mid K_S \rangle} \tag{3.36}$$

$$\omega \equiv \frac{\langle \pi\pi; 2 \mid T \mid K_S \rangle}{\langle \pi\pi; 0 \mid T \mid K_S \rangle} \tag{3.37}$$

I will focus on each of these quantities in turn.

ϵ can be written as

$$\epsilon = \frac{1 + \lambda_0}{1 - \lambda_0} \tag{3.38}$$

with

$$\lambda_0 \equiv \frac{\langle \pi\pi; 0 \mid T \mid \bar{K}^0 \rangle q}{\langle \pi\pi; 0 \mid T \mid K^0 \rangle p}. \tag{3.39}$$

We can write λ_0 as

$$\lambda_0 = \left| \sqrt{\frac{1-\delta}{1+\delta}} \frac{\bar{A}_0}{A_0} \right| e^{i\theta} \tag{3.40}$$

$$= \sqrt{\frac{1-\delta}{1+\delta}} e^{i\theta}. \tag{3.41}$$

We can then rewrite ϵ as:

$$\frac{2\mathrm{Re}\epsilon}{1 + |\epsilon|^2} = \delta, \tag{3.42}$$

$$\frac{2\mathrm{Im}\epsilon}{1 + |\epsilon|^2} = \sqrt{1 - \delta^2} \sin\theta. \tag{3.43}$$

Hence $\epsilon \neq 0$ implies either indirect CP violation ($\delta \neq 0$) or interference CP violation ($\sin\theta \neq 0$).

Next, I'll discuss ϵ_2. It is actually convenient to re-express it in terms of another quantity called, with the benefit of hindsight, ϵ' defined as

$$\epsilon' \equiv \frac{\epsilon_2 - \omega\epsilon}{\sqrt{2}} \tag{3.44}$$

$$= \frac{\langle\pi\pi; 2 \mid T \mid K_L\rangle\langle\pi\pi; 0 \mid T \mid K_S\rangle - \langle\pi\pi; 2 \mid T \mid K_S\rangle\langle\pi\pi; 0 \mid T \mid K_L\rangle}{\sqrt{2}\langle\pi\pi; 0 \mid T \mid K_S\rangle^2} \tag{3.45}$$

$$= \frac{2q}{pA_0^2(1-\lambda_0)^2}\left(\langle\pi\pi; 2 \mid T \mid \bar{K}^0\rangle\langle\pi\pi; 0 \mid T \mid K^0\rangle - \langle\pi\pi; 0 \mid T \mid \bar{K}^0\rangle\langle\pi\pi; 2 \mid T \mid K^0\rangle\right). \tag{3.46}$$

The final line is of the form of Eq. (3.25), which identifies it as a measure of direct CP violation. It will also be useful to define the quantity ϵ'/ϵ which can be written in terms of the $K \to \pi\pi$ amplitudes

$$\frac{\epsilon'}{\epsilon} = \frac{\omega}{\sqrt{2}|\epsilon|}\left(\frac{\mathrm{Im}A_2}{\mathrm{Re}A_2} - \frac{\mathrm{Im}A_0}{\mathrm{Re}A_0}\right). \tag{3.47}$$

Finally, the quantity ω is experimentally known to be small, $1/|\omega| \approx 22.5$. This is known as the $\Delta I = 1/2$ rule, which states that the kaon will decay predominantly into two I=0 pions. The theoretical explanation of this observation is still unknown, but recent lattice studies, including the one this thesis is based on, have shed some light on origin of the $\Delta I = 1/2$ rule. For further discussion, see section 5.7.

3.6 Experimental results

Experimentally we can not determine the amplitudes (which are phase dependent) directly and we are limited to the determination of their magnitudes. The magnitudes of $K_S \to \pi\pi$ decay amplitudes can be calculated from the decay rates given by:

$$\Gamma(K_S \to \pi^+\pi^-) = \frac{1}{16\pi m_K}\sqrt{1 - \frac{4m_\pi^2}{m_K^2}}\left|\sqrt{\frac{1}{3}}\langle\pi\pi; 2 \mid T \mid K_S\rangle + \sqrt{\frac{2}{3}}\langle\pi\pi; 0 \mid T \mid K_S\rangle\right|^2, \tag{3.48}$$

$$\Gamma(K_S \to \pi^0\pi^0) = \frac{1}{32\pi m_K}\sqrt{1 - \frac{4m_\pi^2}{m_K^2}}\left|\sqrt{\frac{2}{3}}\langle\pi\pi; 2 \mid T \mid K_S\rangle - \sqrt{\frac{1}{3}}\langle\pi\pi; 0 \mid T \mid K_S\rangle\right|^2, \tag{3.49}$$

$$\Gamma(K^+ \to \pi^+\pi^0) = \frac{\sqrt{m_{K^+}^2/4 - (m_{\pi^+}^2 + m_{\pi^0}^2)/2 + (m_{\pi^0}^2 - m_{\pi^+}^2)^2/4m_{K^+}^2}}{4\pi m_{K^+}^2}\left|\langle\pi\pi; 2 \mid T \mid K^+\rangle\right|^2. \tag{3.50}$$

Using the set of experimental results ([16]) shown in Table 3.1 (recalling that $\Gamma(A \to B) = \mathrm{Br}(A \to B)/\tau_A$) together with Eqs. (3.48-3.50) and definitions (3.28) gives the following predictions for the decay amplitudes:

$$|A_0| \approx \mathrm{Re}A_0 = 3.3197(14) \times 10^{-7}\mathrm{GeV}, \tag{3.51}$$

$$|A_2| \approx \mathrm{Re}A_2 = 1.570(53) \times 10^{-8}\mathrm{GeV}, \tag{3.52}$$

$$\sqrt{\frac{3}{2}}|A_2^+| \approx \sqrt{\frac{3}{2}}\mathrm{Re}A_2^+ = 1.4787(31) \times 10^{-8}\mathrm{GeV}. \tag{3.53}$$

The rather large difference between $\mathrm{Re}A_2$ and $\sqrt{\frac{3}{2}}\mathrm{Re}A_2^+$ is a consequence of isospin breaking. These results verify than indeed $1/|\omega| \approx 22.5$.

The ratio ϵ'/ϵ can be measured by defining the quantities

$$\eta_f \equiv \frac{\langle \pi\pi; f \mid T \mid K_L \rangle}{\langle \pi\pi; f \mid T \mid K_S \rangle} \tag{3.54}$$

which give

$$\eta_{+-} = \epsilon + \epsilon', \tag{3.55}$$

$$\eta_{00} = \epsilon - 2\epsilon', \tag{3.56}$$

and hence (using the result that ϵ'/ϵ is approximately real)

$$\left|\frac{\eta_{00}}{\eta_{+-}}\right|^2 = 1 - 6\frac{\epsilon'}{\epsilon}. \tag{3.57}$$

The left-hand side of this equation can be determined experimentally by calculating the ratio

$$\left|\frac{\eta_{00}}{\eta_{+-}}\right|^2 = \frac{BR(K_L \to \pi^0\pi^0)BR(K_S \to \pi^+\pi^-)}{BR(K_S \to \pi^0\pi^0)BR(K_L \to \pi^+\pi^-)} \tag{3.58}$$

An experimental value of ϵ'/ϵ is ([16])

$$\frac{\epsilon'}{\epsilon} = 1.65(26) \times 10^{-3}. \tag{3.59}$$

3.7 Two-particle scattering

As an added bonus, we are also able to calculate the two-pion scattering phase shift. The phase shift is the only quantity that the two (pseudo-)scalar meson scattering matrix depends on. To see this, consider the states $\mid E, \mathbf{p}, l, m \rangle$ where E is the total energy, $\mathbf{p}$ is the total momentum, l is the total orbital angular momentum and m is the component

m_{K^+}	493.667(16) MeV
m_{K^0}	497.614(24) MeV
m_{π^+}	139.57018(35) MeV
m_{π^0}	134.9766(6) MeV
τ_{K_s}	$0.89530(5) \times 10^{-10}$ s
τ_{K^+}	$1.2380(21) \times 10^{-8}$ s
$\mathrm{Br}(K_S \to \pi^0\pi^0)$	30.69(5) %
$\mathrm{Br}(K_S \to \pi^+\pi^-)$	69.20(5) %
$\mathrm{Br}(K^+ \to \pi^+\pi^0)$	20.66(8) %
$\delta_2 - \delta_0$	47.7°

Table 3.1: Experimental input used to calculate A_0 and A_2.

of the angular momentum in the z-direction. Then, the S-matrix in the centre-of-mass frame can be written as

$$\langle E, \mathbf{p}, l', m' \mid S \mid E^*, \mathbf{0}, l, m\rangle = \delta(E - E^*)\delta^{(3)}(\mathbf{p})\delta_{ll'}\delta_{mm'}e^{2i\delta_l(E^*)} \tag{3.60}$$

where the function $\delta_l(E^*)$ is called the phase shift. The structure of this equation is motivated as follows. The Kronecker and Dirac deltas arise as a consequence of translational and rotational invariance of the S-operator

$$[P^\mu, S] = [J_3, S] = [\mathbf{J}^2, S] = 0. \tag{3.61}$$

The remaining function can only be a phase because of the unitarity of the S-matrix

$$\left|\langle E, \mathbf{p}, l', m' \mid S \mid E^*, \mathbf{0}, l, m\rangle\right|^2 = 1. \tag{3.62}$$

Finally, the phase $\delta_l(E^*)$ does not depend on m, because rotational invariance implies that the S-operator commutes with the angular momentum raising and lowering operators

$$[J_\pm, S] = 0 \tag{3.63}$$

which results in the condition $\delta_{lm}(E^*) = \delta_{lm+1}(E^*)$ for $l - 1 \leq m < l$. This argument is a special case of the Wigner-Eckart theorem, which will be introduced in section **SEC**.

Using $S = 1 + iT$ shows that the matrix elements of these states behave as

$$\langle E, \mathbf{p}, l, m \mid T \mid E^*, \mathbf{0}, l', m'\rangle = \frac{e^{2i\delta_l} - 1}{i}\delta_{ll'}\delta_{mm'}\delta(\mathbf{p})\delta(E - E^*). \tag{3.64}$$

This relation will be useful in deriving the Lüscher quantisation condition in section 4.12.

The phase shifts δ_l have the following limiting behaviour in the low momentum limit

$$\delta_l(p) \propto p^l \tag{3.65}$$

where p is the magnitude of the momentum of a single particle in the centre-of-mass frame. This means that at low energies the s-wave ($l = 0$) state will dominate. The s-wave phase shift can be further parametrised in terms of the scattering length a_0 defined by

$$a_0 = \lim_{p \to 0} \frac{\tan \delta_0(p)}{p}. \tag{3.66}$$

The scattering length therefore is a constant which contains information about low-energy particle scattering.

Chapter 4

Lattice QCD

Calculation involving hadrons depend on strong interactions, which are difficult to calculate in perturbation theory at low energies. This is because the expansion parameter α_s is of order 1, so the perturbative series does not converge very quickly, if at all. The most promising alternative to perturbation theory in this regime is provided by lattice gauge theories, which are the topic of this chapter. I will discuss the lattice formulation and how quantities calculated on a lattice can be related to physical observables, focusing on the $K \to \pi\pi$ $\Delta I = 3/2$ calculation.

4.1 Lattice formulation

4.1.1 Gauge fields

On the lattice derivatives are replaced with finite differences, which are non-local. As an example, consider an arbitrary field ϕ. Then the continuum derivative of this field is replaced by (for example) a forward derivative:

$$\partial^\mu \phi(x) \to \Delta_F^\mu \phi(x) \equiv \frac{1}{a}\left(\phi(x + a\hat{\mu}) - \phi(x)\right). \tag{4.1}$$

Now suppose that ϕ transforms under the fundamental representation of SU(3): $\phi(x) \to \Omega(x)\phi(x)$, where $\Omega(x) \in SU(3)$. We are looking for a discrete equivalent of a covariant derivative:

$$D^\mu \phi(x) \to \frac{1}{a}\left(\phi(x + a\hat{\mu}) - U(x + a\hat{\mu}, x)\phi(x)\right), \tag{4.2}$$

where U is an $SU(3)$ matrix. We require both terms of the discretised covariant to transform the same way, which imposes the following transformation on U:

$$U(x + a\hat{\mu}, x) \to \Omega(x + a\hat{\mu}) U(x + a\hat{\mu}, x) \Omega^\dagger(x). \tag{4.3}$$

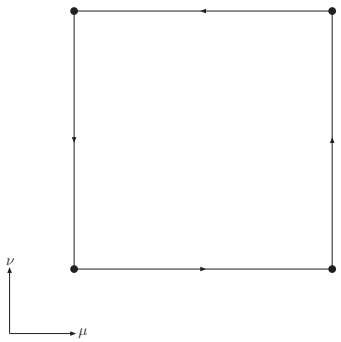

Figure 4.1: Plaquette

Objects transforming in such way are the Wilson lines, defined by:

$$U_P(x,y) = e^{ig\int_P dx'_\mu A^\mu(x')}, \tag{4.4}$$

where the integral is defined along a path P from x to y. The lattice version of the Wilson line (often referred to as the link variable) is:

$$U(x+\mu a, x) = e^{igaA^\mu(x)}. \tag{4.5}$$

There are two ways of constructing gauge-invariant quantities:

- Connecting quark and antiquark fields with a Wilson line constructed out of link variables
- Traces of closed loops constructed out of link variables

To construct a pure gauge action we only require the latter. The simplest object that has this property is the plaquette operator:

$$P^{\mu\nu} = (U(x, x+a\hat{\nu})U(x+a\hat{\nu}, x+a\hat{\mu}+a\hat{\nu})U(x+a\hat{\mu}+a\hat{\nu})U(x+a\hat{\mu}, x))\,, \tag{4.6}$$

illustrated in Fig. 4.1.

The simplest gauge action can be written as:

$$S_{plaq} = \frac{\beta}{4N}\sum_x\sum_{\mu<\nu}\mathrm{ReTr}\,(1-P^{\mu\nu}(x)) = \frac{a^4}{4}\int F^a_{\mu\nu}F^{\mu\nu a} + \mathcal{O}(a^6), \tag{4.7}$$

where N is the number of colours and $\beta = 2N/g^2$ where g^2 is the strong coupling constant. We can see that this action reproduces the continuum Yang-Mills action in the continuum up to terms of order a^6. This can be further improved by considering additional gauge-invariant operators, such as the rectangle $R^{\mu\nu}$ as shown in figure 4.2.

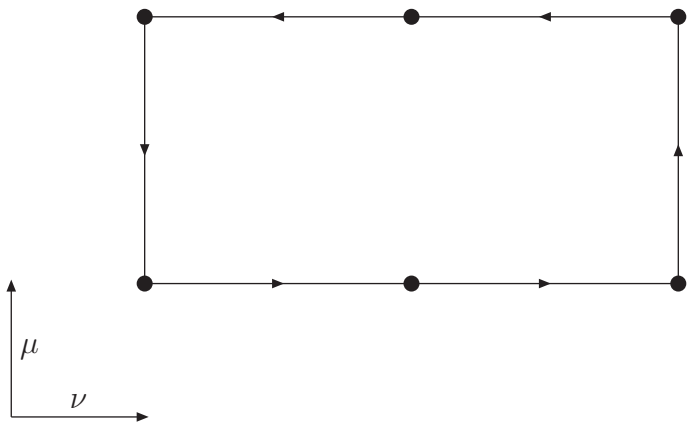

Figure 4.2: Correction to a Wilson plaquette action.

The class of actions improved with the rectangle loop is given by

$$S_I = \frac{\beta}{3}\left((1-8c_1)\sum_{x,\mu<\nu}(\mathrm{ReTr}P^{\mu\nu}) + c_1\sum_{x,\mu\neq\nu}\mathrm{ReTr}R^{\mu\nu}\right). \tag{4.8}$$

The Iwasaki action is defined by the choice $c_1 = -0.331$, which was determined from the renormalisation group analysis in reference [26].

4.1.2 Gauge fixing

It is often convenient to work in a fixed gauge. In our case, the gauge fixing allows us to:

- use non-local (and therefore gauge-dependent) interpolating operators
- use a gauge-dependent (but BRST-invariant) renormalisation scheme (RI-SMOM) and match it to the $\overline{MS}$ scheme

While for the former application any gauge will suffice, the latter forces us to use the same gauge as the one we use for the perturbative RI-SMOM to $\overline{MS}$ matching, i.e. the Landau gauge.

The Landau gauge is defined in the continuum by the condition $\partial_\mu A^\mu = 0$. It will be helpful to notice that this condition is satisfied at the stationary points of the functional

$$W[A] = \int d^4x \sum_{\mu=1}^{4} \mathrm{Tr}A_\mu(x)A^\mu(x). \tag{4.9}$$

This is easily verified by recalling that A_μ transforms as

$$\delta A_\mu = -\frac{1}{g}\partial_\mu\theta + i[A_\mu, \theta] \tag{4.10}$$

where $\theta = \theta^a T^a$ is the gauge parameter. On the lattice, this is equivalent to choosing the gauge parameter matrices Ω such that the functional

$$W = \sum_x \sum_{\mu=1}^{4} \mathrm{Tr}\left(U_\mu(x) + U_\mu^\dagger(x)\right) \tag{4.11}$$

is extremised (recall that U transforms as $\Omega^\dagger U \Omega$).

Similarly, to achieve the Coulomb gauge fixing condition $\nabla \cdot \mathbf{A} = 0$, one can extremise

$$W = \sum_x \sum_{\mu=1}^{3} \mathrm{Tr}\left(U_\mu(x) + U_\mu^\dagger(x)\right), \tag{4.12}$$

where the sum over μ runs only over spatial indices.

In $K \to \pi\pi$ calculation we used Coulomb gauge fixing for the kaon and pion interpolating operators and Landau gauge fixing for renormalisation.

4.1.3 Fermion fields

4.1.3.1 Naive fermion discretisation

Using the prescription for the covariant derivative given by Eq. 4.2, one might expect that the correct lattice prescription for the fermion fields in the Lagrangian would be:

$$\bar{\psi} \not{D} \psi \to \bar{\psi}(x) \left(\psi(x) - U(x, x - a\hat{\mu}\psi(x - a\hat{\mu})\right). \tag{4.13}$$

Unfortunately, this choice suffers from the infamous fermion doubling problem.

To see this, note that the there is a one-to-one correspondence between the poles in momentum space Green's functions and states in the Hilbert space. I am going to show this on an example of a two-point fermion Green's function given by

$$G(p) = \int d^4x \langle 0 \mid T\bar{\psi}(x)\psi(0) \mid 0\rangle e^{ipx}. \tag{4.14}$$

In this equation T is the time-ordering operator defined by

$$T(O_1(x)O_2(y)) = \theta(x^0 - y^0)O_1(x)O_2(y) + \theta(y^0 - x^0)O_2(y)O_1(x), \tag{4.15}$$

where $\theta(x)$ is the Heaviside step function, which gives $+1$ if its argument is positive, $+1/2$ if it is 0 and 0 otherwise. The step function has the following Fourier representation:

$$\theta(x) = \lim_{\epsilon \to 0} \frac{-1}{2\pi i} \int ds \frac{e^{-isx}}{s + i\epsilon}, \tag{4.16}$$

which can be easily verified by contour integration. Inserting this representation into Eq. (4.14) as well as the complete set of states gives:

$$G(p) = \sum_n \int d^4x \int \frac{ds}{2\pi i} \langle 0 \mid \bar{\psi}(0) \mid n \rangle \langle n \mid \psi(0) \mid 0 \rangle e^{i(p-p_n)x} e^{isx^0} \frac{-1}{s + i\epsilon} + \dots \tag{4.17}$$

$$= \sum_n \frac{i(2\pi)^3 \langle 0 \mid \bar{\psi}(0) \mid n \rangle \langle n \mid \psi(0) \mid 0 \rangle}{p^0 - p_n^0 + i\epsilon} \delta^{(3)}(\mathbf{p} - \mathbf{p_n}) + \dots . \tag{4.18}$$

It is clear that the two-point function will have a pole for every state in the Hilbert space that has the same quantum numbers as ψ.

$G(p)$ can be most easily derived using functional methods (4.3):

$$G(p) = \frac{1}{Z[0,0]} \frac{\delta}{\delta \bar{J}} \frac{\delta}{\delta J} Z[J, \bar{J}] \Big|_{J=\bar{J}=0} \tag{4.19}$$

$$= M^{-1}. \tag{4.20}$$

$$Z[J, \bar{J}] = \int \mathcal{D}[\bar{\psi}, \psi, U] e^{-S[\psi, \bar{\psi}, U] + \bar{J}\psi + \bar{\psi}J} \tag{4.21}$$

In continuum free theory with massless fermions, the matrix M in the above expression is simply $i\partial\!\!\!/$, which can be inverted by going to the momentum space to give $p\!\!\!//p^2$. Hence the continuum Green's function has only one pole at $p^2 = 0$.

We now turn to naive lattice fermion discretisation. The matrix M can be expressed, for example, as the following difference of Kronecker deltas: $\frac{1}{2a} \sum_\mu \gamma^\mu (\delta_{x+a\mu} - \delta_{x-a\mu})$, with the inverse given by $\frac{1}{2a \sum_\mu \gamma^\mu \sin ap\mu}$, where p is restricted to the first Brillouin zone $-\pi/a < p \leq \pi/a$. This expression has zeroes when all components of p^μ are either equal to zero or π/a - 16 solution in total.

The additional solutions correspond to additional states in the Hilbert space and are referred to in the literature as 'doublers'. Removing doublers requires a different choice of fermion action. An example is the Wilson action defined by:

$$S_{Wilson} = \sum_x \bar{\psi}(x)(m - \frac{4r}{a})\psi(x) + \frac{1}{2a} \sum_{x,\mu} \bar{\psi}(x + a\hat{\mu})(r - \gamma^\mu) U(x + a\hat{\mu}, x)\psi(x). \tag{4.22}$$

The additional term proportional to r is an irrelevant dimension-5 operator. In practical applications the value of r is typically set to 1. The Fourier space Dirac matrix is:

$$M_{Wilson} = m + \sum_\mu \frac{i}{a} \gamma^\mu \sin(ap_\mu) + \frac{r}{a} \sum_\mu (1 - \cos(ap_\mu)). \tag{4.23}$$

The third term is the new one in comparison to naive fermions. Now even in the zero fermion mass limit, the operator has only one zero at $p^\mu = (0, 0, 0, 0)$, just like in the physical case.

The downside is that the additional Wilson term, $ar\bar{\psi}D^2\psi$ mixes the left and right-chiral fermion fields and hence explicitly breaks chiral symmetry.

4.1.3.2 Domain wall fermions

In the previous section I described Wilson fermions, which remove fermion doublers at the expense of chiral symmetry. According to Nielsen-Ninomiya no-go theorem [27], the following conditions can not be simultaneously satisfied:

1. Absence of doublers
2. Chiral symmetry
3. Locality
4. Even number of dimensions

Wilson fermions are an example of giving up chiral symmetry to ensure the absence of doublers. While the exact chiral symmetry can not be satisfied given other conditions, a lattice version of chiral symmetry defined by the Ginsparg-Wilson relation

$$\gamma^5 D + D\gamma^5 = aD\gamma^5 D \tag{4.24}$$

where D is the Dirac operator and a is the lattice spacing, can be satisfied ensuring chiral symmetry in the continuum limit.

An action which satisfies this property is the overlap fermion action [28].

$$D_{ov} = \frac{1}{a}\left(1 + \gamma^5 \frac{H}{\sqrt{H^2}}\right) \tag{4.25}$$

where $H = \gamma^5 D_{ker}$ and D_{ker} is the kernel which is γ^5-hermitian lattice Dirac operator, such as the Wilson operator. While the overlap fermion maintain the exact chiral symmetry in the Ginsparg-Wilson sense, the calculation of $\sqrt{H^2}$ is particularly expensive making it an unattractive choice for practical purposes.

An alternative proposed by [29] and developed by [30; 31] is to maintain an approximate chiral symmetry by extending the number of dimensions to five. This formulation is known as domain wall fermions (DWF) and it is the formulation used for the calculations in this thesis.

The DWF operator is given by

$$D_{DWF} = \delta_{ss'} D^{\parallel}_{xx'}(M_5) + \delta_{xx'} D^{\perp}_{ss'}(m_f) \tag{4.26}$$

$$D^{\parallel}_{xx'}(M_5) = \frac{1}{2}\sum_{\mu=1}^{4}\Big((1-\gamma_\mu)U_\mu(x)\delta_{x+\hat{\mu},x'} + (1+\gamma_\nu)U^\dagger_\mu(x')\delta_{x-\hat{\mu},x'}\Big) + (M_5+4)\delta_{xx'} \tag{4.27}$$

$$D^{\perp}_{ss'}(m_f) = \begin{cases} \frac{1+\gamma_5}{2}\delta_{1s'} - m_f\frac{1-\gamma_5}{2}\delta_{L_s-1s'} - \delta_{s0} & s=0 \\ \frac{1+\gamma_5}{2}\delta_{s+1s'} + \frac{1-\gamma_5}{2}\delta_{s-1s'} - \delta_{ss'} & 1<s<L_s-2 \\ -m_f\frac{1+\gamma_5}{2}\delta_{0s'} + \frac{1-\gamma_5}{2}\delta_{L_s-2s'} - \delta_{L_s-1s'} & s=L_s-1 \end{cases} \tag{4.28}$$

The 5-dimensional fermion fields constructed using this prescription have the property that, up to terms exponentially suppressed in L_s, their $s=0$ component contains only the right-handed modes while the $s=L_s-1$ component contains only the left-handed modes. The 4-dimensional quark operators can then be constructed from 5-dimensional fields using

$$q = \frac{1+\gamma^5}{2}\Psi(x,0) + \frac{1-\gamma^5}{2}\Psi(x,L_s-1), \tag{4.29}$$

$$\bar{q} = \bar{\Psi}(x,L_s-1)\frac{1+\gamma^5}{2} + \bar{\Psi}(x,0)\frac{1-\gamma^5}{2}. \tag{4.30}$$

As already mentioned, the contamination of left-chiral modes with right-chiral modes and vice versa is exponentially suppressed in L_s, which means that the (lattice) chiral symmetry is restored in the limit $L_s \to \infty$. In practice, we are limited to finite L_s, so there will be some residual chiral symmetry breaking, which can be parametrised with residual mass m_{res}.

Möbius Domain Wall Fermions (MDWF) [32] is a variation of the standard (Shamir) DWF formulation above. The generalisation can be made by introducing parameters b and c so that the 5D component of the DWF operator is

$$D^5_{DWF} = \begin{pmatrix} \tilde{D} & -P_- & 0 & \cdots & 0 & m_f P_+ \\ -P_+ & \tilde{D} & -P_- & \cdots & 0 & 0 \\ 0 & \ddots & \ddots & \cdots & 0 & 0 \\ \vdots & & & & & \vdots \\ 0 & 0 & 0 & \cdots & \tilde{D} & -P_- \\ m_f P_- & 0 & 0 & \cdots & -P_+ & \tilde{D} \end{pmatrix} \tag{4.31}$$

where $P_\pm = \frac{1\pm\gamma^5}{2}$, $\tilde{D} = (1-cD^{\parallel})^{-1}(bD^{\parallel}+1)$ and $D^{\parallel}$ is the Wilson kernel as before. The choice $b=1$ and $c=0$ recovers the original Shamir DWF described by Eq. (4.27). The inclusion of additional parameters has no effect on the physical results, which can

be most easily seen from the mapping between DWF and overlap fermions

$$D_{ov} = \frac{1+m}{2} + \frac{1-m}{2}\gamma^5 \epsilon_{L_s}\left(\gamma^5 D_M\right) \tag{4.32}$$

$$D_M = \frac{(b+c)D^{\|}}{2+(b-c)D^{\|}}. \tag{4.33}$$

In the above equation, $\epsilon_{L_s}(x) = x/|x|$ is the sign function. From this equation it is clear that we are allowed to change b and c freely so long as the sign of D_M does not change. In particular, choosing $b - c = 1$ gives an action equivalent to Shamir DWF, because

$$\epsilon_{L_s}(\alpha\gamma^5 D^M) = \epsilon_{L_s}(\gamma^5 D^M) \tag{4.34}$$

for any $\alpha > 0$ and $\alpha = b + c$. The additional parameter α can be tuned to reduce the chiral symmetry breaking effects. The Möbius DWF formulation used in this project has $b - c = 1$ and $\alpha = b + c = 2$.

4.2 Rotational symmetry

Partial wave states are eigenstates of rotational symmetry, which is broken on the lattice. This section describes the effect of this breaking on two-pion states.

On the lattice the full rotational symmetry is broken to a subgroup which is the symmetry group of a cube. This group consists of 24 transformations (48 with parity) which can be arranged in 5 conjugacy classes:

- The identity (E)
- 6 rotations by $\pi/2$ rotating along the line parallel to the edge of the cube ($6C_4$)
- 3 rotations by π rotating along the line parallel to the edge of the cube ($3C_2$)
- 8 rotations by $2\pi/3$ rotating along the long diagonal ($8C_3$)
- 6 rotations by π rotating along the diagonal of one of the sides ($6C_2$)
- parity transformed versions of the above

Now consider interpolating operators in the momentum space of the form $O_\pi(\mathbf{p})O_\pi(-\mathbf{p})$ with $\mathbf{p} = (\pm 1, \pm 1, \pm 1)$. Since these operators are all parity even (by Bose symmetry) we only need to consider the 24 transformations without parity. There are 5 irreducible representations, which are given in the rows of the character table:

O	E	$6C_4$	$3C_2$	$8C_3$	$6C_2$
A_1	1	1	1	1	1
A_2	1	-1	1	1	-1
E	2	0	2	-1	0
T_1	3	1	-1	0	-1
T_2	3	-1	-1	0	1

As an example, a 3-vector, such as the momentum, transforms according to matrices shown in the appendix. Calculating traces (to get the characters) shows that vectors transform under the T_1 representation.

4.2.1 Representation of $\pi\pi$ interpolating operators

We can construct a vector out of our 4 operators: ((+++),(++-),(+-+),(-++)), where I use the shorthand notation for the signs of each of the components of $\mathbf{p}$. For example (+-+) denotes an operator $O_\pi(\mathbf{p})O_\pi(-\mathbf{p})$ with $p_x = p_z = +1$ and $p_y = -1$. This vector will transform under a 4D representation of cubic symmetry group. The strategy is to work out the characters of this representation and then use the character orthogonality relation:

$$\frac{1}{[g]}\sum_g \chi^{(R_1)}(g)\chi^{(R_2)}(g) = \delta_{R_1 R_2}, \tag{4.35}$$

where g are the group elements, R_1 and R_2 are irreducible representations, χ are the characters and $[g]$ is the number of elements in the group (24).

The characters are defined as traces of the representation matrices, so only the operators which transform to themselves under cubic symmetry transformations will contribute. (To be more precise an operator $O_i \to \sum_j c_{ij}O_j$ will contribute c_{ii} to the trace. Then the trace will be equal to $\sum_i c_{ii}$.) As an example, let's calculate the character of $6C_2$. We can pick any matrix from the $6C_2$ section of the appendix and have the momenta transform accordingly. For the purpose of illustration, let's take:

$$\begin{pmatrix} 0 & 1 & 0 \\ 1 & 0 & 0 \\ 0 & 0 & -1 \end{pmatrix}.$$

We find that under this transformation, exactly two operators remain invariant: (+-+) and (-++), other two operators transform into each other and therefore don't contribute to the trace. The character of C_2 is therefore 2. If we chose a different matrix from $6C_2$ equivalence class, we'd find different operators remaining invariant, but the trace would still be the same (this follows from the definition of an equivalence class and the relation $\mathrm{Tr}(h)=\mathrm{Tr}(g^{-1}hg)$).

Repeating this procedure for other conjugacy classes gives the following table:

O	E	$6C_4$	$3C_2$	$8C_3$	$6C_2$
$\{O_{\pi\pi}\}$	4	0	0	1	2

Finally, using the orthogonality theorem for characters we can see that this representation decomposes into $A_1 + T_2$.

To see which partial waves are contained in these representations, we can repeat the same procedure with spherical harmonics Y_m^l. The representations contained in first three even l (odd values of l are forbidden by parity) are

$$0 \to A_1 \tag{4.36}$$

$$2 \to E + T_2 \tag{4.37}$$

$$4 \to A_1 + E + T_1 + T_2 \tag{4.38}$$

Inverting this relation shows that the s-wave is contained only in A_1 representation and that the next lowest partial wave in A_1 is the g-wave ($l = 4$). Interpolating operators described so far in this section will also contain an unwanted d-wave contribution, because of the presence of T_2 representation. It is much better to construct an interpolating operator that is directly in the A_1 representation, which is given by

$$O_{\pi\pi}^{A_1}(\mathbf{p}) = \sum_{|\mathbf{p}|\in\pm1,\pm1,\pm1} O_\pi(\mathbf{p})O_\pi(-\mathbf{p}). \tag{4.39}$$

4.3 Path integral formulation

While the canonical formalism discussed above has the nice property of manifestly preserving unitarity, it is not very useful for numerical calculation because of the presence of position and momentum operators. It is much more useful to express everything in terms of real numbers and this is what the path integral formulation can achieve.

First, it will be convenient to define the field eigenstates $\mid \phi(t)\rangle$ and the field conjugate eigenstates $\mid \pi(t)\rangle$ such that:

$$\hat{\phi}(t) \mid \phi(t)\rangle = \phi \mid \phi(t)\rangle, \tag{4.40}$$

$$\hat{\pi}(t) \mid \pi(t)\rangle = \pi \mid \pi(t)\rangle, \tag{4.41}$$

where $\hat{\phi}(t)$ and $\hat{\pi}(t)$ are the Heisenberg picture operators and ϕ and π are their respective eigenvalues. We can choose them such that they are orthonormal:

$$\langle \phi_1(t) \mid \phi_2(t)\rangle = \delta(\phi_1 - \phi_2), \tag{4.42}$$

$$\langle \pi_1(t) \mid \pi_2(t)\rangle = \delta(\pi_1 - \pi_2). \tag{4.43}$$

Also, as a consequence of canonical commutation relations, we have:

$$\langle \pi(t) \mid \phi(t) \rangle = \frac{1}{\sqrt{2\pi}} e^{-i \int d^3\vec{x} \pi(\vec{x},t)\phi(\vec{x},t)}. \tag{4.44}$$

It will also be useful to define the Schrödinger picture operators and their eigenstates by:

$$\hat{\phi}(t) = e^{Ht} \hat{\phi} e^{-Ht} \tag{4.45}$$

$$\hat{\pi}(t) = e^{Ht} \hat{\pi} e^{-Ht} \tag{4.46}$$

$$\hat{\phi} \mid \phi \rangle = \phi \mid \phi \rangle, \tag{4.47}$$

$$\hat{\pi} \mid \pi \rangle = \pi \mid \pi \rangle, \tag{4.48}$$

where I used the notation that operators and states with explicit time dependence are understood to be in the Heisenberg picture, while the ones without the explicit time dependence are in the Schrödinger picture. It follows that, up to normalisation, the Heisenberg and Schrödinger picture states are related by:

$$\langle \phi(t) \mid = \langle \phi \mid e^{-Ht}, \tag{4.49}$$

$$\mid \phi(t) \rangle = e^{-Ht} \mid \phi \rangle. \tag{4.50}$$

$$\tag{4.51}$$

Note that in Euclidean space, these state vectors are not related to their duals by complex conjugation. Finally, notice that the completeness relation for Schrödinger picture operators is given by:

$$1 = \int d\phi \mid \phi \rangle \langle \phi \mid = \int d\pi \mid \pi \rangle \langle \pi \mid . \tag{4.52}$$

Consider the matrix element between Heisenberg picture ϕ states at times t and $t + \delta t$ with δt small:

$$\langle \phi'(t + \delta t) \mid \phi(t) \rangle = \langle \phi'(t) \mid e^{-H\delta t} \mid \phi(t) \rangle \tag{4.53}$$

$$= \int d\pi(t) \langle \phi'(t) \mid \pi(t) \rangle \langle \pi(t) \mid e^{-H\delta t} \mid \phi(t) \rangle. \tag{4.54}$$

Taking the Hamiltonian to be order such that all canonical conjugate fields are to the left, the field operators in the Hamiltonian can replaced by their eigenvalues in the

matrix element, resulting in:

$$\langle \phi'(t+\delta t) \mid \phi(t) \rangle = \int d\pi(t) \langle \phi'(t) \mid \pi(t) \rangle \langle \pi(t) \mid \phi(t) \rangle e^{-H(\pi(t),\phi(t))\delta t} \tag{4.55}$$

$$= \int d\pi(t) \frac{1}{2\pi} e^{-H(\pi(t),\phi(t))\delta t - i(\phi'(t)-\phi(t))\pi(t)} \tag{4.56}$$

$$\tag{4.57}$$

Assuming that the Hamiltonian is quadratic in $\pi(t)$, i.e.:

$$H(\pi, \phi) = \pi_i M_{ij}(\phi) \pi_j + V(\phi), \tag{4.58}$$

where the matrix M is symmetric and nonsingular, we can integrate over the fields π resulting in:

$$\langle \phi'(t+\delta t) \mid \phi(t) \rangle = \frac{N}{\sqrt{detM}} e^{-Q(\phi,\bar{\pi})\delta t}, \tag{4.59}$$

where I defined

$$Q(\phi, \bar{\pi}) \equiv H(\bar{\pi}(t), \phi(t)) + i \underbrace{\frac{\phi'(t) - \phi(t)}{\delta t}}_{\dot{\phi}(t)} \bar{\pi}(t), \tag{4.60}$$

N is an overall constant, whose exact value is immaterial, and $\bar{\pi}$ are the fields which minimise the exponent, i.e.:

$$\left(\frac{\delta}{\delta \pi} H(\bar{\pi}(t), \phi(t)) + i\dot{\phi}\pi(t) \right) \Big|_{\pi=\bar{\pi}} = 0, \tag{4.61}$$

$$-i\dot{\phi} = \frac{\delta}{\delta \pi} H(\pi(t), \phi(t)) \Big|_{\pi=\bar{\pi}} \tag{4.62}$$

This means that $\bar{\pi}$ can be interpreted as the momentum conjugate to $-i\phi$ and hence the function Q can be identified with the Euclidean space Lagrangian:

$$\langle \phi'(t+\delta t) \mid \phi(t) \rangle = \frac{N}{\sqrt{detM}} e^{-L(\phi,\dot{\phi})\delta t}. \tag{4.63}$$

The factor of $detM$ is, in the case of QCD, field independent, which means it can be treated as a constant. Similarly, for infinitesimally time separated matrix elements involving operators, which are independent of canonical momenta, gives:

$$\langle \phi'(t+\delta t) \mid O(\phi(t)) \mid \phi(t) \rangle = \frac{N}{\sqrt{detM}} O(\phi(t)) e^{-L(\phi,\dot{\phi})\delta t}. \tag{4.64}$$

A general matrix element can be calculated from the above by inserting complete sets of field states:

$$\langle \phi'(t_f) \mid O_1(t_{O1}) \dots O_n t_{On} \mid \phi(t_i) \rangle = \int d[\phi_1 \dots \phi_k] \langle \phi'(t_f) \mid \phi(t_i) \rangle \tag{4.65}$$

$$= N' \int \mathcal{D}\phi O_1(t_1) O_2(t_2) \dots O_n(t_n) e^{-S}, \tag{4.66}$$

where S is the Euclidean action given by:

$$S = \int dtL. \tag{4.67}$$

The normalisation constant N' can be removed by considering the ratio:

$$\frac{\langle \phi'(t_f) \mid O_1(t_{O1}) \dots O_n(t_{On}) \mid \phi(t_i) \rangle}{\langle \phi'(t_f) \mid \phi(t_i) \rangle} = \frac{\int \mathcal{D}\phi O_1(t_1) O_2(t_2) \dots O_n(t_n) e^{-S}}{\int \mathcal{D}\phi e^{-S}}. \tag{4.68}$$

The left-hand side of the above equation can be rewritten in terms of Schrödinger picture operators and their corresponding eigenstates:

$$\frac{\langle \phi'(t_f) \mid O_1(t_{O1}) \dots O_n(t_{On}) \mid \phi(t_i) \rangle}{\langle \phi'(t_f) \mid \phi(t_i) \rangle} = \frac{\langle \phi' \mid e^{-H(t_f - t_1)} O_1 e^{-H(t_1 - t_2)} \dots O_n e^{-H(t_n - t_i)} \mid \phi \rangle}{\langle \phi' \mid e^{-HT} \mid \phi \rangle} \tag{4.69}$$

When a time extent is finite, $0 \leq t \leq T$, we can choose $t_i = 0$ and $t_f = T$. We also need to choose the boundary condition in the time direction. In this work we will be using periodic boundary conditions, which means that, instead of choosing a fixed value for initial and final states, we demand these states to be equal and integrate over all possible field configurations:

$$C(t_1, t_2, \dots, t_n) \equiv \frac{\int d\phi \langle \phi \mid e^{-H(t_f - t_1)} O_1 e^{-H(t_1 - t_2)} \dots O_n e^{-H(t_n - t_i)} \mid \phi \rangle}{d\phi \langle \phi \mid e^{-HT} \mid \phi \rangle}. \tag{4.70}$$

To relate these correlation functions to Green's functions (and hence the S-matrix), we need to re-express them in terms of matrix elements of physical (unitary) states. This can be done by inserting the complete set of unitary states $1 = \sum\!\!\!\!\!\!\int_n \mid n \rangle \langle n \mid$ (the symbol $\sum\!\!\!\!\!\!\int$ denotes summation over discrete degrees of freedom and an integral over continuous ones) and using the completeness relation 4.52 and the orthonormality :

$$C(t_1, t_2, \dots, t_k) = \frac{\int d\phi \sum\!\!\!\!\!\!\int_{m,n} \langle \phi \mid m \rangle \langle m \mid e^{-H(T - t_1)} O_1 e^{-H(t_1 - t_2)} \dots O_k e^{-H(t_k)} \mid n \rangle \langle n \mid \phi \rangle}{d\phi \sum\!\!\!\!\!\!\int_{m,n} \langle \phi \mid m \rangle \langle m \mid e^{-HT} \mid n \rangle \langle n \mid \phi \rangle} \tag{4.71}$$

$$= \frac{\sum\!\!\!\!\!\!\int_n \langle n \mid e^{-H(T - t_1)} O_1 e^{-H(t_1 - t_2)} \dots O_k e^{-H(t_k)} \mid n \rangle}{\sum\!\!\!\!\!\!\int_n \langle n \mid e^{-HT} \mid n \rangle} \tag{4.72}$$

$$= \frac{\sum\!\!\!\!\!\!\int_n \langle n \mid O_1 e^{-H(t_1 - t_2)} \dots O_k \mid n \rangle e^{-E_n(T - t_1 + t_k)}}{\sum\!\!\!\!\!\!\int_n e^{-E_n T}}. \tag{4.73}$$

This sum contains the desired Green's function contribution $\langle 0 \mid O_1(t_1) O_2(t_2) \dots O_n(t_n) \mid 0 \rangle$, which will furthermore be the dominant contribution provided that $T - t_1 + t_n$ is large.

Some comments:

- Fermionic contributions
  The above derivation is only valid for bosonic degrees of freedom. It can be shown that the path integral result for fermions is similar but with two main differences. The first one is that that the eigenvalues of field operators must be anticommuting (Grassmann) numbers. The second difference is that in equation 4.64 the factor of $detM^{-1/2}$ is replaced by $detM$. Again, in QCD this factor is field independent and will cancel between the numerator and the denominator.

- Vacuum energy
  We can insert complete sets of states between each pair of operators in Eq. 4.73 and divide by the lowest energy state, which is the vacuum energy E_{vac}:

$$\frac{\not\int_{n,n_1,\ldots,n_{k-1}} \langle n \mid O_1 \mid n_1\rangle \ldots \langle n_{k-1} \mid O_k \mid n\rangle e^{-(E_n-E_{vac})(T-t_1+t_k)-\ldots-(E_{k-1}-E_{vac})(t_{k-1})}}{1+\not\int_{n\neq vac} e^{-(E_n-E_{vac})T}}. \tag{4.74}$$

  It is clear that the correlation function only depends on differences of energies and the vacuum energy. Hence we can, without loss of generality, take $E_{vac} = 0$.

- Boundary conditions
  In the above derivation I assumed periodic boundary conditions in time direction, so that $\mid \phi(0)\rangle$ has the same eigenvalues as $\mid \phi(T)\rangle$. I will now describe how antiperiodic and periodic + antiperiodic boundary conditions fit this picture. For antiperiodic boundary conditions we have instead of Eq. (4.70)

$$C(t_1,t_2,\ldots,t_n) \equiv \frac{\int d\phi \langle -\phi \mid e^{-H(t_f-t_1)} O_1 e^{-H(t_1-t_2)} \ldots O_n e^{-H(t_n-t_i)} \mid \phi\rangle}{d\phi\langle -\phi \mid e^{-HT} \mid \phi\rangle}. \tag{4.75}$$

  We can define an operator P_ϕ which flips the sign of the field ϕ, i.e. $P_\phi \mid phi\rangle = \mid -\phi\rangle$. Because the Hamiltonian is quadratic in ϕ, the operator P_ϕ commutes with the Hamiltonian and because $P_\phi^2 = 1$ we have $P_\phi \mid n\rangle = \eta_n \mid n\rangle = \pm \mid n\rangle$, which gives

$$\frac{\not\int_n \langle n \mid \eta_n O_1 e^{-H(t_1-t_2)} \ldots O_k \mid n\rangle e^{-E_n(T-t_1+t_k)}}{\not\int_n \eta_n e^{-E_n T}}. \tag{4.76}$$

  The effect of η_n has no effect on the time dependence of the correlation function, but it does affect the matrix elements.

  More interestingly, we can use P+A boundary conditions in the time direction. In this case for any field ϕ we have

$$\phi(t+T) = \phi(t) + (-\phi(t)) = 0 \tag{4.77}$$

$$\phi(t+2T) = \phi(t). \tag{4.78}$$

Then, between T and 2T, Eq. (4.63) tells us that $\langle\phi(t+\delta t \mid \phi(t)\rangle$ is constant in this interval. Hence

$$\langle\phi_{P+A}(T) \mid O_1(t_1)\dots O_n(t_n) \mid \phi_{P+A}(0)\rangle = \langle\phi_{P+A}(2T) \mid O_1(t_1)\dots O_n(t_n) \mid \phi_{P+A}(0)\rangle \tag{4.79}$$

where the right hand side satisfies periodic boundary conditions by Eq. (4.78) and hence

$$C(t_1,t_2,\dots,t_k)_{P+A} = \frac{\sum\!\!\!\!\!\!\int_n \langle n \mid O_1 e^{-H(t_1-t_2)}\dots O_k \mid n\rangle e^{-E_n(2T-t_1+t_k)}}{\sum\!\!\!\!\!\!\int_n e^{-2E_nT}}. \tag{4.80}$$

The conclusion is that P+A boundary condition have the effect of doubling the time extent and hence suppressing the finite-time effects.

As an example, let's consider a kaon two-point function, defined as:

$$C_K(t) \equiv \langle O_K^\dagger(t) O_K(0)\rangle, \tag{4.81}$$

where O_K is a pseudoscalar operator which have the same quantum numbers as K^0, i.e.:

$$\langle K^0 \mid O_K(t) \mid 0\rangle \neq 0. \tag{4.82}$$

Applying Eq. 4.73, the dominant contributions are:

$$C_K(t) = \langle 0 \mid O_K^\dagger \mid K^0\rangle\langle K^0 \mid O_K \mid 0\rangle e^{-m_K t} + \langle \bar{K}^0 \mid O_K^\dagger \mid 0\rangle\langle 0 \mid O_K \mid \bar{K}^0\rangle e^{-m_K(T-t)}. \tag{4.83}$$

All other contributions are suppressed by a factor smaller than $e^{-m_\pi T}$. The second matrix element can be related to the first one by charge conjugation symmetry:

$$\langle \bar{K}^0 \mid O_K^\dagger \mid 0\rangle \to \langle K^0 \mid O_K^{c\dagger} \mid 0\rangle e^{i(\xi_k+\xi_O)}, \tag{4.84}$$

$$\langle 0 \mid O_K \mid \bar{K}^0\rangle \to \langle 0 \mid O_K^c \mid K^0\rangle e^{-i(\xi_k+\xi_O)}. \tag{4.85}$$

The C-phases cancel in the product of matrix elements and, assuming that the operator transforms as $O_K^c = O_K^\dagger$, the correlation function becomes:

$$C_K(t) = \left|\langle K^0 \mid O_K \mid 0\rangle\right|^2 \left(e^{-m_K t} + e^{-m_K(T-t)}\right) \tag{4.86}$$

An example of an interpolating operator with this property is

$$O_K = \sum_{\mathbf{x},\mathbf{y}} \bar{s}(\mathbf{x},t)\gamma^5 u(\mathbf{y},t). \tag{4.87}$$

Similarly, a two-pion correlation function behaves as

$$C_{\pi\pi}(t) = |N_{\pi\pi}|^2 \left(e^{-E_{\pi\pi}t} + e^{-E_{\pi\pi}(T-t)}\right) + C \tag{4.88}$$

where the constants are explicitly given by

$$N_{\pi\pi} \equiv \langle \pi\pi \mid O_{\pi\pi} \mid 0 \rangle \tag{4.89}$$

$$C \equiv |\langle \pi \mid O_{\pi\pi} \mid \pi \rangle|^2 \, e^{-m_\pi T}. \tag{4.90}$$

4.4 Correlation functions

The correlation functions discussed in the previous section can be written as:

$$\langle O(U, \psi, \bar{\psi}) \rangle = \frac{1}{Z} \int [dU][d\psi][d\bar{\psi}] O(U, \psi, \bar{\psi}) e^{-S[U,\psi,\bar{\psi}]} \tag{4.91}$$

for some function of the fields O. The normalisation Z is chosen such that $\langle 1 \rangle = 1$. The action can be split into a fermionic part and a gauge field part $S = S_{ferm} + S_{gauge}$. The fermionic part has the form $\sum_\alpha \bar{\psi}_{i\alpha} D_{ij\alpha} \psi_{j\alpha}$, where i and j are combined spin and colour indices and α is a flavour index. Integrating out the fermionic degrees of freedom gives:

$$\langle O(U, \psi, \bar{\psi}) \rangle = \frac{1}{Z} \int [dU] \prod_\alpha \det D_{ij\alpha}(U) O'(U, D^{-1}(U)) e^{-S_{gauge}} \tag{4.92}$$

where O' denotes an operator which consists of the sum of all the possible Wick contractions of fermion and antifermion using $D^{-1}(U)$ as a propagator. This means that, to proceed with the calculation, we need to invert the fermion matrix D as well as calculate the the fermionic determinant $\det D$. Unfortunately, the latter tends to be prohibitively expensive to calculate. In the early days of lattice QCD, a common technique was to set the fermionic determinant to 1 (known as 'quenched approximation'). This has an effect of neglecting all the fermion loops in the sea. We can do better by defining a probability density function, which includes the fermionic determinants:

$$P(U) = \frac{1}{Z} \prod_\alpha \det D_\alpha(U) e^{-S_{gauge}} \tag{4.93}$$

which can be interpreted as a probability assuming that the product of fermionic determinants is positive definite. Gauge configurations can be generated according to the desired probability distribution by using a Markov chain Monte Carlo (MCMC) process.

Consider a sequence of gauge configurations U_n constructed in a stochastic way so that the probability that $U_n = U'$ given that $U_{n-1} = U$ is given by $T(U \to U')$, which depends on the initial and final configuration, but not on the index n. The transition probability satisfies $\sum_{U'} T(U \to U') = 1$. Starting from an arbitrary gauge configuration, this procedure will eventually reach equilibrium state, where the probability of reaching any

gauge configuration U' is equal to the probability of going out of it:

$$\sum_U T(U \to U')P(U) = \sum_U T(U' \to U)P(U') \tag{4.94}$$

$$= P(U'), \tag{4.95}$$

where $P(U)$ is the probability that $U_{n-1} = U$. This equation indicates that at equilibrium the probability distribution is fixed at $P(U)$. Our objective now is to find the transition probability $T(U \to U')$, which corresponds to the correct probability distribution $P(U)$. One way of achieving this is by noting that 4.94 can be satisfied by demanding that

$$T(U \to U')P(U) = T(U' \to U)P(U') \tag{4.96}$$

which is known as the detailed balance condition, which can be satisfied by choosing

$$T(U \to U') = \min\left(1, \frac{P(U')}{P(U)}\right). \tag{4.97}$$

To summarise, the MCMC procedure is as follows:

1. Start with an arbitrary gauge configuration U_0.
2. Propose a change to some other gauge configuration U_1.
3. Accept the change with probability $\min\left(1, \frac{P(U_1)}{P(U_0)}\right)$ with $P(U)$ given by Eq. (4.93). Repeat this step until acceptance is reached.
4. Repeat this procedure to obtain $U_2, U_3, \cdots, U_n$.
5. After a sufficiently large number of steps this procedure will reach equilibrium ('thermalise') at which point we can start to take measurements.

There are several options available for choosing an update in step 2, the most common being the Hybrid Monte Carlo approach [33].

For future reference, I will introduce some nomenclature. The quantity measured by index n is the Monte Carlo time measured in Molecular Dynamics (MD) units. The gauge configurations generated in the MCMC procedure are referred to as 'trajectories'. Not all trajectories are used for the measurements and ones that are are referred to as 'configurations'. For example, 80 configurations measured every 20 MD units corresponds to 1600 trajectories in addition to any trajectories used for thermalisation.

4.5 Propagator sources

The evaluation of Eq. (4.93) requires the knowledge of the inverse Dirac operator, which is a square matrix with the side $L^3 \times T \times N_{\text{spins}} \times N_{\text{colours}}$. Performing such an inversion for every quark field on every gauge configuration would be too expensive. However in practice we rarely need the value of the inverse Dirac matrix.

Suppose we choose our interpolating operators such that their dependence on the fermion fields comes through linear combinations of the form

$$\sum_{\mathbf{x}} \eta(\mathbf{x})\psi(\mathbf{x},t). \tag{4.98}$$

Then Wick contracting will give contributions of the form

$$D_f^{-1}(t) \equiv \sum_{\mathbf{x}} \eta(\mathbf{x}) D^{-1}(\mathbf{x},t). \tag{4.99}$$

Hence it is sufficient to only calculate contributions of this form. This can be done by inverting

$$\sum_{y} D(x-y) D_f^{-1}(t) = \eta(\mathbf{x}). \tag{4.100}$$

The matrix $D_f^{-1}(t)$ is a $N_{spins} \times N_{\text{colours}}$ by $L^3 \times T \times N_{\text{spins}} \times N_{\text{colours}}$ rectangular matrix, which is much cheaper to calculate and store than the full D^{-1} matrix. The choice of the source function $\eta(x)$ is non-unique and different choices will correspond to different overlaps of the interpolating operators with physical states. Some of the common choices for the source function are:

- Point sources $\eta(\mathbf{x}) = \delta(\mathbf{x} - \mathbf{x}_0)$
- Wall sources $\eta(\mathbf{x}) = 1$
- Momentum wall sources $\eta(\mathbf{x}) = e^{i\mathbf{p}\cdot\mathbf{x}}$
- Stochastic ('noise') wall sources, where $\eta(x)$ is a random number satisfying $\langle \eta^*(x)\eta(y)\rangle_\eta = \delta(x-y)$, where the angle brackets denote an average over different random number configurations. An example is a $Z_2 \times Z_2$ wall source with $\eta(x) = \frac{1}{\sqrt{2}}(\pm 1 \pm i)$.

It is not known *a priori* what choice of propagator sources will give the best overlap with the desired physical state. A good guideline is to use the interpolating operators which are the creation operators for the desired states in the free theory. For example, to create a $\mid \pi^+(\mathbf{p})\pi^+(-\mathbf{p})\rangle$ state in the free theory we would use:

$$O_{\pi^+\pi^+}(t) = (\bar{d}_p \gamma^5 u)(\bar{d}_{-p}\gamma^5 u), \tag{4.101}$$

where u fields are summed with wall source and d_q are summed with the momentum wall source with momentum q. At first sight this approach requires three inversions: one for the u field and one for each of the d fields. We can save one inversion by using cosine wall sources for the d quarks defined by

$$\eta_{\cos}(t) = \cos(p_x x)\cos(p_y y)\cos(p_z z) \tag{4.102}$$

Noting that $\cos x = (e^{ix} + e^{-ix})/2$ we can see that this source will contain all 8 possible momentum combinations of the form $(\pm 1, \pm 1, \pm 1)$. Using two such sources and projecting the zero total momentum at the sink results in an operator of the form

$$O_{\pi^+\pi^+} = \sum_{p\in\{\pm 1,\pm 1,\pm 1\}} (\bar{d}_p\gamma^5 u)(\bar{d}_{-p}\gamma^5 u). \tag{4.103}$$

Comparing with Eq. (4.39) we can see that this operator is in the A_1^+ irreducible representation of the cubic group, which is convenient for extracting the s-wave phase shift.

4.6 Two pion correlation function

The two-pion correlation is defined as

$$C_{\pi\pi}(t) = \langle O^\dagger_{\pi\pi}(t) O_{\pi\pi}(0)\rangle. \tag{4.104}$$

The $O_{\pi\pi}(t)$ operators in our case are the two-meson operators of the form $[\bar{l}\gamma^5 l][\bar{l}\gamma^5 l](t)$ and the correct isospin projection is achieved by choosing the correct linear combination of contractions, as shown below. In the case of $I = 2$ scattering we use the two-pion interpolating operator constructed out of two pseudoscalar operators with the same quantum numbers as the π^+ meson (the reson will become clear in the following section)

$$O_{\pi\pi}(t) = \left[\bar{d}\gamma^5 u\right]\left[\bar{d}\gamma^5 u\right](t) \tag{4.105}$$

with the d fields multipled by the cosine source described in the previous section.

We only need to use cosine source operator at the source time slice. This is because Eq. (4.103) combined with hypercubic symmetry imply that

$$\langle O_\pi(\mathbf{p}, t) O_\pi(-\mathbf{p}, t) O^{cos}_{\pi\pi}(\mathbf{p}, 0)\rangle \tag{4.106}$$

with $O_\pi(\mathbf{p}, t) = \bar{u}\gamma^5 d_{\mathbf{p}}(t)$ and $O^{cos}_{\pi\pi}$ denotes the cosine source interpolator is equivalent to the correlation function with cosine source and cosine sink.

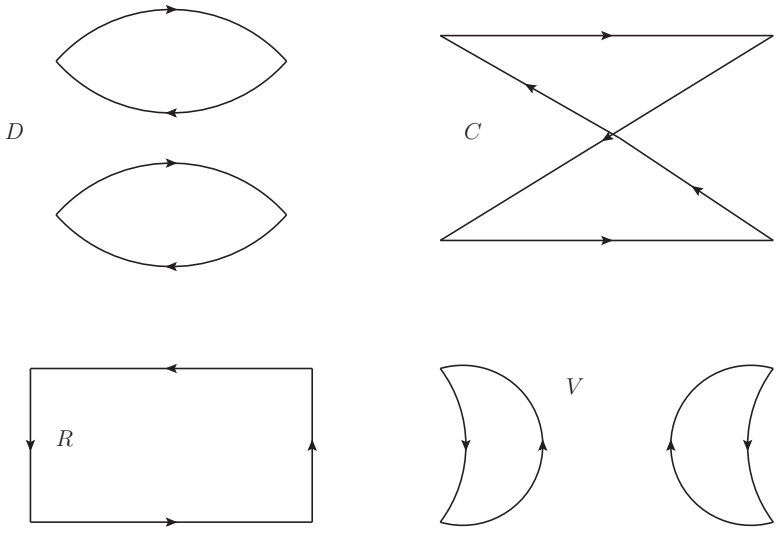

Figure 4.3: Contractions contributing to two pion correlation function

The two pion correlation function has therefore the following time behaviour:

$$C_{\pi\pi}(t) = N_{\pi\pi}(e^{-E_{\pi\pi}t} + e^{-E_{\pi\pi}(T-t)}) + C \tag{4.107}$$

There is an additional complication related to extracting two pion energy. Consider for example the following time ordering:

$$\langle 0 \mid O^{\dagger}_{\pi\pi}(t) O_{\pi\pi}(0) \mid 0 \rangle \xrightarrow[t\to\infty]{T\to\infty} \sum_n \langle 0 \mid O^{\dagger}_{\pi\pi} \mid n \rangle \langle n \mid O_{\pi\pi} \mid 0 \rangle e^{-E_n t} \tag{4.108}$$

Taking a large t limit gives:

- For $(\pi\pi)_{I=2}$ the lowest energy state corresponds to two pions with total momentum 0, which is not a physical contribution. A solution to this problem is discussed in section 4.7.
- $(\pi\pi)_{I=0}$ state has the same quantum numbers as the vacuum, which means that in order to obtain the state with the desired energy and normalisation constant, we first need to subtract the vacuum state. This can be done by subtracting appropriate diagrams from vacuum contractions as discussed below. After subtraction, the problem of zero momentum pions persists and remains the major limitation in determining the $\mathrm{Re}(A_0)$ amplitude at physical kinematics.

To calculate $C_{(\pi\pi)I=2/0}$ which will be used to extract the corresponding two pion energies, we consider the states given by equations 2.59 and 2.66 Next we calculate the Wick contractions that contribute to the amplitude. There are 4 different types of contractions as shown in figure 4.3.

Contributions to each of the amplitudes can be shown to be:

$$ {}_s\langle\pi^+\pi^- \mid \pi^+\pi^-\rangle_s = D - 2R + V \tag{4.109}$$

$$ {}_s\langle\pi^+\pi^- \mid \pi^0\pi^0\rangle = -C + 2R - V \tag{4.110}$$

$$ \langle\pi^0\pi^0 \mid \pi^0\pi^0\rangle = 2D - C - 2R + V \tag{4.111}$$

The index 's' means that the state has been symmetrised:

$$ \mid \pi^+\pi^-_s\rangle = \frac{1}{2}\left(\mid \pi^+(\mathbf{p})\pi^-(-\mathbf{p})\rangle + \mid \pi^-(\mathbf{p})\pi^+(-\mathbf{p})\rangle\right) \tag{4.112}$$

This leads to:

$$ C^{I=2}_{\pi\pi} = 2D - 2C \tag{4.113}$$

$$ C^{I=0}_{\pi\pi} = 2D + C - 6R + 3V \tag{4.114}$$

Note that the R and V contractions do not contribute to the I=2 scattering, which is required by the isospin symmetry.

Presence of the intermediate vacuum state in the V diagram leads to the following complication. Consider insertion of the complete set of vacuum (i.e. gluon) energy states.

$$ V_0 = \sum_n \langle 0 \mid O^\dagger_{\pi\pi} \mid n\rangle\langle n \mid O_{\pi\pi} \mid 0\rangle \xrightarrow{t\to\infty} |\langle 0 \mid O_{\pi\pi} \mid 0\rangle|^2 \tag{4.115}$$

The lowest energy contribution corresponds to the product of two non-interacting pieces. This is not the contribution that we are interested in, and therefore it has to be subtracted explicitly:

$$ V = V_0 - |\langle 0 \mid O_{\pi\pi} \mid 0\rangle|^2 \tag{4.116}$$

This is a difference of two large numbers, which results in large error bars that introduce significant uncertainty to I=0 measurement.

4.7 $K \to \pi\pi$ three point correlation functions

The three point correlation function is defined as:

$$ C_i(0, t_{op}, t_{\pi\pi}) = \langle O_{\pi\pi}(t_{\pi\pi}) Q_i(t_{op} O_K(0)\rangle, \tag{4.117}$$

where O_K and $O_{\pi\pi}$ are the kaon and pion interpolating operators and Q_i are the four-fermion operators in the operator product expansion. This correlation function has the time dependence (assuming $t_{\pi\pi} - t_{op}$, t_{op} and $T - t_{\pi\pi}$ are large enough):

$$C_i(0, t_{op}, t_{\pi\pi}) = \langle \pi\pi_I(t_{\pi\pi}, \mathbf{0}) \mid Q_i(t_{op}) \mid K_I(0, \mathbf{0}) \rangle \tag{4.118}$$

$$= N_{\pi\pi} N_K M_i e^{-(m_K - E_{\pi\pi})t_{op}} e^{-E_{\pi\pi} t_{\pi\pi}} \tag{4.119}$$

with

$$N_{\pi\pi} = \langle 0 \mid O_{\pi\pi} \mid \pi\pi \rangle \tag{4.120}$$

$$N_K = \langle 0 \mid O_K \mid K \rangle. \tag{4.121}$$

In 4.119 we have inserted the complete sets of energy eigenstates of two pion and kaon and took the large time limit. The 'around the world' contributions (i.e. terms proportional to $e^{-E_n T}$ for n other than vacuum in Eq. 4.70) was ignored for simplicity. The phases of N_K, $N_{\pi\pi}$ and M_i are chosen so that all these quantities are real. The energies $E_{\pi\pi}$ and m_K as well as the normalisation constants N_K and $N_{\pi\pi}$ can be obtained from their respective correlation functions in Eq. (4.86) and Eq. (4.107). The matrix elements can then be calculated by taking an appropriate exponential fit.

The major difficulty of this calculation is obtaining pions in a final state with physical momenta. The two pion energy $E_{\pi\pi}$ in equation 4.119 corresponds to the lowest energy state where two pions have a total momentum 0, i.e. a state where both pions are at rest. Naively one might think of calculating the two pion energy by simply subtracting the unphysical ground state. The main limitation of this approach is that in order to reach physical pion momenta a lattice of size $aL = \frac{2\pi}{p_\pi} \approx 6$fm is required, which is larger than any of our ensembles generated so far. Furthermore, extraction of excited states tends to be more noisy than calculating the energy of the ground state. We can avoid the necessity of multi-exponential fits to extract the excited state contribution by utilising the technique suggested in [34; 35] and applied successfully in our original calculation of A_2 [36; 12] and described below.

In $\Delta I = 3/2$ there is an elegant solution to the above problem. Consider twisted boundary condition defined as:

$$\phi(x + L) = e^{i\theta}\phi(x) \tag{4.122}$$

Taking a Fourier transform we find that:

$$\tilde{\phi}(p) e^{ip(x+L)} = \tilde{\phi}(p) e^{i(\theta + px)} \tag{4.123}$$

This condition can be satisfied for arbitrary fields provided that

$$p = \frac{\theta + 2\pi}{L} n, \quad n \in Z \tag{4.124}$$

Since we are interested in the centre-of-mass frame, the most suitable choice of twist angle θ is π corresponding to antiperiodic boundary conditions. Our objective is to construct pions that can have a momentum of $\pm\pi/L$ eliminating the problem of pions at rest and making it possible to study the decay on lattices as small as 3fm.

To do this we impose periodic boundary conditions on u and s quarks and antiperiodic boundary conditions on d quarks. As a consequence, both π^+ and π^- mesons can gain the desired momenta, but π^0 in its lowest energy state will be at rest. In $\Delta I = 3/2$ case this problem can be solved elegantly by applying the Wigner-Eckart theorem. The Wigner-Eckart theorem relates the SU(2) matrix elements of a tensor operator to reduced matrix elements

$$\langle J, M \mid O^j_m \mid j', m' \rangle = C(Jjj', Mmm') N_{Jjj'} \tag{4.125}$$

where $\mid j, m\rangle$ are in the usual representation of SU(2) where m is the eigenvalue of the J_3 operator which in a given representation is within range $-j \leq m \leq j$, $C(J, M; jj'mm')$ are the Clebsch-Gordan coefficients and $N_{Jjj'}$ is a constant. The proof is standard [37; 38] and relies on the observation that $O^j_m \mid j'm'\rangle$ transforms under the direct product representation and therefore must satisfy

$$\mid J, M\rangle = N_{Jjj'} \sum_{mm'} C(Jjj', Mmm') O^j_m \mid j'm'\rangle \tag{4.126}$$

The proportionality constant $N_{Jjj'}$ can not depend on the values of m and m', because that would spoil the transformation properties when both sides of the equation are acted on with a raising or lowering operator. The above equation can be inverted by using the orthogonality property of Clebsch-Gordan coefficients

$$\sum_{J,M} C(Jjj', Mm_1m_2) C(Jjj', Mm_1'm_2') = \delta_{m_1m_1'} \delta_{m_2m_2'} \tag{4.127}$$

and contracted with $\langle J, M \mid$ to recover the Wigner-Eckart theorem.

In our case, we can use the Wigner-Eckart theorem for the isospin to relate $K \to (\pi\pi)_{I=2}$ matrix elements with different values of I_3 to each other. Specifically:

$$\underbrace{\langle (\pi\pi)^{I=2}_{I_3=1} \mid}_{\frac{1}{\sqrt{2}}(\langle\pi^+\pi^0\mid + \langle\pi^0\pi^+\mid)} Q^{\Delta I=3/2}_{\Delta I_3=1/2,i} \mid K^+\rangle = \frac{3}{2} \underbrace{\langle (\pi\pi)^{I=2}_{I_3=2} \mid}_{\langle\pi^+\pi^+\mid} Q^{\Delta I=3/2}_{\Delta I_3=3/2,i} \mid K^+\rangle \,. \tag{4.128}$$

We can therefore relate the physical correlation functions to unphysical ones which are easy to compute on a lattice. One can be worried that imposing different boundary conditions on each of the quarks breaks the isospin symmetry and as a consequence the

outgoing two pion state will be a mixture of states with different isospins. Fortunately, the only isospin state that includes $\pi^+\pi^+$ is $\mid I = 2, I_3 = 2\rangle$, so it can not mix with other states even if the isospin is broken. The $Q^{\Delta I=3/2}_{\Delta I_3=3/2}$ can be obtained from $Q^{\Delta I=3/2}_{\Delta I_3=1/2}$ by applying an isospin raising operator. They are of the form $Q = \sqrt{3}Q'$ with Q' given by:

$$Q'^{(27,1)} = (\bar{s}_i d_i)_L (\bar{u}_j d_j)_L \tag{4.129}$$

$$Q'^{(8,8)} = (\bar{s}_i d_i)_L (\bar{u}_j d_j)_R \tag{4.130}$$

$$Q'^{(8,8)mx} = (\bar{s}_i d_j)_L (\bar{u}_j d_i)_R \tag{4.131}$$

In $\Delta I = 3/2$ case, we calculate the $\langle \pi^+\pi^+ \mid O' \mid K^+ \rangle$ matrix elements which can be related to the $K^0 \to (\pi\pi)_{I=2}$ matrix elements by:

$$M_i^{\Delta I=3/2} \equiv \langle (\pi\pi)^{I=2}_{I_3=0} \mid Q_i \mid K^0 \rangle = \sqrt{\frac{3}{2}} \langle \pi^+\pi^+ \mid Q'_i \mid K^+ \rangle \tag{4.132}$$

Contractions contributing to the above matrix elements are shown in figure 4.4. In this figure, the four-fermion operator is represented by a pair of points to make the spin contractions explicit. The Roman letters indicate colours of quarks entering the four-fermion operator. In the figure contractions C_1,C_2,C_5 and C_7 have the LL operator structure and the remaining ones have the LR structure. Note that because of the left-left Fierz identity Eq. (2.85) we have $C_1 = -C_6$ and $C_2 = -C_5$.

Explicitly we have:

$$M^{\Delta I=3/2}_{(27,1)} = 2\,(C_1 - C_5) \tag{4.133}$$

$$M^{\Delta I=3/2}_{(8,8)} = 2\,(C_3 - C_7) \tag{4.134}$$

$$M^{\Delta I=3/2}_{(8,8)mx} = 2\,(C_4 - C_8) \tag{4.135}$$

We can now write the expressions for the A_2 amplitude in terms of $K^0 \to (\pi\pi)_{I=2}$ ($M_i^{K^0}$), $K^+ \to \pi^+\pi^-$ ($M_i^{K^+}$) and $K^+ \to \pi^+\pi^+$ (M_i) matrix elements:

$$A_2 = \frac{G_F}{\sqrt{2}} V^*_{ud} V_{us} \sum_i C_i(\mu) \left(\frac{1}{\sqrt{2}} M_i^{K^0} \right) \tag{4.136}$$

$$= \frac{G_F}{\sqrt{2}} V^*_{ud} V_{us} \sum_i C_i(\mu) \left(\frac{1}{\sqrt{3}} M_i^{K^+} \right) \tag{4.137}$$

$$= \frac{G_F}{\sqrt{2}} V^*_{ud} V_{us} \sum_i C_i(\mu) \left(\frac{\sqrt{3}}{2} M_i \right). \tag{4.138}$$

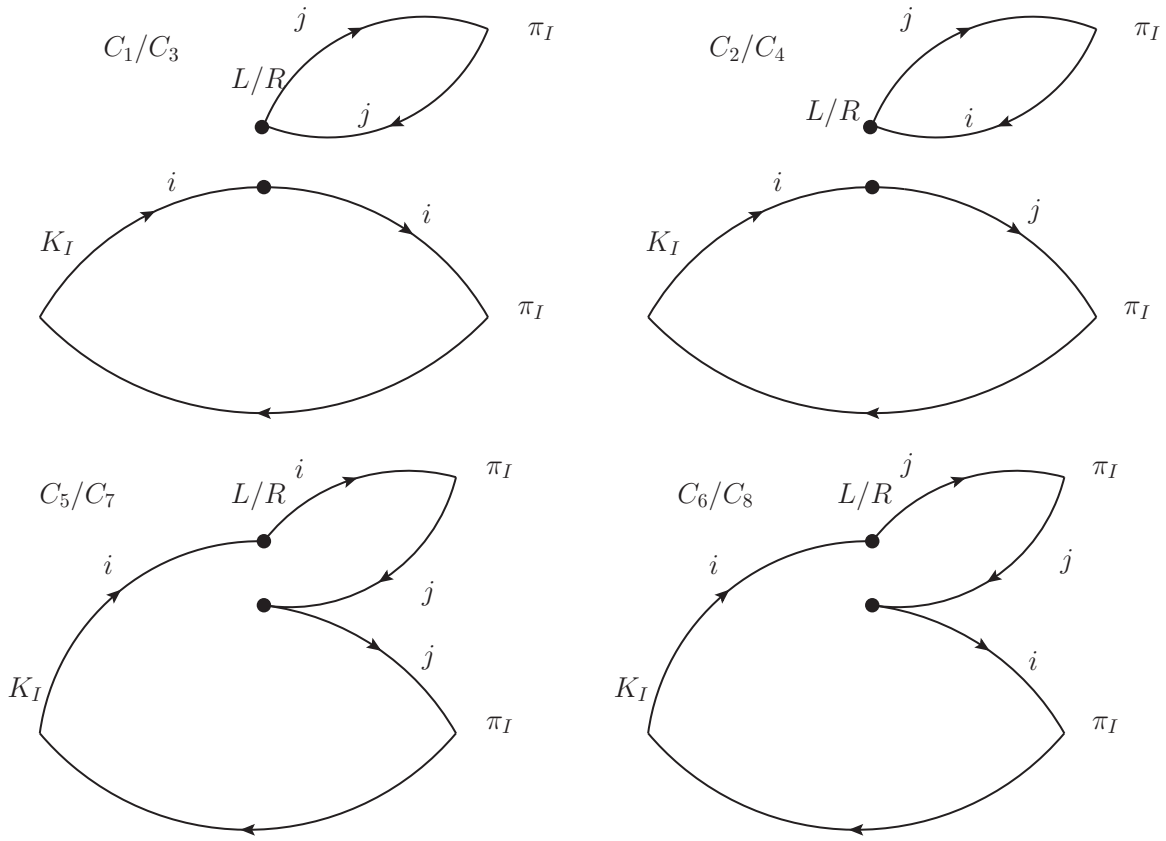

Figure 4.4: $\Delta I = 3/2$ $K \to \pi\pi$ contractions

with

$$M_i^{K^0} \equiv \langle (\pi\pi)^{I=2}_{I_3=0} \mid Q^{\Delta I=3/2}_{\Delta I_3=1/2,i} \mid K^0 \rangle \tag{4.139}$$

$$M_i^{K^+} \equiv \langle (\pi\pi)^{I=2}_{I_3=1} \mid Q^{\Delta I=3/2}_{\Delta I_3=1/2,i} \mid K^+ \rangle \tag{4.140}$$

$$M_i \equiv \langle (\pi\pi)^{I=2}_{I_3=2} \mid Q'^{\Delta I=3/2}_{\Delta I_3=3/2,i} \mid K^+ \rangle. \tag{4.141}$$

The relative factor between the two expressions is due to the different Clebsch-Gordan coefficients.

4.8 All mode averaging

All mode averaging (AMA) is a procedure which allows use to extract maximum amount of information in reasonable computing time. This is achieved by averaging each correlation function over all source and sink times. Normally this procedure would be prohibitively expensive, since it would involve propagator inversions at each time slice. We can avoid this problem by doing the inversions on a selected subset of time slices

('exact' solves) and calculating an estimate on all time slices ('sloppy' solve). A residual is then calculated on time slices that contain exact solves, and is subsequently used to correct the remaining sloppy solves. This procedure is described in [39].

All mode averaging takes about 3 times longer than non-AMA calculation, but results in an error reduction by a factor of 4-5. [40]

4.9 Statistical analysis

In this section we describe main tools used in statistical analysis of the data.

4.9.1 Fitting

As described in chapters 4.6 and 4.7 we often need to fit the data to fit some curve, in our case it is typically a cosh fit. To do this we need to define a notion of a 'quality' of a fit. For an uncorrelated fit such quantity is the χ^2:

$$\chi^2 \equiv \sum_i \frac{(y_i - f(x_i))^2}{\sigma_i^2} \tag{4.142}$$

where y is the dependent variable (in our case the correlation function function), x is the independent variable (in our case the time), σ_i is the standard deviation of the ith measurement and f is the function we are fitting to.

Clearly, the better the data agrees with the prediction given by function f the lower the value of χ^2 will be.

In our case, the function f is determined up to some number of parameters (e.g. N_π and m_π for pion 2-point function). We are interested in values of these parameters that minimise χ^2. The problem is therefore reduced to the least squares fitting.

Typically one expects the value of χ^2 to be equal to the number of degrees of freedom of the theory. A higher value means that the data does not fit the expected curve very well and a lower value indicates that the size of the error bars has been overestimated.

The above analysis does not take into account correlations between values y_i (i.e. the values of correlation function at different time slices). To take them into account we can do a correlated fit.

To do this, we start by evaluating the covariance matrix:

$$Cov_{ij} = (y_i - \langle y_i \rangle)(y_j - \langle y_j \rangle) \tag{4.143}$$

where angle brackets denote the gauge average.

The correlated χ^2 is then given by:

$$\chi^2_{corr} \equiv (y_i - f(x_i))Cov^{-1}_{ij}(y_j - f(x_j)) \tag{4.144}$$

In this project we used exclusively uncorrelated fits, because practice shows that the difference between the two approaches tends to be small.

4.9.2 Error calculation

To get a reliable estimate on the error of any gauge averaged value, we need to take correlations between gauge configurations into account. There are two common procedures which are used to achieve that: bootstrap and jackknife.

In bootstrap the resampling is done by averaging over sets of configurations randomly chosen (with replacement) from the original set of configurations. Using this procedure we can generate a large number of resampled values, which can then be used to calculate the errors using:

$$\sigma^2_B = \frac{N_B - 1}{N_B}\left(\langle \tilde{y}^{B2}_i \rangle - \langle \tilde{y}^B_i \rangle^2\right) \tag{4.145}$$

where $\tilde{y}^B_i = \frac{1}{M_B}\sum_1^{M_B} \mathrm{rand}(y_i)$. In these equations N_B is the number of bootstrap samples, M_B is bootstrap sample size and the rand function chooses a random gauge configuration. Bootstrap resampling can be used to calculate the errors, but it is rather slow.

The jackknife procedure provides a faster alternative to the bootstrap resampling. In jackknife resampling we calculate averages over subsets of gauge configurations, typically consisting of the set of all configurations with one configuration removed. Each quantity is evaluated for each subset of gauge configurations, and the error is given by:

$$\sigma^2_J = (N-1)\left(\langle \tilde{y}^2_i \rangle - \langle \tilde{y}_i \rangle^2\right) \tag{4.146}$$

where

$$\tilde{y}_i = \frac{1}{N}\sum_{j \neq i} y_j. \tag{4.147}$$

4.10 Analytic continuation to Minkowski spacetime

The correlation functions calculated so far were all in Euclidean space-time. However the real-world physics is all in Minkowski spacetime. We therefore need to analytically continue our results. It was shown by Osterwalder and Schrader [41] that, given a certain set of assumptions (namely smoothness, Euclidean covariance, reflection positivity,

permutation symmetry and cluster decomposition) then knowing the correlation function in Euclidean space it is always possible to reconstruct the corresponding Minkowski space correlation function. Unfortunately this is not the case in lattice simulations, where the Euclidean correlation function is known only at a discrete set of points. An alternative approach is to extract physical quantities directly from the Euclidean space correlation functions. Single-particle states are well-described in this approach by the Källen-Lehmann spectral representation.

A problem arises for multi-particle states. As we have seen in section 3.7, the phase shift can be defined in terms of difference of phases between the initial and final states in two-particle scattering. However, in Euclidean space the distinction between initial and final states can not be made. To see how initial and final states separate in Minkowski spacetime, consider Lippman-Schwinger equation

$$\mid \psi_\alpha^\pm\rangle = \mid \phi_\alpha\rangle + \int d\beta \frac{V_{\beta\alpha}}{E_\alpha - E_\beta \pm i\epsilon} \mid \phi_\beta\rangle \tag{4.148}$$

where $\mid \psi_\alpha\rangle$ are eigenstates of the full Hamiltonian, $\mid \phi_\alpha\rangle$ are eigenstates of the free Hamiltonian and $T_{\beta\alpha} = \langle\phi_\beta \mid H_{int} \mid \psi_\alpha\rangle$. In Minkowski space we can define the states at a given time t by taking a superposition of the energy eigenstates

$$\mid \psi(t)^\pm\rangle = \int d\alpha e^{-iE_\alpha t} g(\alpha) \mid \psi_\alpha^\pm\rangle \tag{4.149}$$

$$\mid \phi(t)\rangle = \int d\alpha e^{-iE_\alpha t} g(\alpha) \mid \phi_\alpha\rangle \tag{4.150}$$

where $g(\alpha)$ is some smooth function of α. Then the Lippmann-Schwinger equation can be written as

$$\mid \psi(t)^\pm\rangle = \mid \phi(t)\rangle + \int d\beta \mathcal{J}_\beta^\pm(t) \mid \phi_\beta\rangle \tag{4.151}$$

with

$$\mathcal{J}_\beta^\pm(t) = \int d\alpha \frac{e^{-iE_\alpha t} g(\alpha) V_{\beta\alpha^\pm}}{E_\alpha - E_\beta \pm i\epsilon}. \tag{4.152}$$

When $t > 0$ ($t < 0$), Eq. (4.152) can be calculated by contour integration by closing the contour along the semicircle in the lower (upper) part of the complex plane. If $V_{\beta\alpha}^\pm$ has poles of its own, their residues will be exponentially suppressed in time by the imaginary part of the pole. As a consequence, $\mathcal{J}_\beta^+(t)$ will vanish at $t = -\infty$, while $\mathcal{J}_\beta^-(t)$ will vanish at $t = +\infty$. Eq. (4.151) shows that

$$\lim_{t\to-\infty} \mid \psi^+\rangle = \lim_{t\to-\infty} \mid \phi(t)\rangle \tag{4.153}$$

$$\lim_{t\to\infty} \mid \psi^-\rangle = \lim_{t\to\infty} \mid \phi(t)\rangle \tag{4.154}$$

which are the definitions of 'in' and 'out' states respectively.

In the Euclidean spacetime the situation is different, because the Eq. (4.152) becomes

$$\mathcal{J}_\beta^\pm(t) = \int d\alpha \frac{e^{-E_\alpha t} g(\alpha) V_{\beta\alpha^\pm}}{E_\alpha - E_\beta \pm i\epsilon}, \tag{4.155}$$

which does not vanish regardless of the sign of t. This means that we can not, for example, calculate the $\pi\pi$ phase shift defined as $\langle \pi\pi; out \mid \pi\pi; in \rangle$ (see sec. 3.7).

Another issue of (infinite volume) Euclidean space is that it is only possible to extract the ground states from the spectral decomposition of correlation functions. As an example, consider the two-point function of $\pi\pi$ interpolating operators

$$\langle 0 \mid O_1(x) O_2(0) \mid 0 \rangle = \int \frac{d^3\mathbf{p_1}}{(2\pi)^3 2E_{\mathbf{p_1}}} \int \frac{d^3\mathbf{p_2}}{(2\pi)^3 2E_{\mathbf{p_2}}} \langle 0 \mid O_1 \mid \mathbf{p}_1, \mathbf{p}_2 \rangle \langle \mathbf{p}_1, \mathbf{p}_2 \mid O_2 \mid 0 \rangle e^{-E_{p_1 p_2} t}. \tag{4.156}$$

For large t, the dominant contribution will come from the lowest energy level and it is in fact impossible to extract higher energy levels from the spectrum. These two restrictions are collectively known as the Maiani-Testa no go theorem [42].

The solution of both of these problems is provided by the finite volume. The phase shifts can be calculated by using Lüscher's method, which is described in section 4.12. The solution of the excited states problem is also trivially solved, because the energy levels in the finite volume are discrete.

4.11 Discretisation effects - Symanzik effective theory

In lattice simulations we work with finite lattice spacing a. To relate the lattice results to physical observables, we need to perform measurements at several values of lattice spacing and subsequently extrapolate to $a = 0$ limit. A useful tool which helps in the understanding of the continuum extrapolation is the Symanzik effective theory. It is an effective theory expansion where the order parameter is the lattice spacing i.e.

$$S_{Symanzik} = S_{QCD} + aS_1 + a^2 S_2 + \cdots \tag{4.157}$$

In the above equation, S_{QCD} is the usual QCD action and S_n are corrections which contain dimension $4+n$ operators. Because the observable quantities can not depend on the cutoff (lattice spacing), the coefficient of every operator must have an explicit lattice spacing dependence. The evolution of these coefficients can be described by Wilsonian renormalisation group, but it is difficult to do in practice. As an example take some dimension-6 operator O_6. It will contribute to the Symanzik action as $a^2 C_6(a) O_6$. But C_6 must be dimensionless, so it can only depend on dimensionless quantities. In 2+1 flavour case, they will have the form $C_6(am_l, am_s, a\Lambda_{QCD})$. Assuming the lattice spacing

is small enough so that $am_l, am_s, a\Lambda_{QCD} \ll 1$ we can Taylor expand the coefficients

$$C_6(am_l, am_s, a\Lambda_{QCD}) = C_6(0,0,0) + a(c_l m_l + c_s m_s + c_\Lambda \Lambda_{QCD}) + O(a^2) \tag{4.158}$$

where $C_6(0,0,0)$ is the continuum value of the coefficient. Calculating our quantities at two different values of lattice spacing allows us to take the continuum limit by extrapolating in a (or, if the coefficient proportional to a is zero, by extrapolating in a^2). Continuum limit of more complicated quantities such as Green's functions can be found in the same way.

In the remainder of this section I will argue that for our choice of fermion action (Möbius DWF) the $K \to \pi\pi$ matrix elements will scale as a^2.

Gauge action There is no pure gauge term of dimension 5 in the Symanzik effective action, so the gauge action is automatically $O(a)$ improved.

Fermion action Imposing the equations of motion for the fermion field and ignoring operators which were present at order 4 (such as $m^2\bar{\psi}\psi$, which will renormalises the quark mass) there is only one new dimension-five operator

$$L_1 = c_{SW}\bar{\psi}\sigma^{\mu\nu}G_{\mu\nu}\psi, \tag{4.159}$$

which is known as the Sheikholeslami-Wohlert term or Pauli term or clover term in the literature.

This term however is absent in chiral fermion formulations, because the Ginsparg-Wilson relation 4.24 will not be satisfied at order a if the Dirac operator is shifted by $ac_{SW}\sigma^{\mu\nu}G_{\mu\nu}$. It may seem that the mass term will break the chiral symmetry (and so the Ginsparg-Wilson relation) as well, invalidating the above argument. However, we can use the trick introduced in section 2.5, i.e. replace the mass term with a spurious field. Then the action will preserve the Ginsparg-Wilson relation forbidding the Sheikholeslami-Wohlert term, which has no mass dependence. This shows that chiral fermions in general and domain wall fermions in particular are automatically order a improved.

Pseudoscalar operators To ensure the correct scaling we need to improve not only the action but also the interpolating operators. The pseudoscalar bilinear $\bar{\psi}\gamma^5\psi$ is a dimension 3 operator, so the order a corrections will have to come from the dimension 4 operators. The only dimension-4 operator that can contribute to the process is $m\bar{\psi}\gamma^5\psi$, which just gives corrections to the operator renormalisation and hence is not a new operator in the Symanzik expansion. Hence, the pseudoscalar operators are $O(a)$ improved.

Four-fermion operators The four-fermion operators are dimension-6 operators and will receive $O(a)$ corrections from dimension-7 operators. These dimension-7 operators will necessarily have to contain four fermion fields and the remaining mass dimension can come from either a covariant derivative or a mass factor. The operators containing a derivative such as $(\bar{s}(1-\gamma^5)d)(\bar{q}\not{D}(1-\gamma^5)q)$ or $(\bar{s}\gamma^\mu(1-\gamma^5)d)(\bar{q}\sigma_{\mu\nu}D^\nu q)$ have a different chiral structure than the dimension-6 ones. Explicitly, they contain one left-chiral and three right-chiral fields, which means they will be in either $(\bar{3},15)$, $(\bar{3},\bar{6})$ or $(\bar{3},3)$ representations, which are different from representations of dimension-6 operators. Other dimension-7 operators containing the derivative can be in $(15,\bar{3})$, $(\bar{6},\bar{3})$ and $(15,\bar{3})$, but there are no operators in the same chiral representations as the dimension-6 operators. Similarly, the operators with an explicit mass dependence will correspond to chiral operators with a single mass insertion. However, the mass term term will mix the right and left handed fields resulting in operators which can not mix with dimension-6 operators for the same reason as above (in fact, using equations of motion one can see that $\not{D}\psi = m\psi$, so the mass operators do not need to be considered separately).

The above reasoning applies only if the chiral symmetry holds. Using a non-chiral formulation, such as Wilson fermions, will reintroduce the $O(a)$ effects in $K \to \pi\pi$ matrix elements even if the action itself is $O(a)$ improved. For example, as we have seen in sec. 2.4.3.3, we can expect $a(m_s - m_d)$ mixing between $Q_{X/Y}$ operators and other operators in the theory, which means that these operators will contribute at $O(a)$ even though they are absent in the leading order mixing. Furthermore, there is nothing protecting us from mixing with dimension-7 operators such as $(\bar{s}(1-\gamma^5)d)(\bar{q}\not{D}(1-\gamma^5)q)$.

4.12 Finite volume effects

4.12.1 Lüscher's method

In this section I will describe Lüscher's method which relates the power-like finite volume corrections to the scattering phase shifts, therefore bypassing the Maiani-Testa no go theorem. I will start by describing the differences between finite and infinite volume particle scattering and show how the phase shift comes into play. The discussion in this chapter follows closely [43].

The main difference between finite and infinite volumes is that in finite volume momenta can only take certain discrete values. For example if we choose a box with periodic boundary conditions in a given direction, the momenta in this direction can only assume values which are integer multiples of $2\pi/L$ where L is the box size. This can be seen by taking a Fourier transform of the wavefunction given the condition

$$\psi(x) = \psi(x + L)$$

.

As a consequence all momentum integrals have to be replaced with sums:

$$\int \frac{d^3\mathbf{p}}{(2\pi)^3}\frac{1}{V} \to \sum_{\mathbf{p}} \tag{4.160}$$

Following [43], we can estimate the difference such difference by using the Poisson summation formula:

$$\sum_p f(p) = \sum_x \tilde{f}(x) \tag{4.161}$$

where $\tilde{f}$ is the Fourier transform of f. This formula can be rewritten as:

$$\frac{1}{L^3}\sum_{\mathbf{k}} g(\mathbf{k}) = \int \frac{d^3\mathbf{k}}{(2\pi)^3} g(\mathbf{k}) + \sum_{\mathbf{x}\neq\mathbf{0}} \int \frac{d^3\mathbf{k}}{(2\pi)^3} e^{i\mathbf{x}\cdot\mathbf{k}} g(\mathbf{k}) \tag{4.162}$$

If f has no singularities, then the sum on the right hand side vanishes (by contour integration) and we can simply write that (up to exponential corrections which will be neglected in this chapter):

$$\frac{1}{L^3}\sum_{\mathbf{k}} f(\mathbf{k}) = \int \frac{d^3\mathbf{k}}{(2\pi)^3} f(\mathbf{k}) \tag{4.163}$$

The $\pi\pi$ scattering will involve loop sums (integrals) of the form

$$\sum\!\!\!\!\!\!\int_{\mathbf{q}} I = \int \frac{dq^0}{2\pi} \sum\!\!\!\!\!\!\int_{\mathbf{q}} \frac{f(q)}{\left(q^2 - m^2 + i\epsilon\right)\left((p+q)^2 - m^2 + i\epsilon\right)}. \tag{4.164}$$

Working in the centre-of-mass frame with $p = (E, \mathbf{0})$ the integral over dq^0 (which is an integral both in finite and infinite volume) can be calculated by contour integration to give

$$I = -i\left(\frac{f(\omega_q, \mathbf{q})}{2\omega_q\left((E-\omega_q)^2 - \omega_q^2\right)} + \frac{f(\omega_q + E, \mathbf{q})}{2\omega_q\left((E+\omega_q)^2 - \omega_q^2\right)}\right), \tag{4.165}$$

where $\omega_q \equiv \sqrt{|\mathbf{q}|^2 + m^2|}$. The second term has no pole and therefore does not contain any power-like finite volume corrections. Defining a new 'momentum' variable k as $E = 2\sqrt{k^2 + m^2}$, the first term can be rewritten as

$$I_1 = -i\frac{f(\omega_q, \mathbf{q})(E + 2\omega_q)}{8\omega_q E\left(k^2 - |\mathbf{q}|^2\right)}. \tag{4.166}$$

The conclusion is that the power-like corrections will arise then $k^2 = |\mathbf{q}|^2$, i.e. when the intermediate two-pion state goes on-shell.

To calculate the finite volume corrections in pion scattering, we therefore need to evaluate the sums (and integrals) of the form:

$$S(\mathbf{q}) = \frac{1}{L^3}\sum_{\mathbf{k}} \frac{f(\mathbf{k})}{q^2 - k^2} \tag{4.167}$$

with $q^2 \equiv |\mathbf{q}|^2$ and $k^2 \equiv |\mathbf{k}|^2$ and f being some analytic function of k. To remove the angular dependence, we can expand the function f in spherical harmonics

$$f(\mathbf{p}) = \sum_{l=0}^{\infty}\sum_{m=-l}^{l} f_{lm}(p) p^l Y_l^m. \tag{4.168}$$

Because we are interested in $l = 0$ state, I will focus on the f_{00} term only.

Now the consider the function

$$\frac{1}{L^3}\sum_{\mathbf{k}} \frac{f_{00}(k) - f_{00}(q)}{(q^2 - k^2)^s} = \int \frac{d^3\mathbf{k}}{(2\pi)^3} \frac{f_{00}(k) - f_{00}(q)}{(q^2 - k^2)^s} \tag{4.169}$$

which follows from the Poisson summation formula, because the integrand has no poles (assuming f_{00} is analytic). The exponent s requires further explanation. We want to take $s = 1$, but that would make the integral and the sum containing $f_{00}(q)$ divergent. The condition of convergence of this sum and integral is $\mathrm{Re}(s) > 3/2$. Starting from any s in this region, $s = 1$ can be reached by analytic continuation. This is a different approach to $e^{\alpha(q^2-k^2)}$ UV regulator introduced in [43]. The reason we chose to use analytic continuation approach instead is that the resulting formulae result in a faster numerical convergence. Using the principal value prescription for the integral, the finite volume correction can be rewritten as

$$\frac{1}{L^3}\sum_{\mathbf{k}} \frac{f_{00}(k)}{(q^2 - k^2)^s} - \mathcal{P}\int \frac{d^3\mathbf{k}}{(2\pi)^3} \frac{f_{00}(k)}{(q^2 - k^2)^s} = f_{00}(q)\frac{1}{L^3}\sum_{k} \frac{1}{(q^2 - k^2)^s}. \tag{4.170}$$

The principal value prescription can be related to Feynman $i\epsilon$ prescription by the identity

$$\mathcal{P}\frac{1}{E} = \frac{1}{E + i\epsilon} + i\pi\delta(E) \tag{4.171}$$

resulting in the finite volume correction

$$F \equiv \frac{1}{L^3}\sum_{\mathbf{k}} \frac{f_{00}(k)}{(q^2 - k^2)^s} - \int \frac{d^3\mathbf{k}}{(2\pi)^3} \frac{f_{00}(k)}{(q^2 - k^2)^s + i\epsilon} = \frac{q f_{00}(q)}{8\pi E} - \frac{i f_{00}(q)}{2EL^3}\sum_{k} \frac{1}{(q^2 - k^2)^s}. \tag{4.172}$$

So far we have considered the finite volume correction from a single $\pi\pi$ loop. Full calculation requires the summation of loops shown in Fig. 4.5. By rewriting the finite volume loop contribution as a sum of infinite volume contribution and the correction,

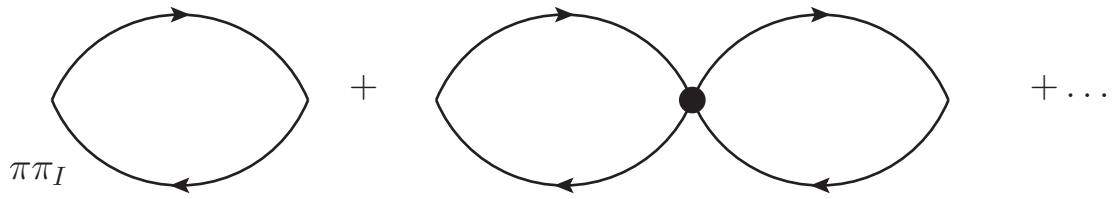

Figure 4.5: Two pion rescattering

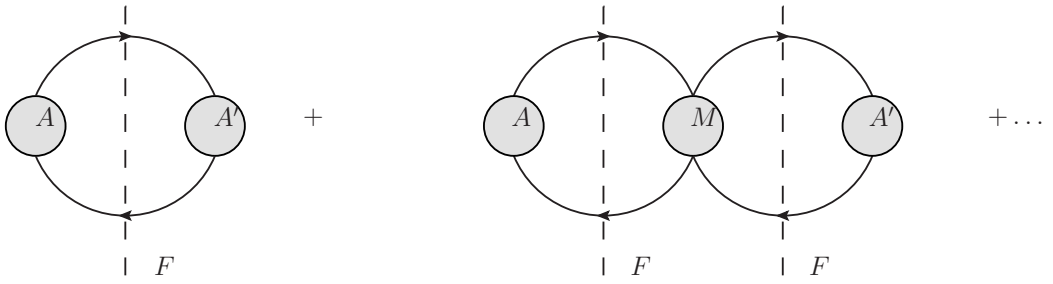

Figure 4.6: Finite volume correction to two pion scattering correlation function

the correction to the $\pi\pi \to \pi\pi$ correlation function can be rewritten as shown in figure 4.6.

Using geometric series, this correction can be rewritten as:

$$\tilde{C}^{FV}(E) = -A'F\frac{1}{1+iMF/2}A \tag{4.173}$$

This correction has poles at $det(1+iMF/2) = 0$. Assuming that A only couples to the s-wave component of the two pion state the above simplifies to $1 + iM_sF_s/2 = 0$, which can be rewritten in terms of the s-wave phase shift δ as:

$$\delta(q) + \phi(q) = n\pi \tag{4.174}$$

with

$$\tan\phi(q) = -\frac{q\pi^{3/2}}{Z_{00}(1;q^2)}, \tag{4.175}$$

$$Z_{00}(s;q^2) = \frac{1}{4\pi}\sum_{n\in Z^3}\frac{1}{((n+(1/2,1/2,1/2))^2-q^2)^s}, \tag{4.176}$$

$$p^2 = \frac{E^2}{4} - m_\pi^2, \tag{4.177}$$

$$q = \frac{Lp}{2\pi}. \tag{4.178}$$

The form of Z_{00} given above is valid for antiperiodic boundary conditions in all 3 directions. The value of Z_{00} for $s = 1$ can be calculated using the method given in the

Appendix A of [44]. This is the Lüscher quantisation condition, first derived in [45]

We can compare the finite volume and infinite volume two pion wavefunctions by comparing the corresponding correlation functions and demanding that they are equal. In infinite volume we have:

$$
\begin{aligned}
C(t) &= \int d^3\mathbf{x} \langle 0 \mid \sigma(\mathbf{x},t)\sigma(0,0) \mid 0\rangle && (4.179)\\
&= \frac{1}{2!}\int d^3\mathbf{x} \int \frac{d^3\mathbf{p}_1}{(2\pi)^3 2E_1} \int \frac{d^3\mathbf{p}_2}{(2\pi)^3 2E_2} \left|\langle 0 \mid \sigma(0,0) \mid E_1,\mathbf{p}_1; E_2,\mathbf{p}_2\rangle\right|^2 e^{-i(E_1+E_2)t} e^{i\mathbf{p}\cdot\mathbf{x}} && (4.180)\\
&= \frac{1}{2}\int \frac{q^2 dq d\Omega}{(2\pi)^3 E^2} \left|\langle 0 \mid \sigma(0,0) \mid E\rangle\right|^2 e^{-iEt} && (4.181)\\
&= \frac{1}{16\pi^2}\int dE \frac{q}{E} \left|\langle 0 \mid \sigma(0,0) \mid E\rangle\right|^2 e^{-iEt} && (4.182)
\end{aligned}
$$

where in second line we inserted a complete set of two particle states with 1/2 indistinguishability factor and shifted the interpolating operators to the origin. In the third line we used the expression for a Dirac delta function to integrate over $\mathbf{x}$ and $\mathbf{p}_2$ and defined $E = 2E_1 = 2E_2$.

In finite volume we have:

$$
\begin{aligned}
C^{FV}(t) &= \int d^3\mathbf{x} \langle 0 \mid \sigma(\mathbf{x},t)\sigma(0,0) \mid 0\rangle_{FV} && (4.183)\\
&= V\sum_n \left|\langle 0 \mid \sigma(0,0) \mid \pi\pi\rangle_{FV}\right|^2 e^{-iEt} && (4.184)\\
&= V\int dE\rho(E) \left|\langle 0 \mid \sigma(0,0) \mid \pi\pi\rangle_{FV}\right|^2 e^{-iEt} && (4.185)
\end{aligned}
$$

where $\rho(E)$ is the density of states function, so that $\rho(E)dE$ counts the number of states between energies E and $E + dE$.

The density of states function can be derived from the quantisation condition (4.174). To do this first note that both $\delta(q)$ and $\phi(q)$ are equivalent to $\delta(q) + \pi$ and $\phi(q) + \pi$ respectively. This means that the constant n in 4.174 can not be a physical quantity in this interpretation. However, if we restrict the phase shift to be in range $-\pi/2 < \delta(q) \leq \pi/2$ and choose the value of $\phi(q)$ to increase by π whenever ϕ crosses a pole, the quantity n will count the number of states with energy below $E(q)$. Then, the number of states between energies E and $E + \delta E$ is given by:

$$
n_{E+\delta E} - n_E = \frac{1}{\pi}\left(\frac{\delta(q(E+\delta E)) - \delta(q(E))}{q(E+\delta E) - q(E)}\right)\left(\frac{\partial q}{\partial E}\delta E + \mathcal{O}(\delta E^2)\right). \qquad (4.186)
$$

In the infinite volume limit the energy levels will get infinitely close together. Then taking δE to be small the above equation reduces to

$$
\rho(E) = \frac{1}{\pi}\left(\frac{\partial\delta(q)}{\partial q} + \frac{\partial\phi(q)}{\partial q}\right)\frac{\partial q}{\partial E}. \qquad (4.187)
$$

By demanding both finite- and infinite-volume correlation functions to be equal we need

$$\mid \pi\pi, E\rangle_\infty = \frac{2E}{q}\sqrt{\pi V\left(\frac{\partial\delta}{\partial q}+\frac{\partial\phi}{\partial q}\right)} \mid \pi\pi, E\rangle_{FV}. \tag{4.188}$$

Similarly for the kaon:

$$\mid K, E_K\rangle_\infty = \sqrt{2E_K V} \mid K, E_K\rangle_{FV} \tag{4.189}$$

Using these results the $K \to \pi\pi$ matrix elements can be related by

$${}_\infty\langle\pi\pi \mid M_i \mid K\rangle_\infty = F_{FV}\langle\pi\pi \mid M_i \mid K\rangle_{FV} \tag{4.190}$$

where F is the Lellouch-Lüscher factor given by

$$F^2 = 8\pi V^2 \frac{m_K E_{\pi\pi}^2}{q^2}\left(\frac{\partial\delta}{\partial q}+\frac{\partial\phi}{\partial q}\right) \tag{4.191}$$

δ is the two-pion s-wave phase shift, which can be calculated using the Lüscher quantisation condition, $\delta(q)+\phi(q) = n\pi$, but the calculation of the derivative in Eq. (4.191) requires an approximation.

4.12.2 Exponential finite volume correction

Having calculated the power corrections we now return to the estimation of exponential finite volume correction. We will rely on ChPT Eqs. (2.161) - (2.164). To one-loop order we write the systematic error associated with the finite-volume corrections in terms of the ratios $\Delta\mathcal{M}_{\log}/\mathcal{M}_{\rm LO}$. These are given by:

$$\begin{aligned}\frac{\Delta\mathcal{M}^{27}_{\log}}{\mathcal{M}^{27}_{\rm LO}} &= \frac{1}{f^2(m_K^2-m_\pi^2)}\left[-\frac{1}{12}m_K^4\left(1-\frac{m_K^2}{m_\pi^2}\right)\Delta\beta(m_\pi^2,m_K^2,m_\eta^2)\right.\\ &+m_K^2\left(\frac{5}{4}\frac{m_K^4}{m_\pi^2}-\frac{13}{4}m_K^2+2m_\pi^2\right)\Delta\beta(m_\pi^2,m_K^2,m_\pi^2)+\\ &(m_K^4-3m_\pi^2m_K^2+2m_\pi^4)\Delta\beta(m_K^2,m_\pi^2,m_\pi^2)+\left(-\frac{1}{4}\frac{m_K^4}{m_\pi^2}-\frac{1}{12}m_K^2+\frac{1}{3}m_\pi^2\right)\Delta\ell(m_\eta^2)\\ &\left.+\left(\frac{-m_K^4}{m_\pi^2}-4m_K^2+4m_\pi^2\right)\Delta\ell(m_K^2)+\left(\frac{5}{4}\frac{m_K^4}{m_\pi^2}-\frac{45}{4}m_K^2+11m_\pi^2\right)\Delta\ell(m_\pi^2)\right]\end{aligned} \tag{4.192}$$

and

$$\begin{aligned}\frac{\Delta\mathcal{M}^{88}_{\log}}{\mathcal{M}^{88}_{\rm LO}} &= \frac{1}{f^2}\left[\left(\frac{5}{4}\frac{m_K^4}{m_\pi^2}-2m_K^2\right)\Delta\beta(m_\pi^2,m_K^2,m_\pi^2)+(m_K^2-2m_\pi^2)\Delta\beta(m_K^2,m_\pi^2,m_\pi^2)\right.\\ &+\frac{1}{4}\frac{m_K^4}{m_\pi^2}\Delta\beta(m_\pi^2,m_K^2,m_\eta^2)-\left(4+\frac{1}{2}\frac{m_K^2}{m_\pi^2}\right)\Delta\ell(m_K^2)\\ &\left.+\left(\frac{5}{4}\frac{m_K^2}{m_\pi^2}-8\right)\Delta\ell(m_\pi^2)-\frac{3}{4}\frac{m_K^2}{m_\pi^2}\Delta\ell(m_\eta^2)\right].\end{aligned} \tag{4.193}$$

The functions $\ell(m^2)$ and $\beta(q^2, m_1^2, m_2^2)$ correspond to diagrams with one and two pseudo-Goldstone boson propagators respectively as illustrated in Fig. 2.10 and they are the only sources of finite-volume corrections. They are given by (in Minkowski spacetime):

$$\ell(m^2) \equiv \nint \frac{dk^0}{2\pi} \frac{i}{k^2 - m^2 + i\epsilon} = \nint \frac{1}{\sqrt{\vec{k}^2 + m^2}}, \tag{4.194}$$

$$\beta(q, m_1, m_2) \equiv \nint \frac{dk^0}{2\pi} \frac{i}{\left(k^2 - m_1^2\right)\left((q+k)^2 - m_2^2\right)} = \nint \frac{\omega_1 + \omega_2}{2\omega_1\omega_2(q_0^2 - (\omega_1 + \omega_2)^2)}, \tag{4.195}$$

where the symbol $\nint$ denotes the summation over $\vec{k}$ in finite volume or the integration in infinite volume. $\omega_1 = \sqrt{\vec{k}^2 + m_1^2}$ and $\omega_2 = \sqrt{(\vec{q} - \vec{k})^2 + m_2^2}$. The difference between the sum and the integral can be calculated using the Poisson summation formula:

$$\frac{1}{L^3} \sum_{\vec{k}} f(\vec{k}) = \int \frac{d^3\vec{k}}{(2\pi)^3} f(\vec{k}) + \sum_{\vec{n} \neq \vec{0}} \int \frac{d^3\vec{k}}{(2\pi)^3} f(\vec{k}) e^{iL\vec{k}\cdot\vec{n}}, \tag{4.196}$$

where the summation on the left-hand side is over all $\vec{k} = \frac{2\pi}{L}\vec{n}$, where $\vec{n}$ is a vector of integers. If f is a function that has no singularities on the real axis, then the second term on the right-hand side gives the exponential finite-volume corrections which we are trying to evaluate.

4.12.2.1 Corrections to $\ell(m^2)$

With periodic boundary conditions, applying the Poisson summation formula (4.196) to ℓ, writing $\vec{k}$ in spherical polar coordinates and integrating over the angles, we obtain for the difference between the finite and infinite-volume values of $\ell(m^2)$ [46]

$$\Delta\ell(m, L) \equiv \frac{m^2}{16\pi^2}\delta_1(mL) \equiv \frac{m}{4\pi^2 L} \sum_{\vec{n} \neq 0} \frac{K_1(|\vec{n}|mL)}{|\vec{n}|}, \tag{4.197}$$

where K_1 is a modified Bessel function of the second kind, $\vec{n}$ is an vector of integers and the sum is over all $\vec{n} \neq (0,0,0) \in \mathbb{Z}^3$.

Since our choice of boundary conditions breaks the isospin symmetry Eq. (4.197) does not give the correct finite-volume corrections for all the instances of ℓ which appear in Eqs. (2.162) and (2.164). Specifically, π^0, K^+ and η satisfy periodic boundary conditions (so that the corresponding finite-volume corrections are indeed given by Eq. (4.197)) whereas $\pi^\pm$ and K^0 satisfy antiperiodic boundary conditions for which the finite-volume corrections to ℓ are different. In the antiperiodic case, we replace $f(\vec{k})$ in Eq. (4.196) by $f(\vec{k} + \vec{q})$, where $\vec{q} = (\frac{\pi}{L})(1,1,1)$. Shifting the integration variable from $\vec{k}$ to $\vec{k} + \vec{q}$, we

find that $\delta_1(mL)$ in Eq. (4.197) is now replaced by:

$$\delta_1^A(mL) = \frac{4}{mL}\sum_{\vec{n}\neq\vec{0}}(-1)^{n_x+n_y+n_z}\frac{K_1(|\vec{n}|mL)}{|\vec{n}|}\,, \tag{4.198}$$

where the index A denotes that the correction is evaluated for a volume with antiperiodic boundary conditions in all spatial directions. The difference from the periodic case is the additional factor $(-1)^{n_x+n_y+n_z}$ in the summands. The known formulae in Eqs. (2.162) and (2.164) do not differentiate between different isospin components, and therefore do not specify which linear combination of periodic and antiperiodic corrections should be used. Since we are only using these formulae for an approximate estimate of the size of the error, we choose to be conservative and to include the larger corrections which are those obtained with the periodic boundary conditions given in Eqs. (4.197).

4.12.2.2 Corrections to $\beta(m_\pi, m_K, m_\pi)$ and $\beta(m_\pi, m_K, m_\eta)$

We now consider the contributions from loops with two meson propagators and which are proportional to the function β. We start by discussing the corrections to $\beta(m_\pi, m_K, m_\pi)$ and $\beta(m_\pi, m_K, m_\eta)$, for which in Minkowski space the external energy is below the corresponding two-particle cut; e.g. in $\beta(m_\pi, m_K, m_\pi)$ the external energy in the centre-of-mass frame is m_π which is clearly smaller than $m_K + m_\pi$. In such situations the finite-volume corrections are exponentially small. We postpone the discussion of the contribution which does contain the two-particle cut, that proportional to $\beta(m_K, m_\pi, m_\pi)$, until the following subsection.

The corrections to $\beta(m_\pi, m_K, m_\pi)$ and $\beta(m_\pi, m_K, m_\eta)$ are proportional to

$$\Delta\beta(q, m_1, m_2) = \sum_{\vec{n}\neq 0}\int\frac{d^3\vec{k}}{(2\pi^3)}\frac{e^{i\vec{k}\cdot\vec{n}}(\omega_1+\omega_2)}{2\omega_1\omega_2(q^2-(\omega_1+\omega_2)^2)} \tag{4.199}$$

with

$$\omega_1^2 = \left|\vec{k}\right|^2 + m_1^2 \qquad \text{and} \qquad \omega_2^2 = \left|\vec{q}+\vec{k}\right|^2 + m_2^2\,. \tag{4.200}$$

Because of the angular dependence inside the integrals, we evaluate the integrals numerically. With the boundary conditions which we are using the corrections with a K^+ and π^- are equal and opposite to those with the neutral mesons. In the estimate of the uncertainty we conservatively do not exploit the cancellation but take the absolute value in each case.

We note that care must be taken when using Eqs. (71) and (73) for the finite-volume corrections to β in Sec. VIII of [24]. In Eq. (4.199) above, the two terms in the factor in the denominator of the integrand $q^2 - (\omega_1 + \omega_2)^2$ come with opposite signs. How this arises in finite-volume Euclidean correlation functions is explained in Appendix 4.12.2.3

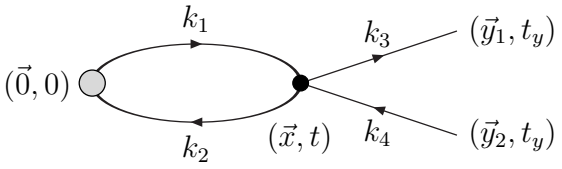

Figure 4.7: Contribution to the correlation function in which two pions are produced by an operator at the origin (grey circle), and rescatter by the strong interactions denoted by the filled circle.

following [47]. The corresponding terms in the denominator of Eq. (73) in [24] appear (incorrectly) with the same sign.

4.12.2.3 $\beta(m_K, m_\pi, m_\pi)$

Kinematically this case is simpler than the two β integrals which were evaluated in Sec.4.12.2.2 since the external particle (K) is now at rest which eliminates the angular dependence from the integral. Furthermore, both internal π^+ propagators satisfy antiperiodic boundary conditions. In this case however, the integral for β has a pole at $\omega_\pi = m_K/2$, so the Poisson summation formula will give both the exponential and power-like corrections. The power corrections are included as the Lellouch-Lüscher factor F in Eq. (4.190) and we do not include these in the estimate of the finite-volume uncertainty. In the case with $q = (m_K, \vec{0})$ and $m_1 = m_2 = m_\pi$, $\beta(m_K, m_\pi, m_\pi)$ in Minkowski space has an imaginary part which leads to finite-volume corrections in Euclidean space which decrease only as inverse powers of the volume and not exponentially. These power corrections are the one-loop chiral perturbation theory (NLO ChPT) contributions to the Lellouch-Lüscher factor F in Eqs. (4.190) and (4.191). This factor is included fully in our analysis and so we must not include it again from NLO ChPT. A detailed study of how the Lellouch-Lüscher factor arises in one-loop ChPT was performed in [47], but we hope that it will be useful to summarise the main points here.

In Minkowski space, performing the k_0 integration in the centre-of-mass frame we obtain

$$\beta(m_K, m_\pi, m_\pi) = \int \frac{d^3\vec{k}}{(2\pi)^3} \frac{1}{\omega(\vec{k})\left[m_K^2 - 4\omega^2(\vec{k}) + i\varepsilon\right]}, \tag{4.201}$$

where $\omega^2(\vec{k}) = \left|\vec{k}\right|^2 + m_\pi^2$.

In finite-volume Euclidean space we evaluate the correlation function illustrated in Fig. 4.7. The kaon propagator is irrelevant for our discussion and so we amputate it, and consider the two pions to be created at the origin, to rescatter and to be annihilated on the timeslice at t_y. After performing the integrals over $\vec{y}_1$, $\vec{y}_2$ (with phase factors $e^{i\vec{q}\cdot\vec{y}_1}$ and $e^{-i\vec{q}\cdot\vec{y}_2}$ respectively) and $\vec{x}$ and exploiting the resulting δ functions, we obtain for

this contribution to the correlation function:

$$I \equiv \int_{-\infty}^{\infty} dt \int \frac{d^3\vec{k}}{(2\pi)^3} \prod_{i=1}^{4} \frac{dE_i}{E_i^2+\omega_i^2}\, e^{i(E_1-E_2)t}\, e^{i(E_3-E_4)(t_y-t)}\,, \tag{4.202}$$

where in a finite volume the integral over $\vec{k}$ is replaced by the corresponding sum. Here $\omega_1^2 = \omega_2^2 = \omega^2(\vec{k}) = \left|\vec{k}\right|^2 + m_\pi^2$ and $\omega_3^2 = \omega_4^2 = \omega^2(\vec{q}) = |\vec{q}|^2 + m_\pi^2$ so that $\omega_{3,4}$ are not integration variables.

The energy integrals can now be performed by contour integration; there are 3 contributions depending on the value of t.

1. The first contribution is from the interval $-\infty < t < 0$ and gives

$$I_1 = \frac{e^{-2\omega(\vec{q})\,t_y}}{32\,\omega^2(\vec{q})} \int \frac{d^3\vec{k}}{(2\pi)^3} \frac{1}{\omega^2(\vec{k})\,(\omega(\vec{k})+\omega(\vec{q}))}\,. \tag{4.203}$$

2. The second contribution comes from the region $0 < t < t_y$ and gives

$$I_2 = \frac{e^{-2\omega(\vec{q})\,t_y}}{32\,\omega^2(\vec{q})} \int \frac{d^3\vec{k}}{(2\pi)^3} \frac{1}{\omega^2(\vec{k})\,(\omega(\vec{k})-\omega(\vec{q}))}(1-e^{-2(\omega(\vec{k})-\omega(\vec{q}))\,t_y})\,. \tag{4.204}$$

3. Finally we have the contribution from the region $t_y < t < \infty$ which gives

$$I_3 = \frac{1}{32\,\omega^2(\vec{q})} \int \frac{d^3\vec{k}}{(2\pi)^3} \frac{e^{-2\omega(\vec{k})\,t_y}}{\omega^2(\vec{k})\,(\omega(\vec{k})+\omega(\vec{q}))}\,. \tag{4.205}$$

The contribution to the amplitude is given by the coefficient of

$$\frac{e^{-2\omega(\vec{q})t_y}}{4\,\omega^2(\vec{q})}.$$

In finite volume the integrals over $\vec{k}$ are replaced by the corresponding sums and we obtain the following three contributions.

$$T_1 = \frac{1}{8L^3} \sum_{\vec{k}} \frac{1}{\omega^2(\vec{k})\,(\omega(\vec{k})+\omega(\vec{q}))} \tag{4.206}$$

from the region $t < 0$.

$$T_2 = \left(\frac{\nu_q t_y}{L^3}\right) \frac{1}{4\,\omega^2(\vec{q})} + \frac{1}{8L^3} \sum_{|\vec{k}|\neq|\vec{q}|} \frac{1}{\omega^2(\vec{k})(\omega(k)-\omega(q))}\,, \tag{4.207}$$

from the region $0 < t < t_y$, where ν_q is the degeneracy of states with $\vec{k} = \vec{q}$. The term proportional to t_y is the FV correction to the two-pion energy and it can be checked

that this is correctly given by the Lüscher quantisation condition [47]. Finally from the region $t_y < t < \infty$ we have

$$T_3 = \left(\frac{\nu_q}{L^3}\right) \frac{1}{16\,\omega^3(q)}\,. \tag{4.208}$$

We now separate the terms with $|\vec{k}| = |\vec{q}|$ from those where $|\vec{k}| \neq |\vec{q}|$. When $|\vec{k}| = |\vec{q}|$, we find a contribution

$$\frac{\nu_q}{L^3}\frac{1}{4\omega^2(\vec{q})}\left\{\frac{1}{4\omega(\vec{q})} + \frac{1}{4\omega(\vec{q})}\right\}, \tag{4.209}$$

where the first term in the braces corresponds to T_1 and the second corresponds to T_3. The contribution from T_3 is cancelled by the FV correction to the matrix element of the two-pion interpolating operator at t_y [47] whereas the one from T_1 is a contribution to the FV effects in the amplitude.

The contributions from $|\vec{k}| \neq |\vec{q}|$ come from T_1 and T_2 and can be combined to give

$$\frac{1}{4\,L^3}\sum_{|\vec{k}|\neq|\vec{q}|}\frac{1}{\omega(\vec{k})\,(\omega^2(\vec{k}) - \omega^2(\vec{q}))}\,. \tag{4.210}$$

Thus in Euclidean finite volume we obtain

$$S_1' + \frac{\nu_q}{16L^3E^3}\,, \tag{4.211}$$

where it is convenient to define

$$S_n' = \frac{\omega^{n-1}(\vec{q})}{4L^3}\sum_{|\vec{k}|\neq|\vec{q}|}\frac{1}{\omega^n(\vec{k})\,(\omega^2(\vec{k}) - \omega^2(\vec{q}))} \tag{4.212}$$

and the corresponding integrals by

$$J_n = \frac{\omega^{n-1}(\vec{q})}{4}\mathcal{P}\int\frac{d^3\vec{k}}{(2\pi)^3}\frac{1}{\omega^n(\vec{k})\,(\omega^2(\vec{k}) - \omega^2(\vec{q}))}\,. \tag{4.213}$$

Relating this sum to the corresponding integral gives the LL-factor [47]. We now make this more specific and determine the exponentially small corrections. In the difference $S_1' - S_0'$ there is no term with a pole at $\omega(k) = \omega(q)$ so that this difference can be related to the corresponding integral using the Poisson summation formula and the exponentially small finite-volume corrections can be identified

$$\begin{aligned} S_1' - S_0' &= -\frac{1}{4L^3\omega(\vec{q})}\sum_{|\vec{k}|\neq|\vec{q}|}\frac{1}{\omega(\vec{k})(\omega(\vec{k}) + \omega(\vec{q}))} && (4.214)\\ &= -\frac{1}{4L^3\omega(\vec{q})}\sum_{\vec{k}}\frac{1}{\omega(\vec{k})(\omega(\vec{k}) + \omega(\vec{q}))} + \frac{\nu_q}{8L^3\omega^3(\vec{q})} \\ &= J_1 - J_0 + \frac{\nu_q}{8L^3\omega^3(\vec{q})} + e_{1,0}\,. && (4.215) \end{aligned}$$

Thus we see that the finite volume and infinite-volume results are related by

$$S_1' + \frac{\nu_q}{16L^3E^3} = J_1 - J_0 + S_0' + \frac{3\nu_q}{16L^3E^3} + e_{1,0}\,, \tag{4.216}$$

where $e_{1,0}$ represent the exponentially small corrections,

$$e_{1,0} = -\frac{1}{8\pi^2\omega(\vec{q})L}\sum_{\vec{n},n\neq 0}\frac{1}{n}\int_0^\infty k\,dk\,\frac{\sin(nkL)}{\omega(k)(\omega(k)+\omega(q))}\,, \tag{4.217}$$

and n and k are $|\vec{n}\,|$ and $|\vec{k}\,|$ respectively. It was shown in [47] that $-J_0 + S_0' + \frac{3\nu_q}{16L^3E^3}$ is precisely the one-loop contribution to the Lellouch-Lüscher factor. The residual exponentially small finite-volume effects are given by $e_{1,0}$. (The ultraviolet divergence cancels in the difference $J_0 - S_0'$, but if the zeta function regularisation is used, as in [45], then $J_0 = 0$.)

We have presented the above detailed discussion because we believe that there is a misunderstanding in the literature. In Eqs. (71) and (73) of [24], the authors take the finite-volume corrections in $\beta(m_K, m_\pi, m_\pi)$ in Euclidean space to be the difference between the momentum integral and the corresponding sum over the integrand in Eq. (4.201) but with the replacement $m_K^2 - 4\omega^2(k) \to m_K^2 + 4\omega^2(k)$ in the denominator. Since there would now be no singularity in the denominator, the finite-volume corrections would be exponential and there would be no Lellouch-Lüscher factor. The above derivation demonstrates instead the origin of the power corrections in the volume.

Throughout the above discussion we assumed periodic boundary conditions in all three spatial directions so that $k_i = n_i \times (2\pi/L)$ where n_i is an integer. In our determination of A_2 we use antiperiodic boundary conditions in all three directions so that

$$e_{1,0} = -\frac{1}{8\pi^2\omega(q)L}\sum_{\vec{n},n\neq 0}\frac{(-1)^{n_x+n_y+n_z}}{n}\int_0^\infty k\,dk\,\frac{\sin(nkL)}{\omega(k)(\omega(k)+\omega(q))}\,. \tag{4.218}$$

4.13 Nonperturbative renormalisation

The Wilson coefficients ($C_i(\mu)$) and composite operators ($Q_i(\mu)$) appearing in Eq. (2.122) are separately renormalisation scheme and scale (μ) dependent. To obtain the physical amplitudes they must be combined in the same scheme and at the same scale. The $C_i(\mu)$ are calculated in perturbation theory for which it is convenient to use the $\overline{MS}$ - NDR scheme (called $\overline{MS}$ in the following). The matrix elements whose calculation is described in Sec. 4.7, on the other hand, are obtained using bare operators with the lattice spacing as the ultraviolet regulator with the lattice discretisation of QCD. We need to relate two different renormalisation schemes to each other. Using Eq. (2.126)

we have

$$Q_i^{R1} = Z_{ij}^{R_1} Q_j^0 \tag{4.219}$$
$$Q_i^{R2} = Z_{ij}^{R_2} Q_j^0 \tag{4.220}$$
$$\tag{4.221}$$

and hence

$$Q_i^{R_1} = Z_{ij}^{R_1} (Z_{jk}^{R_2})^{-1} Q_k^{R_2} \equiv Z_{ij}^{R_2 \to R_1}. \tag{4.222}$$

The matrix $Z_{ij}^{R_2 \to R_1}$ can be calculated by imposing renormalisation conditions R_1 on the Green's functions of operators Q^{R_2}. The operators can be renormalised non-perturbatively, but only into schemes for which the renormalisation condition can be imposed on lattice Green's functions. The $\overline{MS}$ scheme, which is based on dimensional regularisation cannot be simulated in a lattice computation. Our procedure is to start by renormalising the operators non-perturbatively into schemes which can be simulated, specifically the RI-SMOM schemes [48] as described in detail in [12] and briefly summarised below. In this case we have

$$Q_i^{\overline{MS}} = Z_{ij}^{RI \to \overline{MS}} Q_j^{RI} \tag{4.223}$$
$$Q_i^{RI} = Z_{ij}^{lat \to RI} Q_j^{lat}. \tag{4.224}$$

The matching between the RI-SMOM and $\overline{MS}$ schemes is necessarily performed in perturbation theory and is currently known at one-loop order. (In sec 5.3 we also present the matrix elements in two RI-SMOM schemes so that if the perturbative coefficients are calculated to higher order in the future, these matrix elements can be used to reduce the systematic uncertainty in A_2 due to the truncation of the perturbation series.)

We now briefly summarise the renormalisation procedure. We write the five-point amputated Green's functions of the three operators in Eq. (4.129) as a three-component vector $\Lambda = (\Lambda_{(27,1)}, \Lambda_{(8,8)}, \Lambda_{(8,8)\text{mx}}) \equiv (\Lambda_1, \Lambda_2, \Lambda_3)$, and impose a renormalisation condition of the form

$$P\left\{\Lambda^R(\mu)\right\} = F\ , \tag{4.225}$$

where P is a vector of projectors and F the corresponding tree-level matrix. Denoting the tree-level contribution by the superscript (0) and including explicitly the spinor and colour labels, the matrix F is given by

$$P_i\left\{\Lambda_j^{(0)}\right\} \equiv [P_i]^{BA;DC}_{\beta\alpha;\delta\gamma} \left[\Lambda_j^{(0)}\right]^{AB;CD}_{\alpha\beta;\gamma\delta} = F_{ij}. \tag{4.226}$$

Here Greek letters label spinor components, the upper-case Roman letters represent colour indices and $i, j = 1, 2, 3$ denote the operators and projectors. For illustration, the

tree-level value of the Green's function of $Q^{(27,1)}$ is

$$\left[\Lambda^{(0)}_{(27,1)}\right]^{AB;CD}_{\alpha\beta;\gamma\delta} = \left[(\gamma^\mu)_{\alpha\beta}(\gamma^\mu)_{\gamma\delta} + (\gamma^\mu\gamma_5)_{\alpha\beta}(\gamma^\mu\gamma_5)_{\gamma\delta}\right]\delta^{AB}\delta^{CD} - \left[(\gamma^\mu)_{\alpha\delta}(\gamma^\mu)_{\gamma\beta} + (\gamma^\mu\gamma_5)_{\alpha\delta}(\gamma^\mu\gamma_5)_{\gamma\beta}\right]\delta^{AD}\delta^{BC} \,. \tag{4.227}$$

For the renormalisation we only consider the parity-even component of the four-quark operators.

The choice of projectors is not unique and we implement two different sets known as the γ_μ and $\not{q}$-projectors, given explicitly by

$$\left[P^{(\gamma^\mu)}\right]^{JI;LK}_{\beta\alpha;\delta\gamma} = \begin{pmatrix} \left[(\gamma^\mu)_{\beta\alpha}(\gamma^\mu)_{\delta\gamma} + (\gamma^\mu\gamma^5)_{\beta\alpha}(\gamma^\mu\gamma^5)_{\delta\gamma}\right]\delta^{JI}\delta^{LK} \\ \left[(\gamma^\mu)_{\beta\alpha}(\gamma^\mu)_{\delta\gamma} - (\gamma^\mu\gamma^5)_{\beta\alpha}(\gamma^\mu\gamma^5)_{\delta\gamma}\right]\delta^{JI}\delta^{LK} \\ \left[(\gamma^\mu)_{\beta\gamma}(\gamma^\mu)_{\delta\alpha} - (\gamma^\mu\gamma^5)_{\beta\gamma}(\gamma^\mu\gamma^5)_{\delta\alpha}\right]\delta^{JK}\delta^{LI} \end{pmatrix} \tag{4.228}$$

and

$$\left[P^{(\not{q})}\right]^{JI;LK}_{\beta\alpha\beta;\delta\gamma} = \begin{pmatrix} \left[(\not{q})_{\beta\alpha}(\not{q})_{\delta\gamma} + (\not{q}\gamma^5)_{\beta\alpha}(\not{q}\gamma^5)_{\delta\gamma}\right]\delta^{JI}\delta^{LK} \\ \left[(\not{q})_{\beta\alpha}(\not{q})_{\delta\gamma} - (\not{q}\gamma^5)_{\beta\alpha}(\not{q}\gamma^5)_{\delta\gamma}\right]\delta^{JI}\delta^{LK} \\ \left[(\not{q})_{\beta\gamma}(\not{q})_{\delta\alpha} - (\not{q}\gamma^5)_{\beta\gamma}(\not{q}\gamma^5)_{\delta\alpha}\right]\delta^{JK}\delta^{LI} \end{pmatrix} . \tag{4.229}$$

The corresponding matrices F read

$$F^{(\gamma^\mu)} = \begin{pmatrix} 128N(N+1) & 0 & 0 \\ 0 & 128N^2 & 128N \\ 0 & 128N & 128N^2 \end{pmatrix} \tag{4.230}$$

and

$$F^{\not{q}} = q^2 \begin{pmatrix} 32N(N+1) & 0 & 0 \\ 0 & 32N^2 & 32N \\ 0 & 32N & 32N^2 \end{pmatrix} , \tag{4.231}$$

where $N = 3$ is the number of colours.

The final result for the amplitude is, of course, independent of the choice of intermediate scheme defined by P, but comparing the results obtained with different projection operators gives us an estimate of the systematic uncertainty due to the truncation of perturbation theory in relating the RI-SMOM schemes to the $\overline{MS}$ schemes.

The renormalised operators are related to the lattice ones by a matrix relation of the form:

$$Q^{\mathrm{R}}_i(\mu) = Z_{ij}(\mu a)\, Q^{\mathrm{lat}}_j(a). \tag{4.232}$$

In order to extract the renormalisation constants we follow the standard procedure [49; 20] and compute numerically the amputated Green's functions of the bare operators in Eq. (4.129) with particular choices of external momenta (as discussed below) on Landau

gauge-fixed configurations. We next solve equation (4.225) which we rewrite in the form

$$\frac{Z_{ij}(\mu a)}{Z_q^2(\mu a)} P_k \left\{ (\Lambda_j^{\text{bare}}(a) \right\}_{\mu^2=p^2} = F_{ik} \ , \tag{4.233}$$

where $\sqrt{Z_q}$ is the quark field renormalisation constant and μ is the renormalisation scale, which we ultimately choose to be 3 GeV.

The choice of Z_q is also not unique, and we use the following two cases:

$$\frac{Z_q^{(\not{q})}}{Z_V} = \frac{q^\mu}{12q^2} \text{Tr} \Lambda_V^\mu \not{q}, \quad \text{and} \quad \frac{Z_q^{(\gamma_\mu)}}{Z_V} = \frac{1}{48} \text{Tr} \Lambda_V^\mu \gamma^\mu, \tag{4.234}$$

where Λ_V^μ is the three-point amputated Green's function of the local vector current and Z_V is the renormalisation constant of the local vector current. In practice, we multiply each side of Eq. (4.233) by the square of the corresponding side of Eq. (4.234). This eliminates Z_q and after this multiplication the left-hand side of Eq. (4.233) contains the ratio of renormalisation factors Z_{ij}/Z_V^2. Z_V is then calculated by imposing the Ward identity $Z_V \langle P \,|\, V^4 \,|\, P \rangle = 2m_P$, where V^μ is the local vector current and $|P\rangle$ is the state of a pseudoscalar meson P at rest with mass m_P; this is explained in detail in [50].

The choice of projection operator for the four-quark operator and Z_q defines a renormalisation scheme, which we will label (a, b) with $a, b \in \gamma^\mu, \not{q}$ for the choice of $P^{(a)}$ and $Z_q^{(b)}$. In particular, we consider the (γ^μ,γ^μ) and ($\not{q}$,$\not{q}$) schemes, having found in earlier studies that the perturbative conversion to the $\overline{MS}$ scheme is more precise in these schemes. This is based on the observation that the non-perturbative running is generally closer to the perturbative one for these schemes for the four-quark operators in Eq. (4.129) [12; 51]. We follow our previous practice and choose the ($\not{q}$,$\not{q}$) scheme for our central value and the (γ^μ,γ^μ) scheme to estimate the error due to the perturbative conversion to the $\overline{MS}$ scheme.

Chiral symmetry (or specifically its $SU(3)_V$ subgroup) suppresses mixing of operators in different irreducible representations of the chiral symmetry group, so that if the symmetry is exact, Z_{ij} is a block diagonal matrix with a 1×1 block corresponding to the renormalisation of the $(27, 1)$ operator and 2×2 block corresponding to the mixing of $(8, 8)$ and $(8, 8)_{\text{mx}}$ operators. In a massless renormalisation scheme with a chiral discretisation such as the Domain Wall action, we expect a mixing pattern very similar to this, but with a small $O((am_{\text{res}})^2)$ mixing between the blocks.

In order to suppress physical infrared chiral-symmetry breaking effects we choose to impose the renormalisation conditions with the kinematics indicated in Fig. 4.8 with $p_1^2 = p_2^2 = (p_1 - p_2)^2 \equiv \mu^2$. We compute the Green's functions for several momenta and interpolate to $\mu = 3$ GeV using a quadratic ansatz. Using partially twisted boundary conditions, we have a good resolution around the targeted momentum. The momenta in such RI-SMOM schemes are chosen so that there are no "exceptional" channels, i.e.

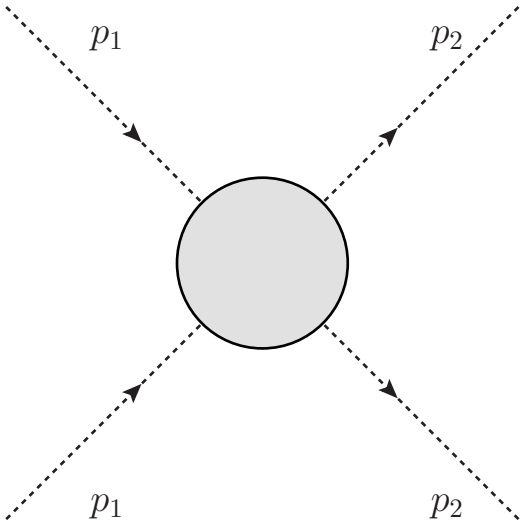

Figure 4.8: Momentum flow defining a renormalisation condition of a four quark operator in RI-SMOM scheme. The momenta are chosen so that $p_1^2 = p_2^2 = (p_1 - p_2)^2 \equiv \mu^2$.

no channels in which the square of the momenta is small [48]. (This is in contrast with the original RI-MOM scheme [49; 20] in which $p_1 = p_2$.) We have already checked that with Domain-Wall fermions and this choice of kinematics the chirally forbidden matrix elements are numerically negligible [12]. In the present computation, we use the 48^3 and 64^3 ensembles which have physical light and strange sea-quark masses. However, the light quark mass is used in all of the valence quarks propagators in the five-point Green's functions, including those for both light and strange quarks. We do not extrapolate either the sea or valence quark masses to zero and, strictly speaking, do not work in the chiral limit. In practice the light quark masses are sufficiently small that their effects are negligible as is the non-zero mass of the strange sea quark. Comparing our results with those of our previous work (with Shamir domain wall fermions) where a chiral extrapolation was performed we find agreement at the per-mille level or better.

4.13.1 Step scaling

The step scaling procedure is the lattice version of the renormalisation group methods described in sec. 2.4.3.4. To see how it works, start with an RI operator renormalised at a scale μ and insert $1 = Z^{-1}(\mu_0, a, m)Z(\mu_0, a, m)$ so that

$$Q^{RI}(\mu) = Z(\mu, m, a)Q^{LAT}(m, a) = Z(\mu, m, a)Z^{-1}(\mu_0, a, m)Z(\mu_0, a, m)Q^{LAT}(m, a), \tag{4.235}$$

where for conciseness of notation I kept the operator index implicit. Then, taking the $m \to 0$ and $a \to 0$ limit, we can see that

$$Q^{RI}(\mu) = \sigma(\mu, \mu_0) Q^{RI}(\mu_0) \tag{4.236}$$

with

$$\sigma(\mu, \mu_0) = \lim_{a,m\to 0} Z(\mu, m, a) Z^{-1}(\mu_0, a, m). \tag{4.237}$$

The matrix σ, which can be calculated nonpertubarively, relates to each other the RI matrix elements at two different scales. Although we did not use step scaling for this particular project, it is one of the potential improvements which can be used to scale our matrix elements to a higher renormalisation scale μ, where the perturbative matching to $\overline{MS}$ scheme is better behaved.

4.14 Differences between $\Delta I = 3/2$ and $\Delta I = 1/2$ calculations

The techniques described previously in this chapter can be used to find the $\Delta I = 3/2$ amplitudes, but the calculation of $\Delta I = 1/2$ proves to be more challenging. This is not only due to an additional level of complication (inclusion of (8,1) operators in the weak Hamiltonian, additional contractions etc.) but also due to more challenging issues described in this section. $\Delta I = 1/2$ amplitudes have been calculated at threshold in [2] and more recently at physical kinematics [13].

4.14.1 Vacuum subtraction

One of the main challenges comes from the fact is that the two-pion I=0 state with zero total momentum has the same quantum numbers as the QCD vacuum. This means that in the spectrum of $K \to (\pi\pi)_{I=0}$ correlation function will behave as

$$\begin{aligned} C^{\Delta I=1/2}_{K\to\pi\pi} &= \langle O^{I=0}_{\pi\pi}(t_{\pi\pi} H_W(t) O_K(0)\rangle && (4.238)\\ &\xrightarrow[t\to\infty]{t_{\pi\pi}-t\to\infty} \langle 0 \mid O^{I=0}_{\pi\pi} \mid 0\rangle\langle 0 \mid H_W \mid K\rangle\langle K \mid O_K \mid 0\rangle && (4.239)\\ &+ \langle 0 \mid O^{I=0}_{\pi\pi} \mid \pi\pi; I=0\rangle\langle \pi\pi; I=0 \mid H_W \mid K\rangle\langle K \mid O_K \mid 0\rangle e^{-E_{\pi\pi}(t_{\pi\pi}-t)} e^{-m_K t} && (4.240)\\ &+ \cdots && (4.241) \end{aligned}$$

where the additional complication comes from the appearance of the first term, which needs to be removed before $K \to \pi\pi$ matrix elements can be extracted. This can be done automatically, by noting that we can shift each of the four-fermion operators in

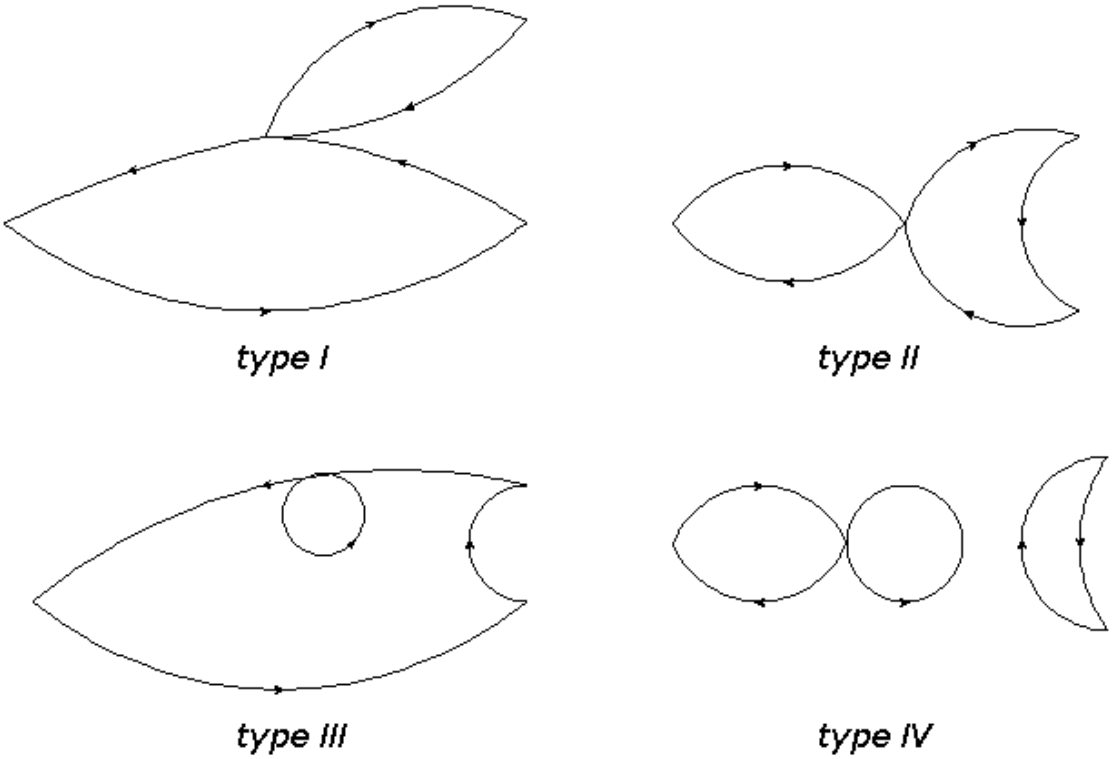

Figure 4.9: Wick contractions contributing to $K \to \pi\pi$ $\Delta I = 1/2$ channel.

the weak Hamiltonian by a multiple of an irrelevant operator $\bar{s}\gamma^5 d$ (c.f. Eq. (2.136)) $O_i^R = O_i + \alpha_i \bar{s}\gamma^5 d$ in such a way that the shifted weak Hamiltonian H_W^R satisfies

$$\langle 0 \mid H_W^R \mid K \rangle = \sum_i C_i \langle 0 \mid Q_i + \alpha_i \bar{s}\gamma^5 d \mid K \rangle = 0. \tag{4.242}$$

This condition will also be useful in the following section.

4.14.2 Dimension-3 operator subtraction

$\Delta I = 1/2$ $K \to \pi\pi$ decays involve contractions given by type 3 and type 4 diagrams shown in Fig. 4.9. These contractions contain loops, which are superficially quadratically divergent. This divergence can be absorbed by counterterms of the form $\bar{s}\gamma^5 d$. Eq. 2.136 shows that these operators can not contribute to $K \to \pi\pi$ matrix elements or indeed to any on-shell matrix elements. The situation is different in lattice simulations where the energies of initial and final states need to be tuned by hand, so in our case $m_K - E_{\pi\pi} \neq 0$. This means that the matrix elements calculated on the lattice will contain a real divergence of order $m_K - E_{\pi\pi}$, but enhanced by inverse powers of lattice spacing. This divergent contribution needs to be renormalised and we can conveniently use Eq. 4.242 as the renormalisation condition.

4.14.3 G-parity

Even after subtracting the vacuum, the lowest energy contribution corresponds to two pions at rest as argued in section 4.7. In the $\Delta I = 3/2$ case we exploit the fact that $\mid \pi^+\pi^+\rangle$ is an I=2 state, which with the help of Wigner-Eckart theorem allows us to remove the π^0 from the final state. This allowed us to break the isospin at the boundary by giving up quarks periodic and down quarks antiperiodic boundary conditions. This trick is no longer feasible for I=0 final state, which contains both $\pi^\pm$ and π^0 particles.

Because we want all pions to have antiperiodic boundary conditions to induce non-zero momenta, a reasonable choice is to use the G-parity boundary conditions, as mentioned in section 2.3.4. This choice creates another difficulty, because kaon is not a G-parity eigenstate. This problem is solved by introducing another flavour, s', which is a G-parity partner of the strange quark, so that

$$s(x+L) = s'(x) \tag{4.243}$$

$$s'(x+L) = -s(x). \tag{4.244}$$

This allows us to construct a G-parity even state (which we want to keep the kaon at rest) $\bar{d}\gamma^5 u + \bar{s}'\gamma^5 u$. To obtain physical results we must subsequently remove the strange quark. In the valence sector there is no problem - the G-parity symmetric kaon interpolator has to be contracted with the weak Hamiltonian, which contains the $\bar{s}$ field. This means that the unphysical part of the kaon interpolator will only contract with the weak Hamiltonian after crossing the boundary resulting in a volume suppression of this contribution. The s' quark will also introduce another sea quark flavour, which will appear in loops. Because s and s' quarks are degenerate, we can remove the additional contribution by taking the square root of their determinants.

Chapter 5

Results

This chapter summarises the results of our calculations. Section 5.1 summarises the ensembles we used in this analysis. Sections 5.2, 5.3 and 5.4 describe the results of the fits, nonperturbative renormalisation and finite volume effects, all of which are necessary ingredients in determining the value of A_2. Section 5.5 describes the breakdown of systematic errors and section 5.6 shows the results of the continuum extrapolation. Finally, section 5.7 contains discussion of the $\Delta I = 1/2$ rule in the light of our results. All the analysis presented in these sections with the exception of determination of renormalisation constants is my original work. The continuum extrapolation was performed jointly with Dr. Chris Kelly. This includes fitting the correlation functions to extract the matrix elements, the analysis of finite volume effects and the error budget.

The final section of this chapter contains a different calculation, which is the determination of $K - \pi$ scattering lengths using our physical point ensembles. This calculation was entirely my original work, including writing the contractions code and the analysis.

5.1 Ensemble parameters

The calculations described below have been performed on two new 2+1 flavour ensembles generated with the Iwasaki gauge action and with Möbius domain wall fermions [50] . The parameters of the ensembles are:

(i) $48^3 \times 96 \times 24$ with $\beta = 2.13$ ($a^{-1} = 1.728(4)\,\text{GeV}$);

(ii) $64^3 \times 128 \times 12$ with $\beta = 2.25$ ($a^{-1} = 2.357(7)\,\text{GeV}$).

These two ensembles use the Möbius variant of domain wall fermions [52] with a Möbius scale factor $\alpha = 2$. For compactness of notation we will refer to these ensembles as 48^3 and 64^3 respectively. The lattice spacing and quark masses were set by choosing the

masses of the pion, kaon and the Ω-baryon to be equal to their physical values. The corresponding sea quark masses are $am_{ud} = 7.8 \times 10^{-4}$ and $am_s = 3.62 \times 10^{-2}$, with the residual mass $am_{res} = 6.19(6) \times 10^{-4}$ for the 48^3 ensemble and $am_{ud} = 6.78 \times 10^{-4}$, $am_s = 2.661 \times 10^{-2}$ and $am_{res} = 2.93(8) \times 10^{-4}$ for the 64^3 ensemble. The two ensembles have approximately the same physical volume with spatial extent $L \simeq 5.5\,\text{fm}$, enabling the continuum extrapolation to be separated from finite-volume effects which we estimate separately. For more details on these ensembles see [50] and we will return briefly to the determination of the lattice spacings in the context of the continuum extrapolation in Sec. 5.6.

The results presented below were obtained using 76 gauge configurations on the 48^3 ensemble and 40 on the 64^3 ensemble. The large statistical uncertainty one expects with a relatively small number of gauge configurations can be significantly reduced if we perform many measurements on each configuration in which the sources and sinks are simply translated in space and time [50]. Performing multiple measurements on the same configuration offers two important opportunities for increased efficiency. First if we can use a low-mode deflation method such as eigCG [53] we will be able the amortise the set-up costs of such an approach over a large number of inversions. Second we can use the all mode averaging technique [39] and perform most of these many inversions at reduced precision and use a relatively few accurate inversions to determine a correction that guarantees systematic double precision but with an additional (usually small) statistical error that reflects the small number of accurate solves. Specifically for the 48^3 ensemble, the eigCG method was used in single precision with 600 approximate low-lying eigenvectors and a stopping residual of 10^{-4}. The approximate (wall source) propagators were computed on all 96 time slices. The accurate solves used to correct the approximation were computed on time slices 0, 76, 72, 68, 64, 60 and 56 with CG stopping residual 10^{-8}. (This choice of time-slice separations is not related to the $K \to \pi\pi$ calculation presented here but to an accompanying calculation of B_K [50].) To ensure that no bias results from the choice of inexact solves for which the correction is calculated, this complete pattern of source time slices for the accurate solves was shifted by a different random time displacement on each configuration. A similar procedure was used on the 64^3 ensemble but with 1500 low-modes and a stopping residual of 10^{-5} for the approximate solves and accurate solves on time slices 0, 103, 98, 93, 88, 83, 78 and 73. On both the ensembles, the accurate CG solves were also computed using eigCG, exploiting the approximate eigenvectors created during the inaccurate applications of eigCG.

Measurements on the 48^3 and 64^3 ensembles are separated by 20 MD and 40 MD units respectively. In order to study the effects of autocorrelations we bin the data. We find that the effects are small, typically leading to a variation of the statistical errors of less than 10%. The results presented below were obtained after binning the 76 configurations of the 48^3 ensemble into 19 bins of 4 configurations and the 40 configurations of the 64^3

	m_π	m_K	$E_{\pi\pi}$	$m_K - E_{\pi\pi}$
48^3 (lattice units)	$8.050(13) \times 10^{-2}$	$2.8867(15) \times 10^{-1}$	$2.873(13) \times 10^{-1}$	$1.4(14) \times 10^{-3}$
64^3 (lattice units)	$5.904(14) \times 10^{-2}$	$2.1531(14) \times 10^{-1}$	$2.1512(68) \times 10^{-1}$	$9(10) \times 10^{-4}$
48^3 (MeV)	139.1(2)	498.82(26)	496.5(16)	2.4(24)
64^3 (MeV)	139.2(3)	507.4(4)	507.0(16)	2.1(26)

Table 5.1: Pion and kaon masses and the I=2 two-pion energies in lattice and physical units measured on the 48^3 and 64^3 ensembles. The momentum of each of the final-state pions is $\pm\pi/L$ in each of the three spatial directions.

ensemble into 8 bins of 5 configurations. The 40 configurations from the 64^3 ensemble are precisely those used in the global analysis reported in [50]. The 76 configurations from the 48^3 ensemble include 73 of the 80 used in [50]. We have however, repeated the relevant analysis of [50], including the determination of the lattice spacings, using precisely the 76 configurations for which we have computed A_2. This makes it possible to compute standard jackknife errors for our physical results which necessarily depend upon the value of the lattice spacing.

The pion (m_π) and kaon masses (m_K) as well as the energies of the $I = 2$ two-pion state ($E_{\pi\pi}$) obtained on the two ensembles are shown in Tab. 5.1. The fitting ranges used for pion and kaon masses as well as two pion energies were from 10 to 86 on the 48^3 ensemble and from 10 to 118 on the 64^3 ensemble. These choices were motivated by the plateaus in the effective mass plots shown in figures 5.1 - 5.2. The effective mass of the kaon, m_K^{eff}, is defined numerically by the ratio:

$$\frac{C_K(t+1)}{C_K(t)} = \frac{\cosh(m_K^{\text{eff}}(t+1-T/2))}{\cosh(m_K^{\text{eff}}(t-T/2))}, \tag{5.1}$$

and the two-pion effective mass, $E_{\pi\pi}^{\text{eff}}$, is found by inverting:

$$\frac{C_{\pi\pi}(t+2) - C_{\pi\pi}(t+1)}{C_{\pi\pi}(t+1) - C_{\pi\pi}(t)} = \frac{e^{-E_{\pi\pi}^{\text{eff}}(t+2)} + e^{-E_{\pi\pi}^{\text{eff}}(T-t-2)} - e^{-E_{\pi\pi}^{\text{eff}}(t+1)} + e^{-E_{\pi\pi}^{\text{eff}}(T-t-1)}}{e^{-E_{\pi\pi}^{\text{eff}}(t+1)} + e^{-E_{\pi\pi}^{\text{eff}}(T-t-1)} - e^{-E_{\pi\pi}^{\text{eff}}t} + e^{-E_{\pi\pi}^{\text{eff}}(T-t)}}. \tag{5.2}$$

The two-point correlation functions C_K and $C_{\pi\pi}$ are defined explicitly in Eq. (4.81) and (4.104) and the differences in the numerator and denominator on the left-hand side of Eq. (5.2) are introduced to eliminate the constant C in Eq. (4.107).

The pion and kaon masses correspond closely to their physical values. We will explain below that the pions are given a momentum π/L in each of the three spatial directions and from the table we see that with this choice $E_{\pi\pi} \simeq m_K$ and the $K \to \pi\pi$ matrix elements correspond to the on-shell (within statistical errors) decay of a kaon in the centre-of-mass frame. We now discuss the evaluation of the matrix elements.

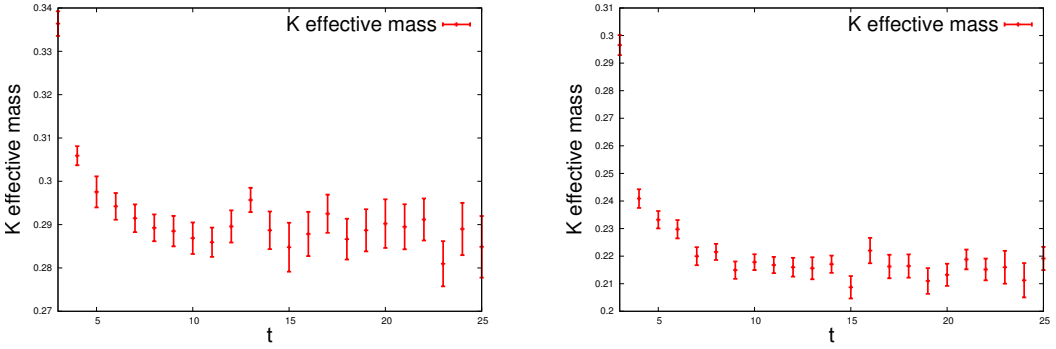

Figure 5.1: Effective mass plots for the kaon correlation functions on the 48^3 ensemble (left) and 64^3 ensemble (right).

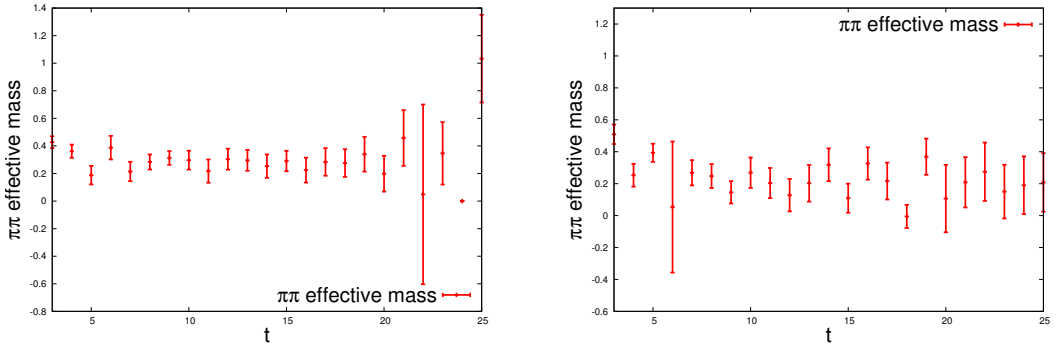

Figure 5.2: Effective mass plots for the two-pion correlation functions on the 48^3 ensemble (left) and 64^3 ensemble (right).

5.2 Matrix elements

We have evaluated $C_i^{K\to\pi\pi}(t_{\rm op})$ given by Eq. (4.117) corresponding to $K^+ \to \pi^+\pi^+$ process as discussed in section 4.7 for a range of values of the source-sink separations $t_{\pi\pi}$. For the 48^3 (64^3) ensemble we performed the calculations for values of $t_{\pi\pi}$ between 24 and 39 (26 and 36). These separations were chosen to be large enough for the plateau region to give a reliable fit and small enough for the around-the-world effects to be small. The fitting ranges were chosen to be from 10 to $t_{\pi\pi} - 10$ for both ensembles. These choices are motivated by the locations of plateau regions in Fig. 5.3.

For illustration, in Fig. 5.3 we plot $C_i^{K\to\pi\pi}(t_{\rm op})$ computed on each of the two ensembles for $t_{\pi\pi} = 26$. The observed plateaus are a manifestation of the fact that the volumes have been tuned so that $E_{\pi\pi} \simeq m_K$ (cf. Eq. (4.119)).

As a check, we can also construct the time-independent ratio of the correlation functions:

$$\frac{C^i_{K\to\pi\pi}(t)}{C_K(t)\, C^{I=2}_{\pi\pi}(t_{\pi\pi}-t)} = \frac{M_i^{\rm bare}}{N_{\pi\pi} N_K}. \tag{5.3}$$

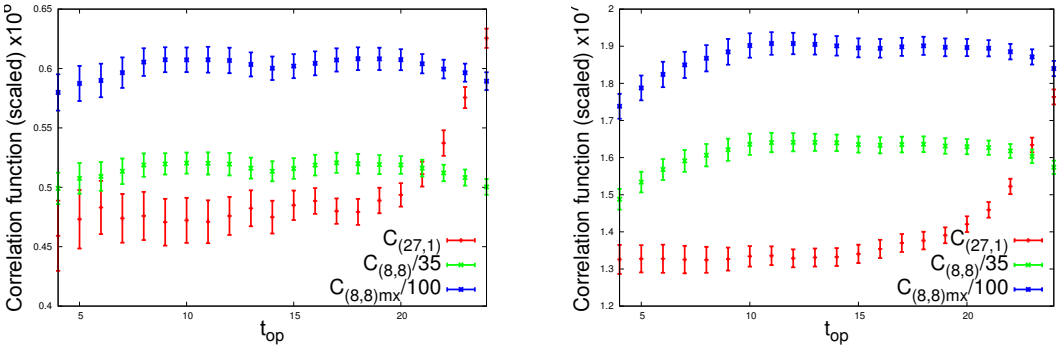

Figure 5.3: $K \to \pi\pi$ three-point correlation function on the 48^3 lattice (left) and 64^3 lattice (right) with a kaon-pion separation of $t_{\pi\pi} = 26$.

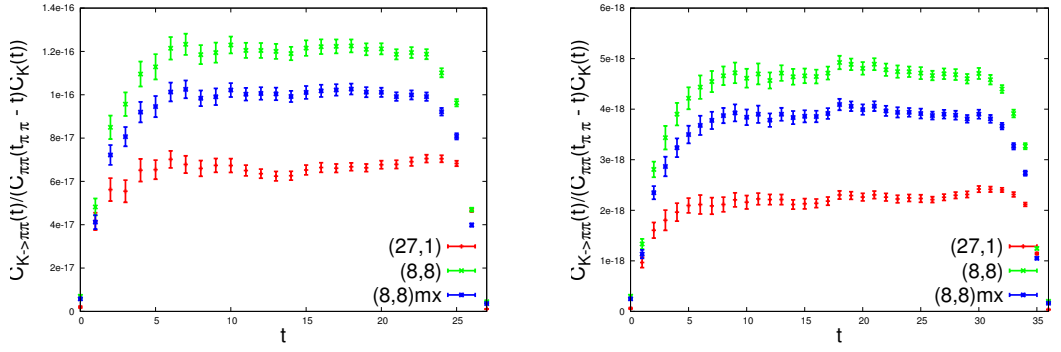

Figure 5.4: Ratios of $K \to \pi\pi$ three-point correlation function to the two point functions (Eq. (5.3)) on the 48^3 lattice (left) and the 64^3 lattice (right) with a kaon-pion separation of $t_{\pi\pi} = 26$.

This ratio is plotted for $t_{\pi\pi} = 26$ in Fig. 5.4. As anticipated, all three operators exhibit a constant behaviour in the region where the contribution from excited states is negligible. Eq. (5.3) is expected to hold in the region $0 \ll t \ll t_{\pi\pi} \ll T$, where T is the total time extent of the lattice. In this region 'around-the-world' effects arising from different time orderings of the operators can be neglected.

The values of the bare $K^+ \to \pi^+\pi^+$ matrix elements are shown in Tab. 5.2. The entries have been obtained by performing weighted averages (under the jackknife) over the values obtained for each choice of $t_{\pi\pi}$, i.e.

$$M_i = \frac{\sum_{t_{\pi\pi}} M_i(t_{\pi\pi})/\delta M(t_{\pi\pi})^2}{\sum_{t_{\pi\pi}} 1/\delta M(t_{\pi\pi})^2} \tag{5.4}$$

where $M_i(t_{\pi\pi}$ is the matrix element evaluated using source-sink separation $t_{\pi\pi}$ and $\delta M_i(t_{\pi\pi}$ is the corresponding statistical error.

	$a^3 M^{\text{bare}}_{(27,1)}$	$a^3 M^{\text{bare}}_{(8,8)}$	$a^3 M^{\text{bare}}_{(8,8)\text{mx}}$
48^3 ensemble	$7.400(70) \times 10^{-5}$	$9.171(69) \times 10^{-3}$	$3.058(23) \times 10^{-2}$
64^3 ensemble	$2.742(22) \times 10^{-5}$	$3.942(39) \times 10^{-3}$	$1.308(13) \times 10^{-2}$

Table 5.2: Results for the bare $K^+ \to \pi^+\pi^+$ matrix elements in lattice units. Only statistical errors are shown.

5.3 NPR

In the calculation of $Z_{ij}^{lat\to RI}$ we find that all the chirally forbidden renormalisation factors mixing (27,1) and (8,8) representations are smaller than 10^{-5}, so we set the corresponding matrix elements of $P_i\{\Lambda_j\}$ to zero and finally obtain the lattice to RI-SMOM renormalisation matrices:

$$Z^{(\gamma^\mu,\gamma^\mu)}_{\beta=2.13}(\mu = 3\,\text{GeV}) = \begin{pmatrix} 0.4617(3) & 0 & 0 \\ 0 & 0.5302(4) & -0.07018(6) \\ 0 & -0.0386(1) & 0.4451(5) \end{pmatrix} \tag{5.5}$$

$$Z^{(\not{q},\not{q})}_{\beta=2.13}(\mu = 3\,\text{GeV}) = \begin{pmatrix} 0.4822(3) & 0 & 0 \\ 0 & 0.5305(4) & -0.07135(7) \\ 0 & -0.0637(1) & 0.5052(6) \end{pmatrix} \tag{5.6}$$

for the 48^3 ensembles and

$$Z^{(\gamma^\mu,\gamma^\mu)}_{\beta=2.25}(\mu = 3\,\text{GeV}) = \begin{pmatrix} 0.5194(2) & 0 & 0 \\ 0 & 0.5774(2) & -0.0751(1) \\ 0 & -0.02797(7) & 0.4431(6) \end{pmatrix} \tag{5.7}$$

$$Z^{(\not{q},\not{q})}_{\beta=2.25}(\mu = 3\,\text{GeV}) = \begin{pmatrix} 0.5399(2) & 0 & 0 \\ 0 & 0.5782(2) & -0.0761(1) \\ 0 & -0.05230(4) & 0.4990(5) \end{pmatrix} \tag{5.8}$$

for the 64^3 ensembles. With momentum sources [54], only few configurations are needed to obtain an excellent statistical precision. The number of Landau gauge-fixed configurations used to obtain these results varies between 5 and 15. The statistical errors were estimated with 200 bootstrap samples. The matrices in Eqs. (5.5) – (5.8) are the ones used in Eq. (4.232) to obtain the operators renormalised in the RI-SMOM schemes at the scale $\mu = 3\,\text{GeV}$ from the corresponding lattice bare operators.

The procedure described above enables us to calculate the matrix elements of the operators in Eq. (4.129) in the (continuum) RI-SMOM schemes with a very small systematic uncertainty due to the renormalisation. The Wilson coefficients however, are computed in the $\overline{MS}$ scheme and so we have to match the RI-SMOM schemes to the $\overline{MS}$ one.

	48^3 Ensembles	64^3 Ensembles
$\mathrm{Re}(A_2)$ (γ^μ, γ^μ)	$1.346(11)_{\mathrm{stat}}(1)_{\mathrm{NPR}} \times 10^{-8}\,\mathrm{GeV}$	$1.4029(93)_{\mathrm{stat}}(11)_{\mathrm{NPR}} \times 10^{-8}\,\mathrm{GeV}$
$\mathrm{Im}(A_2)$ (γ^μ, γ^μ)	$-5.739(46)_{\mathrm{stat}}(8)_{\mathrm{NPR}} \times 10^{-13}\,\mathrm{GeV}$	$-6.143(73)_{\mathrm{stat}}(9)_{\mathrm{NPR}} \times 10^{-13}\,\mathrm{GeV}$
$\mathrm{Re}(A_2)$ $(\not{q}, \not{q})$	$1.386(12)_{\mathrm{stat}}(1)_{\mathrm{NPR}} \times 10^{-8}\,\mathrm{GeV}$	$1.4386(95)_{\mathrm{stat}}(11)_{\mathrm{NPR}} \times 10^{-8}\,\mathrm{GeV}$
$\mathrm{Im}(A_2)$ $(\not{q}, \not{q})$	$-6.174(49)_{\mathrm{stat}}(9)_{\mathrm{NPR}} \times 10^{-13}\,\mathrm{GeV}$	$-6.548(78)_{\mathrm{stat}}(10)_{\mathrm{NPR}} \times 10^{-13}\,\mathrm{GeV}$

Table 5.3: The amplitude A_2 calculated using two different intermediate RI-SMOM schemes. The two errors, labelled by "stat" and "NPR", are the statistical uncertainties in the evaluation of the bare matrix elements and Z_{ij} respectively. Discrepancies in the results in the two schemes are attributed to the truncation in the matching to the $\overline{\mathrm{MS}}$ scheme.

We repeat that this matching is perturbative and at present is only known to one-loop order [55]; this limitation amplifies the uncertainty due to the renormalisation. This uncertainty could be reduced by extending the perturbative calculations to higher orders. Future lattice calculations could also help here by using step scaling to run the renormalisation constants obtained in the RI-SMOM schemes non-perturbatively to larger momentum scales. The perturbative matching to the $\overline{MS}$ scheme can then be performed at these larger scales where the coupling constant is smaller, leading to smaller uncertainties. We now estimate the current uncertainty due to the matching.

To estimate the uncertainty due to the truncation of the perturbative matching factors, we note that the matrix elements in the $\overline{MS}$ scheme should be independent of the choice of intermediate RI-SMOM scheme. Differences in the results are observed (see Table 5.3) and attributed to the truncation. Following the procedure in [36; 12] we take the result obtained using the $(\not{q}, \not{q})$ intermediate scheme as our central value and the difference of the results obtained using the two schemes as an estimate of the systematic error. This uncertainty is marked as "NPR (perturbative)" in the error budgets presented in Tables 5.9 and 5.10 in Sec. 5.5. The uncertainties marked as "NPR (nonperturbative)" are the statistical errors in the evaluation of Z_{ij}.

5.4 Two-meson phase shift and finite volume effects

We now proceed to discuss the calculation of the finite volume effects and the Lellouch-Lüscher factor given by Eq. (4.191). This requires the knowledge of the derivative of the phase shift, while Lüscher's quantisation condition Eq. (4.174) gives only the the value of the phase shift at a given momentum. The results presented in Table 5.4 were obtained using the approximation that δ is a linear function of the momentum between 0 and p. Since the second term in the parentheses on the right-hand side of Eq. (4.191) is much smaller than the first and given the remaining systematic uncertainties discussed in Sec. 5.5, this procedure gives an adequate approximation. In order to estimate

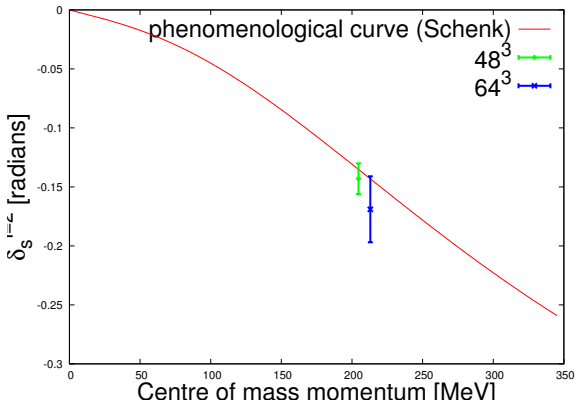

Figure 5.5: Comparison of $I = 2$ two-pion s-wave phase shifts calculated using Lüscher's formula with the phenomenological curve from Ref. [1]. The computed results are consistent with the phenomenological curve.

the error due to this approximation we also evaluate the derivative $\frac{\partial\delta}{\partial p}$ using the phenomenological curve of Ref. [1] illustrated in Fig. 5.5; we take the difference of the two procedures as an estimate of the corresponding uncertainty. For our central value we use the linear approximation for the derivative of the phase shift so that it is independent of phenomenological estimates.

At the pion momentum which corresponds to the decay of a physical kaon to two pions ($p = 207\,\mathrm{MeV}$) the value of the derivative of the phase shift with respect to the momentum obtained from the phenomenological curve is $9.53 \times 10^{-4}\,\mathrm{MeV}^{-1}$. Converting this to $\frac{\partial\delta}{\partial q}$ gives -0.216 for the 48^3 and -0.221 for the 64^3 ensembles. While this makes a significant difference to the derivative of the phase shift, it represents a relatively small uncertainty in the Lellouch-Lüscher factor $F \propto \frac{\partial\delta}{\partial q} + \frac{\partial\phi}{\partial q}$. This sum is dominated by the $\frac{\partial\phi}{\partial q}$ term and thus the difference in the Lellouch-Lüscher factor between both approaches to calculating $\frac{\partial\delta}{\partial q}$ amounts to 1.1% and 0.6% on the 48^3 and 64^3 ensembles respectively.

When quoting our central value we include the Lellouch-Lüscher factor evaluated as described in the preceding paragraph. In order to estimate the size of the remaining exponential finite-volume effects we use chiral perturbation theory equations (4.192) and (4.193) and include the corresponding effects in our systematic uncertainty. Since we are only calculating an estimate, we do not use partially twisted chiral perturbation theory, but take both the sea and valence d-quarks to satisfy antiperiodic boundary conditions. The results are shown in table 5.5.

5.5 Error budget

In this section we discuss the two remaining systematic errors: those which arise because the meson masses and the two-pion energy are not quite physical and those introduced

	$E_{\pi\pi}$	q	δ (radians)	$\frac{\partial\delta}{\partial q}$	$\frac{\partial\phi}{\partial q}$
48^3	0.2873(13)	0.9087(61)	−0.158(22)	−0.174(24)	3.7147(20)
64^3	0.21512(68)	0.9157(43)	−0.184(16)	−0.201(17)	3.7171(15)

Table 5.4: Contributions to the Lellouch-Lüscher factor on the 48^3 and 64^3 ensembles. The rate of change of the phase shift was calculated by using a linear approximation in momentum as explained in the text.

Quantity	48^3 lattice	64^3 lattice
L	5.48 fm	5.36 fm
$\Delta l(m_\pi^2)$	$14.32\,\mathrm{MeV}^2$	$16.39\,\mathrm{MeV}^2$
$\Delta l(m_K^2)$	$(9.05\times10^{-4})\,\mathrm{MeV}^2$	$(1.03\times10^{-3})\,\mathrm{MeV}^2$
$\Delta l(m_\eta^2)$	$(1.32\times10^{-4})\,\mathrm{MeV}^2$	$(1.52\times10^{-4})\,\mathrm{MeV}^2$
$\Delta\beta(m_\pi, m_K, m_\eta)$	3.0×10^{-7}	3.0×10^{-7}
$\Delta\beta(m_\pi, m_K, m_\pi)$	5.0×10^{-5}	5.2×10^{-5}
$\Delta\beta(m_K, m_\pi, m_\pi)$	6.67×10^{-5}	6.97×10^{-5}
$\frac{\Delta M_{(27,1)}}{M_{(27,1)}}$	0.022	0.024
$\frac{\Delta M_{(8,8)}}{M_{(8,8)}}$	0.024	0.026

Table 5.5: Contributions to our estimate of the exponentially suppressed finite-volume errors.

by the perturbative Wilson coefficients. Finally all of the systematic errors in our results for the real and imaginary parts of A_2 are summarised Tables 5.9 and 5.10, respectively.

The volume, boundary conditions and quark masses have been chosen to enable simulations of physical $K \to \pi\pi$ decays. Nevertheless, since the volume and quark masses have to be chosen *a priori*, the output values of the meson masses and two-pion energies will be a little different from the physical values (see Tab. 5.1). In order to estimate the corresponding uncertainty we follow the procedure described in [56; 12] and outlined below. We use measurements on 60 quenched configurations on a 24^3 lattice with $a^{-1} = 1.31\,\mathrm{GeV}$ performed with 3 values of the light-quark masses, 5 strange-quark masses and the application of antiperiodic boundary conditions in $n_{\mathrm{tw}} = 0$, 1, 2 and 3 directions. These measurements are used to determine the coefficients in the following phenomenological formulae:

$$m_{xy}^2 = B_0(m_x + m_y) + B_1, \tag{5.9}$$

$$E_{\pi\pi}^2(n_{\mathrm{tw}}) = A_0(n_{\mathrm{tw}})m_l + A_1(n_{\mathrm{tw}}), \tag{5.10}$$

$$A_2 = C_0(n_{\mathrm{tw}})m_s + C_1(n_{\mathrm{tw}})m_l + C_2(n_{\mathrm{tw}}), \tag{5.11}$$

where m_l and m_s are the masses of the light and strange quarks, m_{xy} is the mass of the meson consisting of x and y valence quarks (which can be either light or strange) and n_{tw} is the number of directions in which the antiperiodic boundary conditions would

$n_{\rm tw}$	0	1	2	3
A_0	17.53(16)	17.14(73)	14.9(2.3)	24.5(9.5)
A_1	0.0273(12)	0.1038(60)	0.202(18)	0.196(82)
B_0	2.124	2.124	2.124	2.124
B_1	0.00692	0.00692	0.00692	0.00692
$\mathrm{Re}C_0(\mathrm{GeV})$	$1.016(55)\times10^{-7}$	$1.43(11)\times10^{-7}$	$1.53(25)\times10^{-7}$	$1.78(54)\times10^{-7}$
$\mathrm{Re}C_1(\mathrm{GeV})$	$1.697(89)\times10^{-6}$	$1.29(18)\times10^{-6}$	$1.45(38)\times10^{-6}$	$4.22(97)\times10^{-6}$
$\mathrm{Re}C_2(\mathrm{GeV})$	$2.53(51)\times10^{-9}$	$1.08(12)\times10^{-8}$	$1.68(25)\times10^{-8}$	$-2(67)\times10^{-10}$
$\mathrm{Im}C_0(\mathrm{GeV})$	$-1.06(31)\times10^{-12}$	$-4.6(3.3)\times10^{-13}$	$4.4(7.4)\times10^{-13}$	$2(11)\times10^{-13}$
$\mathrm{Im}C_1(\mathrm{GeV})$	$5.54(79)\times10^{-11}$	$3.39(91)\times10^{-11}$	$2.1(1.6)\times10^{-11}$	$-1.8(3.2)\times10^{-11}$
$\mathrm{Im}C_2(\mathrm{GeV})$	$-1.689(64)\times10^{-12}$	$-1.392(66)\times10^{-12}$	$-1.24(12)\times10^{-12}$	$-7.5(1.9)\times10^{-13}$

Table 5.6: Parameters used for extrapolations on the 24^3 quenched ensembles.

have to be imposed on the quenched lattice to get the correct two-pion energy. Note that $n_{\rm tw}$ does not have to be an integer, and is given instead by $p^2 = n_{\rm tw}\pi^2/L^2$, where p is the centre-of-mass momentum of each pion. The full list of coefficients A, B and C obtained from these quenched configurations was presented in [56] and is reproduced in Tab. 5.6.

We can use the coefficients in Tab. 5.6 to determine A_2 on the quenched ensembles for any choice of $\{m_\pi, m_K, E_{\pi\pi}\}$. We exploit this possibility for three sets of parameters: (i) the physical masses $m_K = E_{\pi\pi} = 493.7\,\mathrm{MeV}$, $m_\pi = 139.6\,\mathrm{MeV}$; (ii) the values from the 48^3 simulation given in the third row of Tab. 5.1 and (iii) the values from the 64^3 simulation given in the fourth row of Tab. 5.1. We denote the corresponding three estimates of A_2 by $A_2^{\mathrm{q;phys}}$, $A_2^{\mathrm{q;48}}$ and $A_2^{\mathrm{q;64}}$ respectively, where the superscript q reminds us that the results were obtained on the quenched ensembles. We use the differences $A_2^{\mathrm{q;48}} - A_2^{\mathrm{q;phys}}$ and $A_2^{\mathrm{q;64}} - A_2^{\mathrm{q;phys}}$ as estimates of the systematic error due to unphysical kinematics.

The results are:

$$\mathrm{Re}(A_2^{\mathrm{q;phys}}) = 2.25\times10^{-8}\,\mathrm{GeV}, \quad \mathrm{Im}(A_2^{\mathrm{q;phys}}) = -1.344\times10^{-12}\,\mathrm{GeV}, \tag{5.12}$$

$$\mathrm{Re}(A_2^{\mathrm{q;48}}) = 2.29\times10^{-8}\,\mathrm{GeV}, \quad \mathrm{Im}(A_2^{\mathrm{q;48}}) = -1.341\times10^{-12}\,\mathrm{GeV}, \tag{5.13}$$

$$\mathrm{Re}(A_2^{\mathrm{q;64}}) = 2.36\times10^{-8}\,\mathrm{GeV}, \quad \mathrm{Im}(A_2^{\mathrm{q;64}}) = -1.329\times10^{-12}\,\mathrm{GeV}. \tag{5.14}$$

The differences in Eqs. (5.12) - (5.14) translate to an estimated 1.8% error on $\mathrm{Re}(A_2)$ and 0.2% error on $\mathrm{Im}(A_2)$ on the 48^3 ensemble and a 4.5% difference for $\mathrm{Re}(A_2)$ and 1.1% difference for $\mathrm{Im}(A_2)$ on the 64^3 ensemble. These numbers are obtained from the difference of the simulated results from those at the physical point (normalised by the result at the physical point). These uncertainties are included in Tabs. 5.9 and 5.10 under the label "unphysical kinematics".

To estimate the error in the Wilson coefficients, we compare the results for A_2 using Wilson coefficients calculated at leading order and next to leading order. We have used the set of coefficients evaluated in the $\overline{MS}$ scheme at 3 GeV, which are shown

	(27,1)	(8,8)	$(8,8)_{\text{mx}}$
z_i^{LO}	0.26696	4.260055×10^{-5}	-1.0063×10^{-5}
y_i^{LO}	-0.0035185	-2.026445×10^{-4}	2.447741×10^{-4}
z_i^{NLO}	0.290342	4.70099×10^{-5}	-5.22390×10^{-5}
y_i^{NLO}	-0.00397252	-8.09555×10^{-5}	3.26016×10^{-4}

Table 5.7: Wilson coefficients at 3 GeV in the $\overline{MS}$ scheme at leading order (LO) and next-to-leading order (NLO).

	LO	NLO
$\text{Re}(A_2)$ 48^3	$1.293(11) \times 10^{-8}$	$1.386(12) \times 10^{-8}$
$\text{Im}(A_2)$ 48^3	$-5.551(45) \times 10^{-13}$	$-6.174(49) \times 10^{-13}$
$\text{Re}(A_2)$ 64^3	$1.3410(89) \times 10^{-8}$	$1.4386(95) \times 10^{-8}$
$\text{Im}(A_2)$ 64^3	$-6.037(71) \times 10^{-13}$	$-6.548(78) \times 10^{-13}$

Table 5.8: Comparison of matrix elements calculated with leading order (LO) and next-to-leading order (NLO) Wilson coefficients.

$\text{Re}A_2$ systematic errors	48^3	64^3	cont.
NPR (nonperturbative)	0.1%	0.1%	0.1%
NPR (perturbative)	2.9%	2.5%	2.9%
Finite volume corrections	2.2%	2.4%	2.4%
Unphysical kinematics	1.8%	4.5%	4.5%
Wilson coefficients	6.8%	6.8%	6.8%
Derivative of the phase shift	1.1%	0.6%	1.1%
Total	8%	9%	9%

Table 5.9: Systematic error breakdown for $\text{Re}\, A_2$

in table 5.7 [57], and the standard parametrisation of Wilson coefficients was used, i.e. $C_i = z_i + \tau y_i$ where τ is the ratio of CKM matrix coefficients $\tau = -\frac{V_{ts}^* V_{td}}{V_{us}^* V_{ud}}$. The results for matrix elements calculated at leading and next-to-leading orders are shown in Tab. 5.8. From the differences between the entries in the columns marked as LO and NLO we estimate that the uncertainties are 6.8% for $\text{Re}(A_2)$ on both sets of ensembles and 10% (8%) for $\text{Im}(A_2)$ on the 48^3 (64^3) ensembles.

Tables 5.9 and 5.10 show our estimates of systematic errors associated with the results for $\text{Re}(A_2)$ and $\text{Im}(A_2)$ presented in this paper. The evaluation of the continuum limit of A_2 is discussed in following section. As will be seen, the systematic error associated with this extrapolation is negligible with respect to the statistical errors. Consequently no discretisation error is shown in Tables 5.9 and 5.10. The values in the column marked "cont." are the errors assigned to our continuum-extrapolated results, and are simply the larger of the corresponding entries from the 48^3 and 64^3 columns. We can see that the dominant contribution to the systematic error for both real and imaginary parts of A_2 on both ensembles comes from the uncertainty in Wilson coefficients.

ImA_2 systematic errors	48^3	64^3	cont
NPR (nonperturbative)	0.1%	0.1%	0.1%
NPR (perturbative)	7.0%	6.2%	7.0%
Finite volume corrections	2.4%	2.6%	2.6%
Unphysical kinematics	0.2%	1.1%	1.1%
Wilson coefficients	10%	8%	10%
Derivative of the phase shift	1.1%	0.6%	1.1%
Total	12%	10%	12%

Table 5.10: Systematic error breakdown for Im A_2

	48I	64I	phys.
m_π/m_Ω	0.08296(17)	0.08220(19)	0.08073
m_K/m_Ω	0.29740(32)	0.29982(37)	0.29643

Table 5.11: The ratios of the pion and kaon mass to the Omega baryon mass on the 48^3 and 64^3 ensembles as well as the physical value.

5.6 Continuum extrapolation

In this section we discuss the extrapolation of the results obtained on the 48^3 and 64^3 ensembles to the continuum limit. We divide this discussion into two parts. In the first we present the complete physical results for the complex amplitude A_2 in the continuum limit. As we will observe, the dominant error in our result comes from the perturbative error assigned to the Wilson coefficients. This may be reduced in the future if higher order perturbation theory results become available or if lattice step-scaling methods are used to allow present perturbative results to be applied at a higher energy scale. Therefore, in the second part we determine the continuum limit of the individual matrix elements themselves, normalised in the regularisation-independent $(\not{q},\not{q})$ and (γ,γ) schemes.

5.6.1 Continuum limit of Re(A_2) and Im(A_2)

As already mentioned in Sec. 5.5 the quark masses used in these ensembles are very slightly larger than their physical values. This is illustrated in Tab. 5.11, in which we compare the physical and simulated values of the dimensionless quantities m_π/m_Ω and m_K/m_Ω, which are highly sensitive to the light and heavy quark masses respectively. In order to determine the values of the lattice spacing we must therefore perform a short chiral extrapolation; this is achieved using a simultaneous chiral and continuum 'global fit' that incorporates data from both ensembles. Since the (renormalised) quark masses on the two ensembles are very similar, we must include additional ensembles in order to have a sufficient spread of masses for the determination of the chiral dependence. The full set of ensembles and details of this procedure can be found in [50].

The determination of A_2 presented here was performed using 76 configurations of the 48^3 ensemble, whereas the lattice spacings in [50] were computed using 80. In order to preserve the full correlations between the jackknife samples of A_2 and the corresponding superjackknife samples of the lattice spacing, we repeated the global fit analysis using the same 76 configurations. The details of the binning are also different. In [50] we binned the 48^3 data over 5 successive measurements (100 MD time units) in order to take into account the observed autocorrelations in the data, whereas in the present calculation, we construct 19 bins each of 4 configurations. These differences lead to determined values of the lattice spacings in Eq. (5.15) below which are a little different from those in [50]. For the 64^3 ensembles we use the same set of 40 configurations for the evaluation of A_2 and the same binning as in the global fit in [50].

In order to estimate the systematic errors due to the chiral extrapolation and finite volume in the determination of the lattice spacings, we have performed our fits using three different chiral ansätze: NLO SU(2) chiral perturbation theory, with and without finite-volume corrections (referred to as the ChPTFV and ChPT forms respectively), and a linear ansatz (referred to as the 'analytic' form). In practice we found the lattice spacings obtained from all three ansätze to be consistent to within a fraction of the statistical error due to the dominance of the near-physical data, hence we treat these systematic errors as negligible. The final results for the values of the lattice spacing are:

$$a_{64}^{-1} = 2.3584(70)\ \text{GeV} \quad \text{and} \quad a_{48}^{-1} = 1.7280(41)\ \text{GeV}\,, \tag{5.15}$$

where the errors are statistical only.

The lattice matrix elements M_i scale as a^3 and so small differences in the lattice spacing become amplified. We have performed the continuum extrapolation of A_2 using the lattice spacings obtained with each of the three chiral ansätze; the extrapolated values are given in Tab. 5.12. In figure 5.6 we show the continuum extrapolation in the $(\not{q}, \not{q})$ scheme using the lattice spacings obtained with the ChPTFV chiral ansatz. We use results obtained with this ansatz as our central values for each lattice spacing and for the extrapolated value in the continuum.

We obtain an estimate of the component of the chiral extrapolation error arising from the lattice spacing determination by taking the difference between the continuum values obtained using the ChPTFV and analytic lattice spacings. The full jackknife differences are $0.3(2.6) \times 10^{-10}$ and $0.1(1.2) \times 10^{-14}$ for the real and imaginary parts respectively. As with the lattice spacings, we cannot resolve these differences within the statistical error, hence we set the chiral error to zero. On the other hand the jackknife differences between the ChPTFV and ChPT ansätze are resolvable as they differ only in small Bessel function corrections and are thus highly correlated: we obtain $3.4(1.0) \times 10^{-11}$ and $1.59(47) \times 10^{-15}$ for the real and imaginary parts respectively. Nevertheless, these errors are only 5–8% of the statistical error and can therefore also be neglected. This

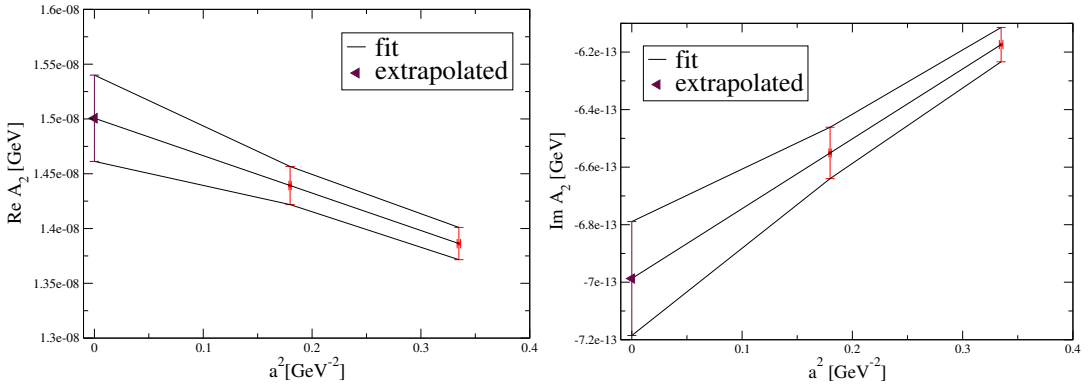

Figure 5.6: The continuum extrapolation of $\mathrm{Re}(A_2)$ (left) and $\mathrm{Im}(A_2)$ (right). The points at finite lattice spacing are taken from Tab. 5.3 for the $(\not{q},\not{q})$ intermediate renormalisation scheme.

Ansatz	$\mathrm{Re}(A_2)$ ($\times 10^{-8}$ GeV)	$\mathrm{Im}(A_2)$ ($\times 10^{-13}$ GeV)
ChPTFV	1.501(39)	-6.99(20)
ChPT	1.494(38)	-6.96(19)
analytic	1.494(43)	-6.96(21)

Table 5.12: The continuum values of $\mathrm{Re}(A_2)$ and $\mathrm{Im}(A_2)$ determined using the lattice spacings obtained with each of the three chiral ansätze.

Systematic errors in $\mathrm{Im}A_2/\mathrm{Re}A_2$	48^3	64^3	cont
NPR (nonperturbative)	0.1%	0.1%	0.1%
NPR (perturbative)	7.6 %	6.7 %	7.6 %
Finite volume corrections	3.5 %	3.5 %	3.5 %
Unphysical kinematics	1.8 %	4.6%	4.6%
Wilson coefficients	12.0 %	10.5 %	12.0%
Derivative of the phase shift	0	0	0
Total	14.7%	13.7%	15.3%

Table 5.13: Systematic error breakdown for $\mathrm{Im}A_2/\mathrm{Re}A_2$.

leads to the result:

$$\mathrm{Re}(A_2) = 1.501(39)\times 10^{-8}\ \mathrm{GeV} \qquad \text{and} \qquad \mathrm{Im}(A_2) = -6.99(20)\times 10^{-13}\ \mathrm{GeV}\,, \quad (5.16)$$

where the errors are statistical.

Our final result for A_2 is obtained by assigning the 9% and 12% systematic errors from Tabs. 5.9 and 5.10 as the systematic errors to be associated with the values for $\mathrm{Re}(A_2)$ and $\mathrm{Im}(A_2)$ given in Eq. (5.16):

$$\boxed{\mathrm{Re}(A_2) = 1.50(4)_{\mathrm{stat}}(14)_{\mathrm{syst}}\times 10^{-8}\ \mathrm{GeV}; \qquad \mathrm{Im}(A_2) = -6.99(20)_{\mathrm{stat}}(84)_{\mathrm{syst}}\times 10^{-13}\ \mathrm{GeV}\,.} \quad (5.17)$$

In order to estimate the unknown quantity $\mathrm{Im}A_0$, we combine our results for A_2 with the experimental values of $\mathrm{Re}A_0 = 3.3201(18)\times10^{-7}$ GeV and $\epsilon'/\epsilon = (1.65\pm0.26)\times10^{-3}$ [16]. To this end we start by evaluating the ratio $\mathrm{Im}A_2/\mathrm{Re}A_2$, taking account any statistical correlations between the real and imaginary parts by performing the analysis within the jackknife procedure. On the two ensembles we find

$$\left(\frac{\mathrm{Im}A_2}{\mathrm{Re}A_2}\right)_{48^3} = -4.45(5)_{\mathrm{stat}}(65)_{\mathrm{syst}}\times10^{-5} \quad \text{and} \quad \left(\frac{\mathrm{Im}A_2}{\mathrm{Re}A_2}\right)_{64^3} = -4.55(5)_{\mathrm{stat}}(62)_{\mathrm{syst}}\times10^{-5}. \tag{5.18}$$

The systematic errors for this ratio are given in Table 5.13; they are generally combined in quadrature except for that due to the derivative of the phase shift because the Lellouch-Lüscher factor cancels in the ratio. It is interesting to note that if instead of adding the errors in the Wilson coefficients for $\mathrm{Re}A_2$ and $\mathrm{Im}A_2$ in quadrature as in Tab. 5.13, we had calculated the ratios with the coefficients at leading and next-to-leading order respectively and taken the difference as a measure of the uncertainty we would have obtained a much smaller answer (3.6% instead of 12%). Since the operators which give the dominant contributions to the real and imaginary parts are different, and in the absence of an understanding which might suggest a correlation between their Wilson coefficients, we prefer to be cautious and take the larger uncertainty. We find a similar feature in the NPR perturbative error.

The continuum extrapolation of the dimensionless ratio $\mathrm{Re}A_2/\mathrm{Im}A_2$ is milder than that of $\mathrm{Re}A_2$ and $\mathrm{Im}A_2$ separately and we obtain

$$\left(\frac{\mathrm{Im}A_2}{\mathrm{Re}A_2}\right)_{\mathrm{continuum}} = -4.67(72)\times10^{-5}. \tag{5.19}$$

Using this ratio, we can calculate the electroweak penguin contribution to ϵ'/ϵ, given by:

$$\left(\frac{\epsilon'}{\epsilon}\right)_{\mathrm{EWP}} \equiv \frac{\omega}{\sqrt{2}\,|\epsilon|}\frac{\mathrm{Im}A_2}{\mathrm{Re}A_2} = -6.6(10)\times10^{-4}, \tag{5.20}$$

where we have used the values $\omega \equiv \frac{\mathrm{Re}A_2}{\mathrm{Re}A_0} = 0.04454(12)$ and $|\epsilon| = 2.228(11)\times10^{-3}$ from [12]. This value for $(\epsilon'/\epsilon)_{\mathrm{EWP}}$ is consistent with our previously quoted value $-6.25(44)(119)\times10^{-4}$ [12]. Finally, for $\mathrm{Im}A_0$ we find

$$\mathrm{Im}A_0 = \mathrm{ReA}_0\left(\frac{\mathrm{Im}A_2}{\mathrm{Re}A_2} - \frac{\sqrt{2}|\epsilon|}{\omega}\frac{\epsilon'}{\epsilon}\right) = -5.40(64)\times10^{-11}\,\mathrm{GeV}\,. \tag{5.21}$$

The results in Eqs. (5.20) and (5.21) were obtained using our result for $\mathrm{Im}A_2/\mathrm{Re}A_2$ in Eq. (5.19). If instead we take $\mathrm{Im}A_2$ from our calculation, Eq. (5.17), and combine it with the experimental result $\mathrm{Re}A_2 = 1.4787(31)\times10^{-8}\,\mathrm{GeV}$ we obtain, $\mathrm{Im}A_2/\mathrm{Re}A_2 = -4.73(58)\times10^{-5}$, $(\epsilon'/\epsilon)_{\mathrm{EWP}} = -6.69(82)\times10^{-4}$ and $\mathrm{Im}\,A_0 = -5.42(63)\times10^{-11}\,\mathrm{GeV}$.

Ensemble	Scheme	$M^{K^+}_{(27,1)}$ [GeV^3]	$M^{K^+}_{(8,8)}$ [GeV^3]	$M^{K^+}_{(8,8)\text{mx}}$ [GeV^3]
48^3	$(\not{q},\not{q})$	0.04761(39)(133)	0.7026(52)(183)	3.892(28)(101)
64^3	$(\not{q},\not{q})$	0.04848(32)(247)	0.8412(88)(244)	4.140(44)(120)
48^3	(γ,γ)	0.04473(37)(128)	0.7112(53)(185)	3.471(26)(90)
64^3	(γ,γ)	0.04664(31)(238)	0.8477(88)(246)	3.724(40)(108)
Continuum	$(\not{q},\not{q})$	0.0506(13)(26)	1.003(22)(30)	4.43(12)(13)
Continuum	(γ,γ)	0.0489(13)(25)	1.007(23)(30)	4.02(10)(12)

Table 5.14: Results for the $K^+ \to (\pi\pi)_{I=2}$ matrix elements $M_i^{K^+}$ (defined in Eq. (4.141)) in two non-exceptional RI-SMOM renormalisation schemes at the scale 3 GeV. The first error is statistical, while the second one is the systematic uncertainty estimated as described in the text.

5.6.2 Continuum limit of the RI-SMOM matrix elements

From the error budget in Tab. 5.13 we see that the dominant uncertainty is due to the Wilson coefficients, which we take to be the difference between the leading and next-to-leading order contributions as defined in [21], where the calculations were based on [58; 59; 60]. In case the Wilson coefficients in the RI-SMOM schemes become known with better precision in the future, we present in Tab. 5.14 the $K^+ \to \pi^+\pi^0$ matrix elements $M_i^{K^+}$ defined in Eq. (4.141), with the operators Q_i in Eqs. (2.102) - (2.104) renormalised in the $(\not{q},\not{q})$ and (γ,γ) renormalisation schemes at a renormalisation scale of 3 GeV. These matrix elements together with the new Wilson coefficients would enable an improved evaluation of A_2, without the need to recompute the matrix elements. The systematic errors for the (27,1) operator are estimated using the entries in Tab. 5.9 with the NPR(perturbative) and Wilson coefficient errors set to zero. This gives the errors of 2.8%, 5.1% and 5.2% for the 48^3 and 64^3 ensembles and in the continuum limit respectively. For the (8,8) operators using the entries in Tab. 5.10, the same procedure leads to systematic errors of 2.6%, 2.9% and 3.0% for the 48^3 and 64^3 ensembles and in the continuum respectively.

5.7 $\Delta I = 1/2$ rule

Before briefly summarising our results and discussing prospects for future calculations we confirm our finding, first presented in [2], that there is a significant cancellation between the two dominant contributions to $\mathrm{Re}\, A_2$. As explained above, $\mathrm{Re}(A_2)$ is dominated by the matrix element of the $(27,1)$ operator and is proportional to the sum of the two contractions C_1 and C_2 in Fig. 4.4. While naïve factorisation, frequently used for phenomenological estimates, suggests that $C_1 = 3\,C_2$ because of the colour suppression in C_2, we find a strong cancellation between these two contributions. For the 48^3 and 64^3 ensembles studied in this paper, we illustrate this cancellation in Fig. 5.8. (In Sec. 5.2 we

explain that the numerical results in this paper were obtained from correlation functions with even values of $t_{\pi\pi}$. The choice of $t_{\pi\pi} = 27$ for the 48 ensembles in Fig. 5.8 is made to ensure that the cancellation is illustrated at the same value of $t_{\pi\pi}$ in physical units on the two sets of ensembles.) As explained in [2] we believe that this cancellation is a significant component in explaining the $\Delta I = 1/2$ rule. Although we have not completed the calculation of A_0 at this stage, we note that the contributions of the $(27, 1)$ operator all contribute with the same sign. A similar partial cancellation occurs between the two corresponding contractions in the evaluation of the B_K parameter of neutral kaon mixing as pointed out in [61] and subsequently confirmed in [2; 62].

Our *ab initio* determination of A_2 shows clearly that phenomenological approaches based on the dominance of naïve factorisation are not consistent. We note however, that there were non-lattice studies based on chiral perturbation theory and the $1/N$ expansion, where N is the number of colours, which indicated that C_2 may have the opposite sign to C_1 [63; 64]. Of course, as illustrated in our results above, the $1/N$ expansion *per se* is not a good approximation; C_2 is suppressed by $1/N$ and yet is comparable to C_1. In different ways, the authors of [63; 64] combine the expansion with leading short- and long-distance logarithms. In [63] the authors use an Ansatz for matching the perturbative short-distance contributions and long-distance effects based on a chiral Lagrangian for mesons. In [64] the authors compare the experimental value of $\mathrm{Re}A_2$ with the leading term of the expansion to deduce that C_2 should be negative. For recent discussions of these two early approaches, stimulated by our lattice QCD result [2; 12] and written by subsets of their original authors, we refer the reader to [65; 66].

In order to have a fully quantitative understanding of the $\Delta I = 1/2$ rule, to determine ϵ'/ϵ and to compare the result to the experimental value $\epsilon'/\epsilon = (1.65 \pm 0.26) \times 10^{-3}$ we need to perform the evaluation of A_0 at physical kinematics. A key ingredient which makes the calculation of A_2 feasible is the use of the Wigner-Eckart theorem described in Sec. 5.2. Together with the choice of volume and the use of antiperiodic boundary conditions for the d-quark in all three spatial directions, it ensures that the energy of the two-pion ground state is equal to m_K. Unfortunately this approach cannot be directly applied to the calculation of A_0; in particular the breaking of isospin symmetry by the boundary conditions invalidates the calculation. For example, the π^0 remains at rest with the antiperiodic boundary conditions, whereas the charged pions have nonzero momentum. More sophisticated boundary conditions mixing quarks and antiquarks and an isospin rotation, the so-called *G-parity* boundary conditions [67; 34; 68; 69; 70], must therefore be used instead for both the valence and the sea quarks. The evaluation of A_0 with G-parity boundary conditions is well underway and exciting progress has recently been reported in [71] and we anticipate the first complete calculation of A_0, albeit on a single lattice spacing, within the next year.

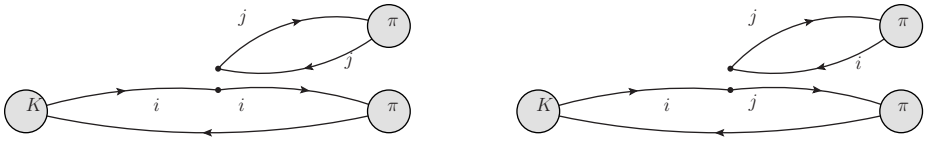

Figure 5.7: Dominant contractions contributing to Re(A_2) - C_1 (left) and C_2 (right)

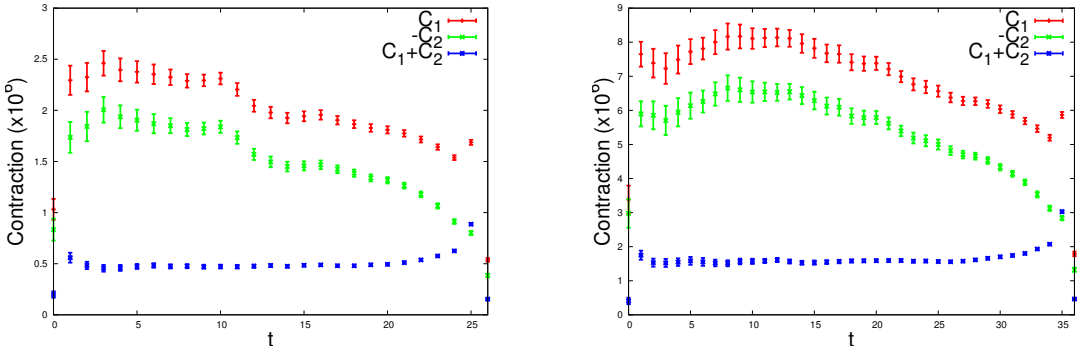

Figure 5.8: Cancellation of dominant contributions to Re(A_2) on the 48^3 ensembles with a K - $\pi\pi$ separation of 27 and the 64^3 ensembles with separation 36.

5.8 $K\pi$ scattering

In this section I will describe a different calculation which was done using the same 48^3 and 64^3 ensembles, which is the calculation of $K-\pi$ scattering lengths at physical kinematics. This calculation has been described in [4]. While this calculation is not in itself related to the $K \to \pi\pi$ decays, the techniques used are the same as in the case of $\pi\pi$ scattering, exploiting mostly Lüscher's quantisation condition (4.174). However, it is an interesting illustration of the effect of finite time extent (sometimes called 'thermalisation effects' referring to finite temperature calculations).

For this calculation we use stochastic $Z2 \times Z2$ sources with $\eta(x) = \pm 1 \pm i$ as described in section 4.5 with point sinks. The inversions are done on every second timeslice on the 48^3 ensemble and every fourth on the 64^3 ensemble.

The $K-\pi$ correlation functions are given by

$$C^I_{K\pi}(t) \equiv \langle K^\dagger(t+2)\pi^\dagger(t)\pi(2)K(0)\rangle \tag{5.22}$$

where the operator $\pi(2)K(0)$ is understood to be taken in the correct isospin projection - either 3/2 or 1/2.

The Wick contractions are shown in Figures 5.9, 5.10. For 'D' and 'C' contractions, the propagator sources are all located on the meson source planes (e.g. t=0 and t=2).

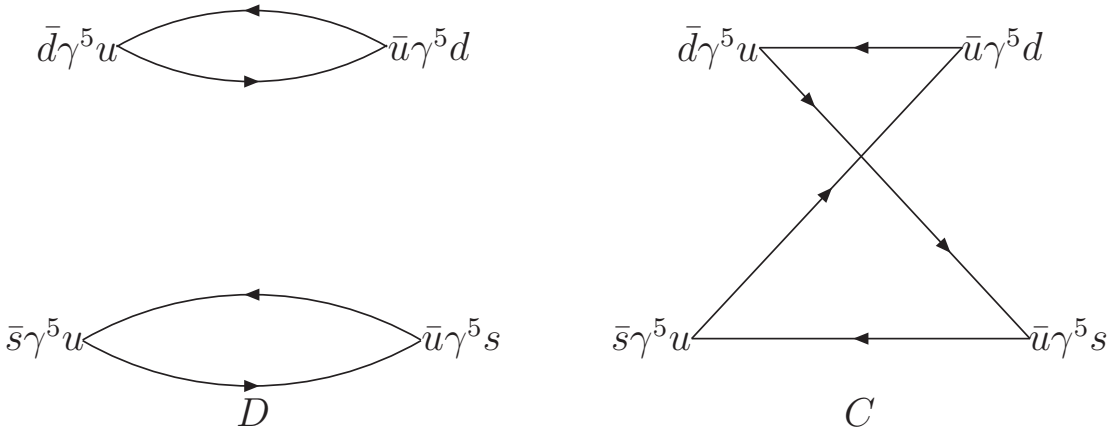

Figure 5.9: Contraction corresponding to $K\pi$ I=3/2 scattering: D (left) and C(right)

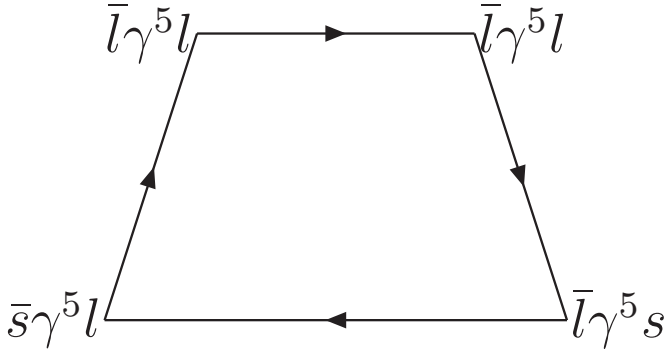

Figure 5.10: Additional contraction in the $K\pi$ I=1/2 scattering: R

For the 'R' contractions, the source planes correspond to the opposite vertices of the rectangle. The correlation functions can be written in terms of these contractions as

$$C_{K\pi}^{I=3/2} = D - C \tag{5.23}$$

$$C_{K\pi}^{I=1/2} = D + \frac{1}{2}C - \frac{3}{2}R. \tag{5.24}$$

We can do this because in the limit of the large number of random source vectors, the stochastic sources reduce to the meson point sources.

The time dependence of these functions follows from Eq. 4.73 and is given by

$$\begin{aligned}
C_{K\pi}^{I}(t) &= \langle K^\dagger(t+2)\pi^\dagger(t)\pi(2)K(0)\rangle && (5.25)\\
&= |\langle K\pi \mid \pi(2)K(0) \mid 0\rangle|^2\, e^{-E_{K\pi}(t+2)} && (5.26)\\
&+ |\langle 0 \mid \pi(2)K(0) \mid K\pi\rangle|^2\, e^{-E_{K\pi}(T-t-2)} && (5.27)\\
&+ |\langle K \mid \pi(2)K(0) \mid \pi\rangle|^2\, e^{-m_\pi(T-t-2)} e^{-m_K(t+2)} && (5.28)\\
&+ |\langle \pi \mid \pi(2)K(0) \mid K\rangle|^2\, e^{-m_K(T-t-2)} e^{-m_\pi(t+2)} && (5.29)\\
&+ \ldots .
\end{aligned}$$

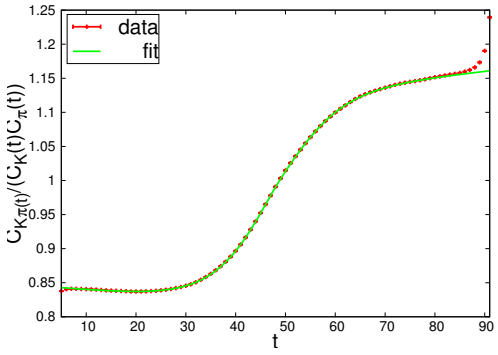

Figure 5.11: Ratio of $C_{K\pi}(t)/(C_K(t)C_\pi(t))$ with the best fit curve.

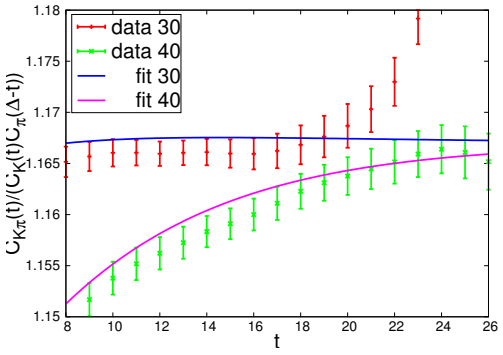

Figure 5.12: Fits for K-to-π matrix elements with K-pi separation of 30 and 40.

For sufficiently large time extent, T, contributions from the terms given by Eqs. (5.27-5.29) will be negligible in comparison to the term given by Eq. (5.26). In this case the correlation function has a time dependence given by a single exponential. Our experience with π-π scattering shows that the most accurate estimate of the ground state energy can be obtained by considering the ratio of the two-pion correlation function to the single pion two-point functions [12]. In K-π scattering case, the corresponding ratio would be:

$$\frac{C_{K\pi}(t)}{C_\pi(t)C_K(t)} \approx Ae^{-\Delta Et} \approx A(1-\Delta Et), \tag{5.30}$$

where $\Delta E = E_{K\pi} - m_K - m_\pi$ and A is a constant. The second approximation in the above equations comes from assuming that ΔE is small. We therefore expect the ratio to be approximately linear for some $0 \ll t \ll T/2$. An example of such ratio plot is shown in Fig. 5.11. We can see that the data points for the ratio do not match the single exponential behaviour. From this observation we can conclude that 'around-the-world' effects given by equations (5.27-5.29) should be included in the fitting procedure. This requires a five-parameter fit, where the parameters are $E_{K\pi}$ and four normalisation constants which appear in terms given by equations (5.26-5.29). Such fit turns out to be stable, but fitting five parameters simultaneously can result in a large statistical error. We can extract $K \to \pi$ matrix elements from:

$$\begin{aligned} C(t) &= \langle \pi(\Delta)\pi(t+2)K(t)K(0)\rangle & (5.31)\\ &= \langle 0 \mid \pi \mid \pi\rangle\langle \pi \mid \pi(2)K(0) \mid K\rangle\langle K \mid K \mid 0\rangle e^{-m_\pi(\Delta-t)}e^{-m_K t} & (5.32)\\ &+ \langle \pi \mid \pi \mid 0\rangle\langle 0 \mid \pi(2)K(0) \mid K\pi\rangle\langle K\pi \mid K \mid \pi\rangle e^{-m_\pi(T-\Delta)}e^{-E_{K\pi}t} & (5.33)\\ &+ \ldots, \end{aligned}$$

with other contributions negligible in comparison. The construction of these correlation functions requires no additional inversions in our setup.

Table 5.15 shows $K-\pi$ scattering lengths calculated using both approaches and their

$a_0 m_\pi$	48^3	64^3	continuum
I=3/2	-0.068(8)	-0.068(7)	-0.07(2)
I=1/2	0.16(1)	0.16(1)	0.16(3)
I=3/2	-0.063(8)	-0.059(5)	-0.06(1)
I=1/2	0.178(9)	0.170(9)	0.16(2)

Table 5.15: $K-\pi$ scattering lengths calculated using 5-parameter (top 2 rows) and 3-parameter (bottom 2 rows) fits and their continuum extrapolation

	$a_0^{3/2} m_\pi$	$a_0^{1/2} m_\pi$
Büttiker et. al. [72]	-0.0448(77)	0.224(22)
$\mathcal{O}(p^4)$ ChPT	-0.05(2)	0.19(2)
NPLQCD [73]	-0.0574(16) $\begin{pmatrix} +24 \\ -58 \end{pmatrix}$	0.1725(13) $\begin{pmatrix} +23 \\ -156 \end{pmatrix}$
Fu [74; 75]	-0.0512(18)	0.1819(35)
PACS-CS [76]	-0.0602(31)(26)	0.183(18)(35)
this work (5p)	-0.07(2)	0.16(3)
this work (3p)	-0.06(1)	0.16(2)

Table 5.16: Comparison of presented results for $K\pi$ scattering lengths (bottom two rows) with experimental (top two rows) and lattice results.

continuum extrapolation. It can be seen that 3-parameter fit produces smaller statistical errors than the 5-parameter fit. The comparison of our results with previous ones is shown in table 5.16. Our results are in good agreement with the previous ones. Furthermore, our error in the $I = 1/2$ channel is comparable with other collaborations. However, unlike others we did not rely on ChPT at any point during our calculation, so we are free of any systematic errors associated with the chiral extrapolation. This is the first calculation of this quantity directly at the physical point.

Chapter 6

Conclusions

This chapter summarises our findings from Chapter 5.

We have calculated the $\Delta I = 3/2$ amplitude, which we found to be:

$$\boxed{\mathrm{Re}(A_2) = 1.50(4)_{\mathrm{stat}}(14)_{\mathrm{syst}} \times 10^{-8}\ \mathrm{GeV}; \qquad \mathrm{Im}(A_2) = -6.99(20)_{\mathrm{stat}}(84)_{\mathrm{syst}} \times 10^{-13}\ \mathrm{GeV}\,.} \tag{6.1}$$

This is consistent with both the previous continuum result [12], which was

$$\mathrm{Re}A_2 = 1.381(46)_{\mathrm{stat}}(258)_{\mathrm{syst}} \times 10^{-8}\mathrm{GeV}; \qquad \mathrm{Im}A_2 = -6.54(46)_{\mathrm{stat}}(120)_{\mathrm{syst}} \times 10^{-13}\mathrm{GeV}; \tag{6.2}$$

and is also in good agreement with the experimental result

$$|A_0| \approx \mathrm{Re}A_0 = 3.3197(14) \times 10^{-7}\mathrm{GeV}, \tag{6.3}$$

$$|A_2| \approx \mathrm{Re}A_2 = 1.570(53) \times 10^{-8}\mathrm{GeV}, \tag{6.4}$$

$$\sqrt{\frac{3}{2}}|A_2^+| \approx \sqrt{\frac{3}{2}}\mathrm{Re}A_2^+ = 1.4787(31) \times 10^{-8}\mathrm{GeV}. \tag{6.5}$$

The major improvement over the previous result is that the discretisation errors are well-controlled and are no longer the dominant source of systematic error. The systematic error is now instead dominated by the error on the Wilson coefficients, which can be improved either by improving the perturbative calculation or by using the step scaling procedure to move the renormalisation scale higher than 3 GeV, where the perturbation theory is better behaved.

Another interesting conclusion is that we have reproduced the cancellation in the $\mathrm{Re}A_2$ amplitude first reported in [2]. We believe that this cancellation gives a significant contribution to the $\Delta I = 1/2$ rule. A more recent development is the first ever calculation of A_0 in [13]. The result is $\mathrm{Re}(A_0) = 3.3201(18) \times 10^{-7}$ GeV and $\mathrm{Im}(A_0) = -1.90(123)(104) \times$

10^{-11} GeV. This gives the first theoretical prediction for ϵ'/ϵ, which is

$$\mathrm{Re}(\epsilon'/\epsilon) = 1.38(515)(443) \times 10^{-4} \tag{6.6}$$

which is 2.1σ smaller than the experimental value of $16.6(23) \times 10^{-4}$. This discrepancy may be the first sign of new physics, but we need to reduce the error before it becomes significant.

Some of the future work to improve the error may include increasing statistics or generating finer (i.e. smaller lattice spacing) ensembles (for example 2+1+1 flavour physical point). There is also a possibility of applying the aforementioned step scaling to higher scale to reduce the perturbative error. A more challenging task would be to include isospin breaking effects, which as can be seen from the experimental input, can be as large as 10% (c.f. Eq. (6.4) and Eq. (6.5)).

We have also calculated the $K\pi$ scattering lengths using the same ensembles. In this calculation we found significant contributions from finite time effects, which we control using one of the two approaches: either by directly fitting the correlation function to a 5-parameter form or by using $K \to \pi$ and $\pi \to K$ correlation function (which we call a 3-parameter fit). We find that 3-parameter fit gives a considerably smaller errors, and the scattering lengths calculated using this method are

$$a_0^{I=3/2} m_\pi = -0.06(1); \qquad a_0^{I=1/2} m_\pi = 0.16(2). \tag{6.7}$$

These numbers are in agreement with both dispersive calculations based on the experimental input, as well as the previous lattice calculations. While the error bars are larger than those in the previous calculations due to limited statistics, we should emphasise that this is the first calculation of this quantity performed directly at the physical point and is therefore independent of chiral perturbation theory.

Appendix A

Conjugacy classes of the cubic symmetry group

This section contains matrices which correspond to the transformation of a vector under cubic symmetry group, arranged by their conjugacy classes.

A.1 E

$$\begin{pmatrix} 1 & 0 & 0 \\ 0 & 1 & 0 \\ 0 & 0 & 1 \end{pmatrix}$$

A.2 $6C_4$

$$\begin{pmatrix} 1 & 0 & 0 \\ 0 & 0 & 1 \\ 0 & -1 & 0 \end{pmatrix}, \begin{pmatrix} 1 & 0 & 0 \\ 0 & 0 & -1 \\ 0 & 1 & 0 \end{pmatrix}, \begin{pmatrix} 0 & 0 & -1 \\ 0 & 1 & 0 \\ 1 & 0 & 0 \end{pmatrix}, \begin{pmatrix} 0 & 0 & 1 \\ 0 & 1 & 0 \\ -1 & 0 & 0 \end{pmatrix}, \begin{pmatrix} 0 & -1 & 0 \\ 1 & 0 & 0 \\ 0 & 0 & 1 \end{pmatrix}, \begin{pmatrix} 0 & 1 & 0 \\ -1 & 0 & 0 \\ 0 & 0 & 1 \end{pmatrix}$$

A.3 $3C_2$

$$\begin{pmatrix} 1 & 0 & 0 \\ 0 & -1 & 0 \\ 0 & 0 & -1 \end{pmatrix}, \begin{pmatrix} -1 & 0 & 0 \\ 0 & 1 & 0 \\ 0 & 0 & -1 \end{pmatrix}, \begin{pmatrix} -1 & 0 & 0 \\ 0 & -1 & 0 \\ 0 & 0 & 1 \end{pmatrix}$$

A.4 $\mathbf{8}C_3$

$$\begin{pmatrix} 0 & 0 & 1 \\ 1 & 0 & 0 \\ 0 & 1 & 0 \end{pmatrix}, \begin{pmatrix} 0 & 1 & 0 \\ 0 & 0 & 1 \\ 1 & 0 & 0 \end{pmatrix}, \begin{pmatrix} 0 & 0 & -1 \\ 1 & 0 & 0 \\ 0 & -1 & 0 \end{pmatrix}, \begin{pmatrix} 0 & 1 & 0 \\ 0 & 0 & -1 \\ -1 & 0 & 0 \end{pmatrix},$$
$$\begin{pmatrix} 0 & -1 & 0 \\ 0 & 0 & 1 \\ -1 & 0 & 0 \end{pmatrix}, \begin{pmatrix} 0 & 0 & -1 \\ -1 & 0 & 0 \\ 0 & 1 & 0 \end{pmatrix}, \begin{pmatrix} 0 & -1 & 0 \\ 0 & 0 & -1 \\ 1 & 0 & 0 \end{pmatrix}, \begin{pmatrix} 0 & 0 & 1 \\ -1 & 0 & 0 \\ 0 & -1 & 0 \end{pmatrix}$$

A.5 $\mathbf{6}C_2$

$$\begin{pmatrix} 0 & 1 & 0 \\ 1 & 0 & 0 \\ 0 & 0 & -1 \end{pmatrix}, \begin{pmatrix} 0 & -1 & 0 \\ -1 & 0 & 0 \\ 0 & 0 & -1 \end{pmatrix}, \begin{pmatrix} -1 & 0 & 0 \\ 0 & 0 & 1 \\ 0 & 1 & 0 \end{pmatrix}, \begin{pmatrix} -1 & 0 & 0 \\ 0 & 0 & -1 \\ 0 & -1 & 0 \end{pmatrix},$$
$$\begin{pmatrix} 0 & 0 & 1 \\ 0 & -1 & 0 \\ 1 & 0 & 0 \end{pmatrix}, \begin{pmatrix} 0 & 0 & -1 \\ 0 & -1 & 0 \\ -1 & 0 & 0 \end{pmatrix}$$

References

[1] A. Schenk, *Absorption and dispersion of pions at finite temperature*, *Nucl.Phys.* **B363** (1991) 97–116.

[2] **RBC Collaboration, UKQCD Collaboration** Collaboration, P. Boyle et al., *Emerging understanding of the Δ I = 1/2 Rule from Lattice QCD*, *Phys.Rev.Lett.* **110** (2013) 152001, [hep-lat/12].

[3] T. Blum et al., *$K \to \pi\pi$ $\Delta I = 3/2$ decay amplitude in the continuum limit*, *Phys. Rev.* **D91** (2015), no. 7 074502, [arXiv:1502.00263].

[4] T. Janowski, P. A. Boyle, A. Jüttner, and C. Sachrajda, *K-π scattering lengths at physical kinematics*, *PoS* **LATTICE2014** (2014) 080.

[5] J. H. Christenson, J. W. Cronin, V. L. Fitch, and R. Turlay, *Evidence for the 2 π Decay of the k(2)0 Meson*, *Phys. Rev. Lett.* **13** (1964) 138–140.

[6] **NA31** Collaboration, H. Burkhardt et al., *First Evidence for Direct CP Violation*, *Phys. Lett.* **B206** (1988) 169–176.

[7] L. K. Gibbons et al., *Measurement of the CP violation parameter $Re(\epsilon'/\epsilon)$*, *Phys. Rev. Lett.* **70** (1993) 1203–1206.

[8] **NA48** Collaboration, V. Fanti et al., *A New measurement of direct CP violation in two pion decays of the neutral kaon*, *Phys. Lett.* **B465** (1999) 335–348, [hep-ex/9909022].

[9] **KTeV** Collaboration, A. Alavi-Harati et al., *Measurements of direct CP violation, CPT symmetry, and other parameters in the neutral kaon system*, *Phys. Rev.* **D67** (2003) 012005, [hep-ex/0208007]. [Erratum: Phys. Rev.D70,079904(2004)].

[10] M. K. Gaillard and B. W. Lee, *$\Delta I = 1/2$ Rule for Nonleptonic Decays in Asymptotically Free Field Theories*, *Phys. Rev. Lett.* **33** (1974) 108.

[11] G. Altarelli and L. Maiani, *Octet Enhancement of Nonleptonic Weak Interactions in Asymptotically Free Gauge Theories*, *Phys. Lett.* **B52** (1974) 351–354.

[12] T. Blum, P. Boyle, N. Christ, N. Garron, E. Goode, et al., *Lattice determination of the $K \to (\pi\pi)_{I=2}$ Decay Amplitude A_2*, *Phys.Rev.* **D86** (2012) 074513, [hep-lat/12].

[13] Z. Bai et al., *Standard-model prediction for direct CP violation in $K \to \pi\pi$ decay*, arXiv:1505.07863.

[14] F. Jegerlehner and A. Nyffeler, *The Muon g-2*, *Phys. Rept.* **477** (2009) 1–110, [arXiv:0902.3360].

[15] **LHCb** Collaboration, C. Langenbruch, *Latest results on rare decays from LHCb*, in *50th Rencontres de Moriond on EW Interactions and Unified Theories La Thuile, Italy, March 14-21, 2015*, 2015. arXiv:1505.04160.

[16] **Particle Data Group** Collaboration, K. Olive et al., *Review of Particle Physics*, *Chin.Phys.* **C38** (2014) 090001.

[17] J. F. Nieves and P. B. Pal, *Generalized Fierz identities*, *Am. J. Phys.* **72** (2004) 1100–1108, [hep-ph/0306087].

[18] S. Bertolini, J. O. Eeg, and M. Fabbrichesi, *Studying epsilon-prime / epsilon in the chiral quark model: gamma(5) scheme independence and NLO hadronic matrix elements*, *Nucl. Phys.* **B449** (1995) 197–228, [hep-ph/9409437].

[19] N. Ishizuka, K. I. Ishikawa, A. Ukawa, and T. Yoshié, *Calculation of $K \to \pi\pi$ decay amplitudes with improved Wilson fermion action in lattice QCD*, arXiv:1505.05289.

[20] A. Donini, V. Gimenez, G. Martinelli, M. Talevi, and A. Vladikas, *Nonperturbative renormalization of lattice four fermion operators without power subtractions*, *Eur.Phys.J.* **C10** (1999) 121–142, [hep-lat/9902030].

[21] G. Buchalla, A. J. Buras, and M. E. Lautenbacher, *Weak decays beyond leading logarithms*, *Rev.Mod.Phys.* **68** (1996) 1125–1144, [hep-ph/9512380].

[22] C. W. Bernard, T. Draper, A. Soni, H. D. Politzer, and M. B. Wise, *Application of Chiral Perturbation Theory to $K \to 2\pi$ Decays*, *Phys. Rev.* **D32** (1985) 2343–2347.

[23] V. Cirigliano and E. Golowich, *Analysis of $O(p^2)$ corrections to $< \pi\pi|Q(7,8)|K >$*, *Phys. Lett.* **B475** (2000) 351–360, [hep-ph/9912513].

[24] C. Aubin, J. Laiho, S. Li, and M. Lin, *$K \to \pi$ and $K \to 0$ in 2+1 Flavor Partially Quenched Chiral Perturbation Theory*, *Phys.Rev.* **D78** (2008) 094505, [hep-lat/08].

[25] J. Laiho and A. Soni, *On lattice extraction of $K \to \pi\pi$ amplitudes to O(p**4) in chiral perturbation theory*, *Phys.Rev.* **D65** (2002) 114020, [hep-ph/hep].

[26] Y. Iwasaki, *Renormalization Group Analysis of Lattice Theories and Improved Lattice Action: Two-Dimensional Nonlinear O(N) Sigma Model*, *Nucl. Phys.* **B258** (1985) 141–156.

[27] H. B. Nielsen and M. Ninomiya, *No Go Theorem for Regularizing Chiral Fermions*, *Phys. Lett.* **B105** (1981) 219.

[28] R. Narayanan and H. Neuberger, *Chiral determinant as an overlap of two vacua*, *Nucl. Phys.* **B412** (1994) 574–606, [hep-lat/9307006].

[29] D. B. Kaplan, *A Method for simulating chiral fermions on the lattice*, *Phys. Lett.* **B288** (1992) 342–347, [hep-lat/9206013].

[30] Y. Shamir, *Chiral fermions from lattice boundaries*, *Nucl. Phys.* **B406** (1993) 90–106, [hep-lat/9303005].

[31] V. Furman and Y. Shamir, *Axial symmetries in lattice QCD with Kaplan fermions*, *Nucl. Phys.* **B439** (1995) 54–78, [hep-lat/9405004].

[32] R. C. Brower, H. Neff, and K. Orginos, *Mobius fermions: Improved domain wall chiral fermions*, *Nucl. Phys. Proc. Suppl.* **140** (2005) 686–688, [hep-lat/0409118]. [,686(2004)].

[33] S. Duane, A. D. Kennedy, B. J. Pendleton, and D. Roweth, *Hybrid Monte Carlo*, *Phys. Lett.* **B195** (1987) 216–222.

[34] C. Kim, *$I = 2$ $\pi\pi$ scattering using G parity boundary condition*, *Nucl.Phys.Proc.Suppl.* **129** (2004) 197–199, [hep-lat/0311003].

[35] C. Kim, *$\Delta(I) = 3/2$ $K \to \pi\pi$ with physical final state*, *Nucl.Phys.Proc.Suppl.* **140** (2005) 381–383.

[36] T. Blum, P. Boyle, N. Christ, N. Garron, E. Goode, et al., *The $K \to (\pi\pi)_{I=2}$ Decay Amplitude from Lattice QCD*, *Phys.Rev.Lett.* **108** (2012) 141601, [arXiv:1111.1699].

[37] H. Georgi, *Lie Algebras In Particle Physics: from Isospin To Unified Theories*. Frontiers in Physics. Perseus Books, Advanced Book Program, 1999.

[38] H. Jones, *Groups, Representations and Physics*. CRC Press, 1998.

[39] T. Blum, T. Izubuchi, and E. Shintani, *A new class of variance reduction techniques using lattice symmetries*, hep-lat/12.

[40] R. Mawhinney, *Weak decay measurements from 2+1 flavor dwf ensembles*, Presented at Lattice 2013 conference, Mainz, 2013.

[41] K. Osterwalder and R. Schrader, *AXIOMS FOR EUCLIDEAN GREEN'S FUNCTIONS*, *Commun. Math. Phys.* **31** (1973) 83–112.

[42] L. Maiani and M. Testa, *Final state interactions from Euclidean correlation functions*, *Phys. Lett.* **B245** (1990) 585–590.

[43] C. Kim, C. Sachrajda, and S. R. Sharpe, *Finite-volume effects for two-hadron states in moving frames*, *Nucl.Phys.* **B727** (2005) 218–243, [hep-lat/he].

[44] **CP-PACS** Collaboration, T. Yamazaki et al., *$I = 2$ $\pi\pi$ scattering phase shift with two flavors of O(a) improved dynamical quarks*, *Phys. Rev.* **D70** (2004) 074513, [hep-lat/0402025].

[45] L. Lellouch and M. Luscher, *Weak transition matrix elements from finite volume correlation functions*, *Commun.Math.Phys.* **219** (2001) 31–44, [hep-lat/he].

[46] C. Aubin and C. Bernard, *Pion and kaon masses in staggered chiral perturbation theory*, *Phys.Rev.* **D68** (2003) 034014, [hep-lat/0304014].

[47] C. D. Lin, G. Martinelli, E. Pallante, C. Sachrajda, and G. Villadoro, *$K^+ \to \pi^+\pi^0$ decays on finite volumes and at next-to-leading order in the chiral expansion*, *Nucl.Phys.* **B650** (2003) 301–355, [hep-lat/0208007].

[48] C. Sturm, Y. Aoki, N. Christ, T. Izubuchi, C. Sachrajda, et al., *Renormalization of quark bilinear operators in a momentum-subtraction scheme with a nonexceptional subtraction point*, *Phys.Rev.* **D80** (2009) 014501, [hep-ph/090].

[49] G. Martinelli, C. Pittori, C. T. Sachrajda, M. Testa, and A. Vladikas, *A General method for nonperturbative renormalization of lattice operators*, *Nucl.Phys.* **B445** (1995) 81–108, [hep-lat/he].

[50] **RBC, UKQCD** Collaboration, T. Blum et al., *Domain wall QCD with physical quark masses*, arXiv:1411.7017.

[51] **RBC, UKQCD** Collaboration, R. Arthur, P. Boyle, N. Garron, C. Kelly, and A. Lytle, *Opening the Rome-Southampton window for operator mixing matrices*, *Phys.Rev.* **D85** (2012) 014501, [arXiv:1109.1223].

[52] R. C. Brower, H. Neff, and K. Orginos, *The Möbius Domain Wall Fermion Algorithm*, arXiv:1206.5214.

[53] A. Stathopoulos and K. Orginos, *Computing and deflating eigenvalues while solving multiple right hand side linear systems in quantum chromodynamics*, *SIAM J.Sci.Comput.* **32** (2010) 439–462, [arXiv:0707.0131].

[54] M. Gockeler, R. Horsley, H. Oelrich, H. Perlt, D. Petters, et al., *Nonperturbative renormalization of composite operators in lattice QCD*, *Nucl.Phys.* **B544** (1999) 699–733, [hep-lat/9807044].

[55] C. Lehner and C. Sturm, *Matching factors for Delta S=1 four-quark operators in RI/SMOM schemes*, *Phys.Rev.* **D84** (2011) 014001, [hep-ph/110].

[56] M. Lightman, $\Delta I = 3/2$ $K \to \pi\pi$ *Decays Using Lattice QCD with Domain Wall Fermions*. PhD thesis, Columbia University, 2011.

[57] E. J. Goode, *The Evaluation of $K \to \pi\pi$ Decay Amplitudes from Lattice Quantum Chromodynamics*. PhD thesis, University of Southampton, 2012.

[58] A. J. Buras, M. Jamin, and M. E. Lautenbacher, *The Anatomy of epsilon-prime / epsilon beyond leading logarithms with improved hadronic matrix elements*, *Nucl.Phys.* **B408** (1993) 209–285, [hep-ph/9303284].

[59] M. Ciuchini, E. Franco, G. Martinelli, and L. Reina, *ϵ'/ϵ at the Next-to-leading order in QCD and QED*, *Phys.Lett.* **B301** (1993) 263–271, [hep-ph/9212203].

[60] M. Ciuchini, E. Franco, G. Martinelli, L. Reina, and L. Silvestrini, *An Upgraded analysis of epsilon-prime epsilon at the next-to-leading order*, *Z.Phys.* **C68** (1995) 239–256, [hep-ph/9501265].

[61] L. Lellouch, *Flavor physics and lattice quantum chromodynamics*, in *Modern perspectives in lattice QCD: Quantum field theory and high performance computing. Proceedings, International School, 93rd Session, Les Houches, France, August 3-28, 2009*, pp. 629–698, 2011. arXiv:1104.5484.

[62] **ETM** Collaboration, N. Carrasco, V. Lubicz, and L. Silvestrini, *Vacuum Insertion Approximation and the I=1/2 rule: A lattice QCD test of the nave factorization hypothesis for K , D , B and static mesons*, *Phys.Lett.* **B736** (2014) 174–179, [arXiv:1312.6691].

[63] W. A. Bardeen, A. Buras, and J. Gerard, *A Consistent Analysis of the $\Delta I = 1/2$ Rule for K Decays*, *Phys.Lett.* **B192** (1987) 138.

[64] A. Pich and E. de Rafael, *Weak K amplitudes in the chiral and 1/n(c) expansions*, *Phys.Lett.* **B374** (1996) 186–192, [hep-ph/9511465].

[65] A. J. Buras, J.-M. Gérard, and W. A. Bardeen, *Large N Approach to Kaon Decays and Mixing 28 Years Later: $\Delta I = 1/2$ Rule, $\hat{B}_K$ and ΔM_K*, *Eur.Phys.J.* **C74** (2014), no. 5 2871, [arXiv:1401.1385].

[66] A. Pich, *Theoretical overview of kaon decays*, *J.Phys.Conf.Ser.* **556** (2014), no. 1 012045, [arXiv:1410.3783].

[67] U. Wiese, *C periodic and G periodic QCD at finite temperature*, *Nucl.Phys.* **B375** (1992) 45–66.

[68] C. Kim and N. H. Christ, *G parity boundary conditions and $\Delta I = 1/2$, $K \to \pi\pi$ decays*, *PoS* **LAT2009** (2009) 255, [arXiv:0912.2936].

[69] **RBC, UKQCD** Collaboration, C. Kelly, *Progress towards $\Delta I = 1/2$ $K \to \pi\pi$ decays with G-parity boundary conditions*, *PoS* **LATTICE2012** (2012) 130.

[70] **RBC, UKQCD** Collaboration, C. Kelly, T. Blum, N. Christ, A. Lytle, and C. Sachrajda, *Progress Towards an ab initio, Standard Model Calculation of Direct CP-Violation in K-decays*, *PoS* **LATTICE2013** (2014) 401.

[71] C. Kelly and D. Zhang, *Lattice measurement of the $\delta i = 1/2$ contribution to standard model direct cp-violation in $k \to \pi\pi$ decays at physical kinematics*, in *PoS LATTICE 2014 365,366*, 2015.

[72] P. Buettiker, S. Descotes-Genon, and B. Moussallam, *A new analysis of π K scattering from Roy and Steiner type equations*, *Eur. Phys. J.* **C33** (2004) 409–432, [hep-ph/0310283].

[73] S. R. Beane, P. F. Bedaque, T. C. Luu, K. Orginos, E. Pallante, A. Parreno, and M. J. Savage, *π K scattering in full QCD with domain-wall valence quarks*, *Phys. Rev.* **D74** (2006) 114503, [hep-lat/0607036].

[74] Z. Fu, *Lattice study on πK scattering with moving wall source*, *Phys. Rev.* **D85** (2012) 074501, [arXiv:1110.1422].

[75] Z. Fu, *The preliminary lattice QCD calculation of κ meson decay width*, *JHEP* **01** (2012) 017, [arXiv:1110.5975].

[76] **PACS-CS** Collaboration, K. Sasaki, N. Ishizuka, M. Oka, and T. Yamazaki, *Scattering lengths for two pseudoscalar meson systems*, *Phys. Rev.* **D89** (2014), no. 5 054502, [arXiv:1311.7226].